Estimation of hydrogen redistribution in zircaloy cladding of spent fuel under thermal conditions of dry storage and evaluation of its influence on mechanical properties of the cladding

M. Sugisaki, K. Hashizume, Y. Hatano

Department of Nuclear Engineering, Faculty of Engineering, Kyushu University, Japan

Abstract. Hydrogen redistribution processes in Zircaloy cladding of spent fuel were evaluated under thermal conditions of dry storage. Charpy impact tests were carried out from room temperature to 250°C on two kinds of Zircaloy specimens charged with 400 ppm of hydrogen: specimens in which hydrogen (hydride) is uniformly distributed and specimens in which it is non-uniformly distributed. These tests show that the impact strength of the specimen with non-uniform hydrogen distribution is larger than that of the specimen with uniform distribution. These results suggest that the impact strength of the cladding having large amounts of hydrogen is degraded during dry storage; for example, in the case of the cladding with 400 ppm hydrogen, the uniform distribution of hydrogen is realized when the cladding is heated to 480°C.

1. Introduction

Recently, interim dry storage has been undertaken in several countries, and some criteria for the safety of facilities have been assessed from several points of view [1-8]. One perspective is the thermal condition of the spent-fuel elements when heated to temperatures up to 200°C to 300°C, depending on the burnup, the period of cooling in the water pool, and the nature of the cover gas. In this temperature region, thermal effects could bring about some chemical reactions or degradation of physical properties of the fuel elements; for example, the thermal criteria for creep of the fuel cladding tubes have been studied. With respect to the mechanical properties of the cladding tubes, hydrogen embrittlement may be an important problem. Zircaloy fuel-cladding tubes absorb hydrogen during service in water-cooled reactors, and the hydrides, ZrH_{2-x} (δ-phase), precipitate non-uniformly, i.e., they are concentrated in the outer periphery (cooler region) of the fuel tubes and lead to hydrogen embrittlement of the tubes. This non-uniform distribution of hydrogen (hydride) may be maintained during interim storage in a water pool, because the cladding tubes are not heated to temperatures that would result in hydrogen redistribution. In the case of dry storage, however, there would be a possibility that redistribution of hydrogen (hydride) is appreciable and the mechanical properties of the cladding tubes appreciably change, because the diffusion coefficient of hydrogen is of the order of magnitude 10^{-6} to 10^{-7} cm^2/s in the temperature region expected for dry storage. Therefore, it may be important to investigate the redistribution behaviour of hydrogen (hydride) in Zircaloy cladding tubes under thermal conditions of dry storage and to evaluate the influence of redistribution of hydride precipitates on mechanical properties such as impact properties.

This paper provides a report of a recent experimental study of the Charpy impact test of two kinds of Zircaloy-2 specimens with uniform or non-uniform distribution of hydride and discusses the effect of the non-uniformity of the hydride distribution on hydrogen embrittlement. Also reported is the numerical calculation of the redistribution process of the hydride under the thermal gradient that was applied to the preparation of the specimens for the Charpy impact tests. Finally, the paper discusses the possibility of the redistribution of hydrogen (hydride) under the thermal conditions of dry storage and proposes a criterion for the thermal condition of the dry storage facility.

2. **Charpy imact test**

2.1. Specimen preparation

The Charpy impact test was carried out on two kinds of specimens: a specimen in which hydrogen and hydride are uniformly distributed and the other is one in which they are non-uniformly distributed. Hydrogenation of specimens was carried out in the following manner. Specimens of rectangular prisms (10 x 5 mm in section; 50 mm in length) were cut from a Zircaloy-2 rod (diameter 12 mm), the composition of which is summarized in Table 1. They were loaded with hydrogen with a gas absorption method at 520°C. The hydrogen content was adjusted as 100 or 400 ppm. Then these specimens were vacuum-sealed in a quartz glass tube and isothermally heated at 500°C for 17 days to achieve uniform distribution of hydrogen. The uniform distribution of hydrogen was confirmed by quantitative analysis based on the vacuum extraction method at high temperatures. In these specimens, α- and δ-phases are randomly distributed. The phase diagram and the detailed solubility curve of hydrogen in zirconium are shown in Figs. 1 and 2 [9]. The specimen with the non-uniform distribution of hydrogen was prepared by making use of thermomigration of hydrogen. The principle of redistribution of hydrogen by thermomigration is explained by the diffusion flux of hydrogen J under thermal gradient dT/dx, as described by the equation

$$J = - D (dC/dx + Q^*C/RT^2 \; dT/dx) \qquad (4.1)$$

where

D is the diffusion coefficient of hydrogen
C is the hydrogen concentration
Q* is the heat of transport
R is the gas constant
T is the temperature

and x is the space coordinate.

Hydrogen atoms are driven to the lower or higher temperature side by the thermal gradient, depending on the sign of the heat of transport Q*. In the case of hydrogen in zirconium and Zircaloy, the sign of Q* is positive (i.e., hydrogen atoms are driven to the lower temperature side). The magnitude of Q* has been determined by many researchers [10-17]. On the basis of these studies, the value of +27 kJ/mol was adopted in the present analysis. The apparatus for the thermomigration heat treatment is schematically depicted in Fig. 3. In the present experiment, the thermal gradient was applied to the specimen on the 5- or 10-mm side with heat reservoirs as shown in Fig 4. These specimens will be Type-A or -B hereafter, as is depicted in the figure. The magnitude of the thermal gradient was adjusted as 80°C/cm and the temperature of the lower side surface of the specimen was about 280°C.

Table 1a. Composition of Zircaloy-2 Specimen for Charpy Impact Test

Element	Cr	Fe	Ni	O	Sn	Zr
Composition (wt%)	0.10~0.11	0.16~0.18	0.06~0.07	0.11~0.13	1.40~1.48	balance

Table 1b. Impurity Content of Specimen (as-received material)

Element	H	N	C	Al	Si	Hf
Content (ppm)	3~8	26~29	81~97	21~27	40~50	51~52

To determine the duration of the heat treatment of thermomigration, the hydrogen redistribution process was calculated by numerical analysis of the above diffusion equation. The numerical analysis was performed on the following assumptions, which have been previously adopted by Markowitz and others [11-12]:

(1) The diffusion of hydrogen in the δ-phase was neglected because the diffusion coefficient of hydrogen was much smaller than that in the α-phase [18]. The cross section of α-phase effective for the diffusion at a position x was determined by the ratio of the amount of α-phase to that of δ-phase present at that position in which the density difference between α- and δ-phases was neglected

(2) When the hydrogen concentration in Zircaloy exceeds the solubility in the α-phase, the δ-phase of zirconium hydride precipitates. The solubility data for zirconium was used, and the difference in the solubility between Zircaloy and zirconium was neglected. The rate of the phase change from the δ-phase to the α-phase or vice versa was considered to be so fast that the phase change was immediately realized. The hydrogen concentration of δ-phase in equilibrium with the α-phase was assumed as $ZrH_{1.4}$, independent of temperature.

An example of the results of the numerical analysis is shown in Fig. 5. As seen in this figure, in an early stage of diffusion annealing, hydrogen concentration at the high temperature side rapidly decreases to the terminal solubility of α-phase, and hydrogen atoms are concentrated at a colder side (i.e., the hydride phase is transported from a hotter side to the colder one. In an intermediate stage, a step-like hydrogen distribution is built up, and its plateau gradually approaches to the colder side.

On the basis of this analysis, the duration time of heat treatment for the thermomigration was determined as 24 or 100 days in the case of Type-A specimens and 9 days in the case of Type-B specimens. The concentration distribution of hydrogen in these specimens was analysed by the vacuum extraction method. The measured hydrogen profile is compared with that obtained by the above numerical analysis in Fig. 6. The characteristics of the hydrogen profiles are consistent with each other. The measured hydrogen concentration distribution is also shown in Figs. 7 and 8.

2.2. Charpy impact test

Charpy impact tests were carried out for the V-notched specimens. The position of the V-notch is shown in Fig. 9. In the case of Type-A specimens, the V-notch was made on either the surface of the specimen, which was heat-treated for 24 days, or the surface of the α-phase for the specimen heat-treated for 100 days. The Charpy test was carried out in a temperature region from room temperature to 250ºC. The results are summarized in Table 2 (at end of paper) and depicted in Figs. 10 to 12 for convenience of comparison. The characteristics of the present results are summarized as follows:

1. The impact strength decreases with increase of the hydrogen content because of the formation of hydride.

2. Impact strength recovers when the distribution of the hydride becomes non-uniform.

The first result is already well known, but the second result has not necessarily been explicitly recognized. The recovery of the ductility may be attributable to the fact that the single-phase region appears because the hydride is concentrated at a colder side by thermomigration. These

results suggest that the impact strength of the Zircaloy cladding would be degraded when the distribution of the hydride becomes uniform.

3. Redistribution of hydride under thermal conditions of dry storage

3.1. Hydrogen pick-up during reactor service

To evaluate the redistribution of hydride under thermal conditions of dry storage, an initial distribution must be assumed. The supposition in the present analysis is that the initial distribution of the hydride inside the fuel cladding which is placed under the thermal condition of dry storage, is the same as that built-up during reactor service.

The process of hydrogen pick-up may be modelled as follows:

1. Some of hydrogen atoms, released by the reaction of zirconium with water, penetrate through the zirconium oxide layer, dissolve in the Zircaloy matrix, and diffuse into the bulk metal. The present analysis only considers the hydrogen distribution in the Zircaloy matrix, not the hydrogen transport in the zirconium oxide layer. The dissolving rate of hydrogen atoms into the Zircaloy matrix is generally dependent on the temperature of the cladding, so the rate of hydrogen pick-up is dependent on the longitudinal position. The hydrogen diffusion in these directions can be separately treated, because the diffusion path length is very short in the radial direction compared to that in the longitudinal direction. In addition, the stationary distribution of hydrogen in the radial direction can be assumed because the time required for hydrogen to diffuse over the distance corresponding to the thickness of the cladding is very short compared to the time scale of reactor service. The thermal gradient imposed on the cladding is large in the radial direction, so the effect of thermomigration must be considered in the calculation of diffusion in the radial direction.

2. The concentration of hydrogen inside the cladding gradually increases with burnup, and the hydride precipitates when the hydrogen concentration exceeds the solubility limit of the α-phase. The precipitation starts near the outer periphery of the cladding, because the solubility limit is lowest near the outer periphery, where the cladding temperature is lowest. As a result, the hydride is concentrated near the outer periphery, which is in contact with the reactor coolant.

3. When the fuel elements are cooled down after reactor service, the precipitation of hydride occurs in the whole region of the cladding, because the amount of hydrogen picked-up usually exceeds the solubility limit in the lower temperature region. Such distribution of the hydride may be maintained during the interim storage in a water pool, so this distribution can be assumed to be an initial state for dry storage.

The actual calculation was carried out for PWR and BWR fuel elements. The heat of transport Q* was assumed to be independent of the temperature, and the magnitude of thermal gradients is assumed to be independent of position in the radial direction. The reduction of the thickness of the cladding tube from corrosion was taken into consideration. The calculation was carried out assuming a rate of burnup such that 30 Gwd/t was realized in 33 months. The rate of corrosion was assumed to be constant. The oxide thickness was taken as 80 μm after 55 GWd/t. The fraction of hydrogen pick-up was based on the assumption of 8 % of hydrogen atoms released by the corrosion reaction penetrated through the oxide layer and dissolved into the Zircaloy matrix. These values lead to 400 ppm as the total hydrogen absorbed during a reactor service of 55 GWd/t. The temperature distribution inside the cladding was assumed as

that of the usual PWR or BWR. As a typical example, the distribution of hydrogen in the radial direction of the BWR fuel cladding at a reactor temperature is shown in Fig. 13. In the calculation, the thickness of the cladding wall is 0.85 mm and the temperatures of the inner and outer surfaces are 368 and 295ºC, respectively. The region in which hydrogen concentration sharply increases mainly consists of δ-phase, and the inner region consists of α-phase, in which the hydrogen concentration ranges from 15 to ~70 ppm.

3.2. Redistribution of hydride under isothermal condition

When the spent-fuel assemblies are placed into dry storage, redistribution of the hydride in the cladding may be brought about by the temperature rise from decay heat. During dry storage, the temperature of the cladding is almost uniform in the transverse direction because the decay heat is not so large as to produce thermal gradients in the radial direction. The temperature distribution in the longitudinal direction, however, is not uniform, because the decay heat is largest in the longitudinally central part. An example of the data measured for spent-fuel elements placed under several ambient gas conditions is shown in Fig. 14.

The redistribution process of hydride in the longitudinal and radial directions was carried out with the same method of finite difference as described in the previous section. The initial distribution of the hydride is also assumed to be the same as described in the previous section.

In the case of calculation in the radial direction, several temperatures were supposed (i.e., 300ºC, 400ºC, and 480ºC). The calculated results are shown for BWR cladding in Figs. 15 through 17. The characteristics of these results are summarized as follows:

1. The stationary distribution is attained in a comparatively short time even at 573ºK. It should be noted that the uniform distribution is not attained in the stationary state. The reason is that hydrogen redistribution does not proceed over the solubility limit.

2. Appreciable amounts of hydrogen are redistributed to the inner side. The amount of hydrogen atoms transported to the inner side increases with increase of temperature. This is ascribed to the fact that the solubility limit increases with temperature.

3. The uniform distribution is realized when the temperature is raised up to 480ºC.

4. This is attributable to the fact that 400 ppm of hydrogen corresponds to the solubility limit at this temperature.

In the case of redistribution in the longitudinal direction, the calculation was carried out for the most severe case of the thermal condition as depicted in Fig. 14. The calculated results are shown in Figs. 18 and 19. As is seen in these figures, appreciable redistribution is not realized in a short time. Consequently, the redistribution process of hydrogen in the cladding of the spent fuel under the isothermal condition is summarized as follows:

1. Appreciable redistribution in a radial direction is easily realized in a comparatively short time at temperatures near 300ºC to 400ºC.

2. Appreciable redistribution in a longitudinal direction is not realized.

3.3. Impact of redistribution of hydride on the safety criteria of dry storage facilities

As just discussed, the appreciable redistribution of hydride is brought about in the radial direction in comparatively short times at temperatures near 300ºC to 400ºC. This result

suggests that the impact strength of the fuel cladding appreciably decreases if it picks up large amounts of hydrogen.

It should be noted here, however, that the completely uniform distribution is not necessarily brought about. The hydride is uniformly distributed in the radial direction of cladding in several hours when the cladding is heated up to dry storage temperatures, when the total amount of absorbed hydrogen can be dissolved in the α-phase. In the case of 400 ppm hydrogen, the temperature is about 480ºC.

From the viewpoint of hydrogen redistribution, then, the allowable maximum temperature must be determined as one at which the total amount of absorbed hydrogen can be dissolved in the α-phase.

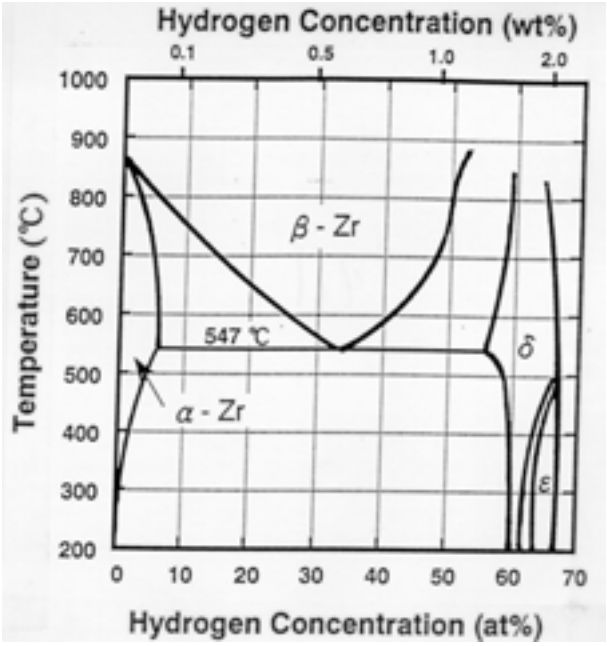

Figure 1. Phase diagram of hydrogen-zirconium system.

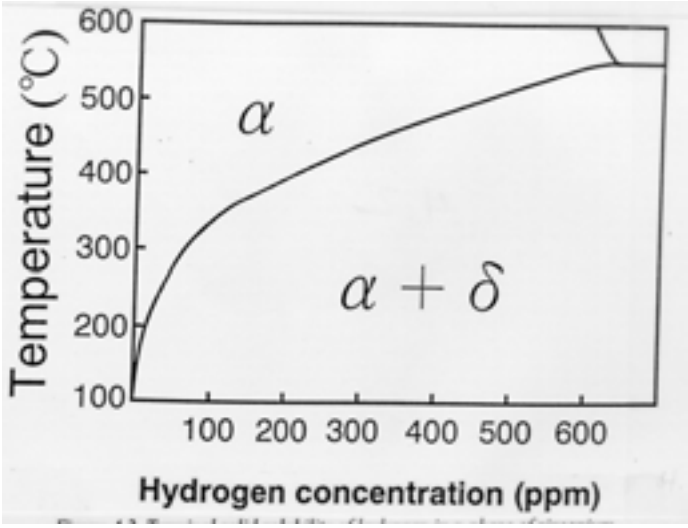

Figure 2. Terminal solid solubility of hydrogen in α-phase of zirconium.

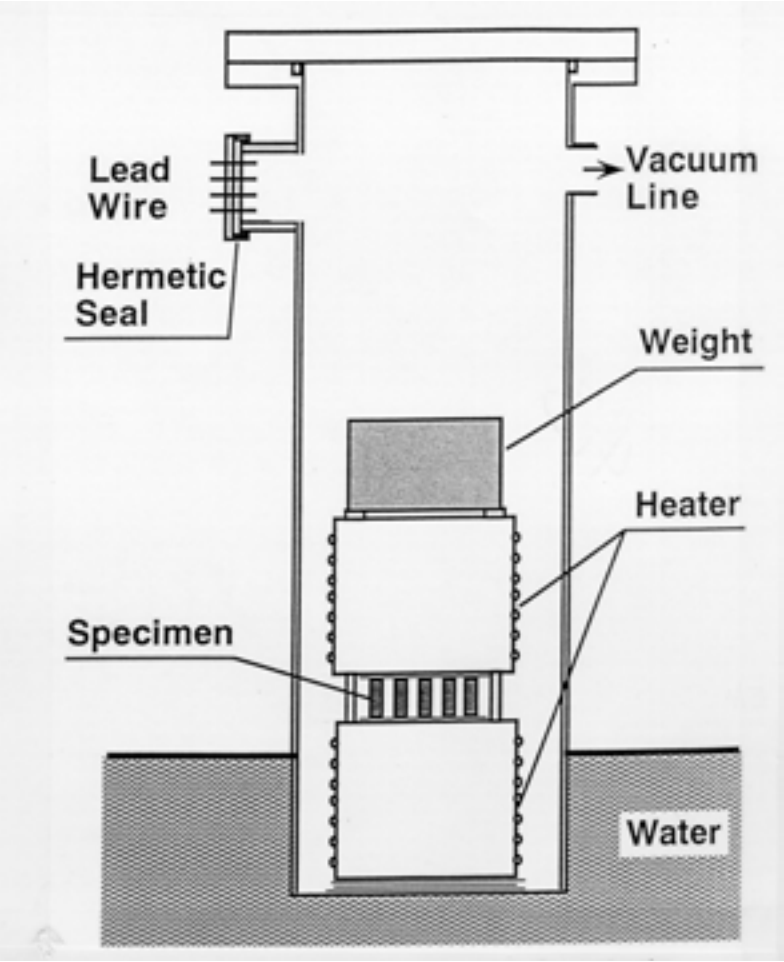

Figure 3. Apparatus for heat treatment for thermomigration.

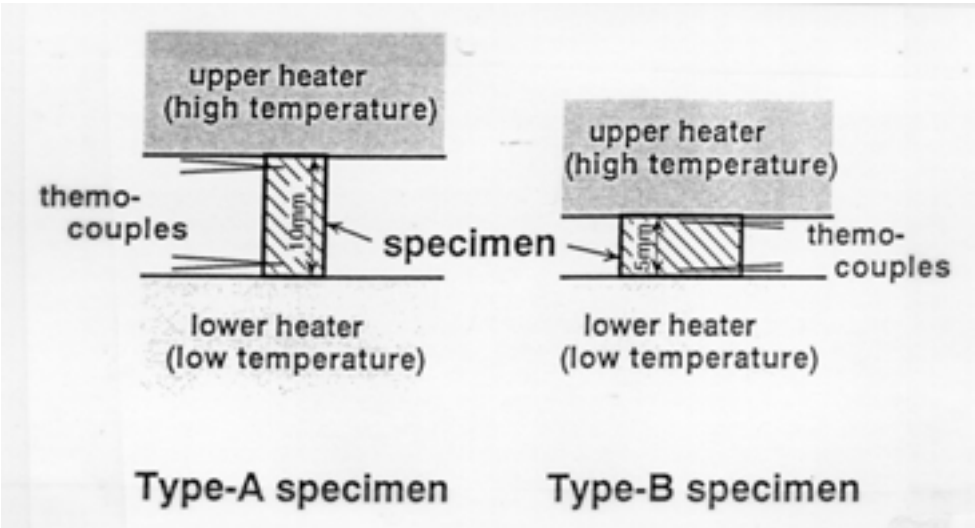

Figure 4. Schematic description of thermal gradient imposed to specimens.

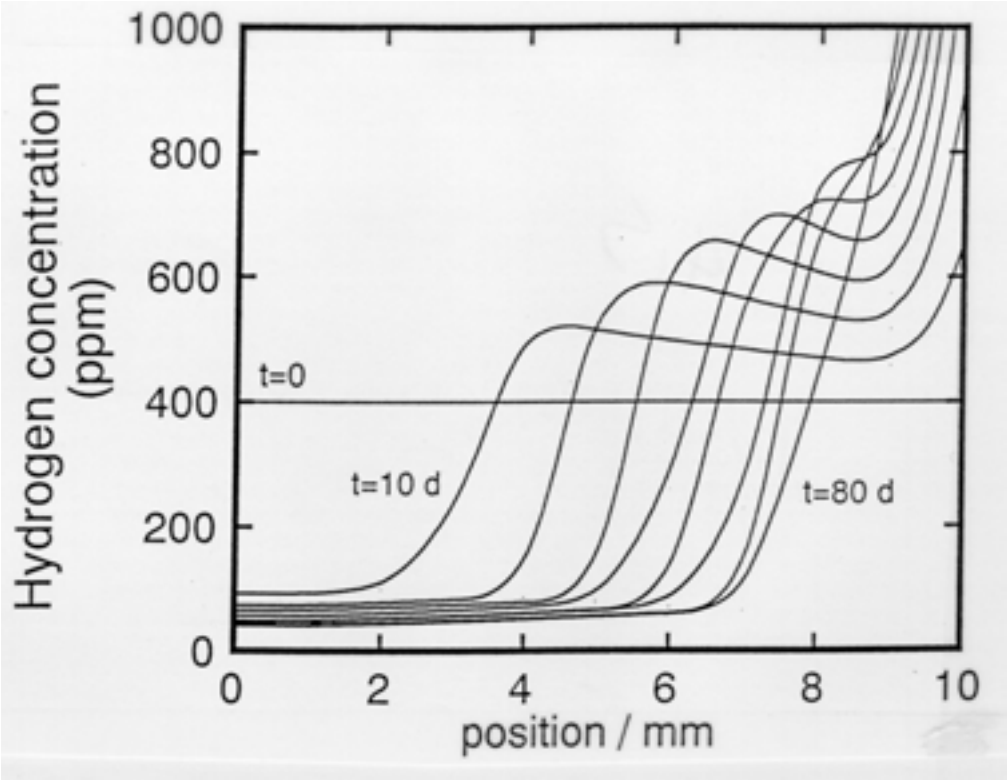

Figure 5. Change of hydrogen concentration distribution with time from thermomigration. Average temperature is 594°K, and the magnitude of thermal gradient is 80°K/cm.

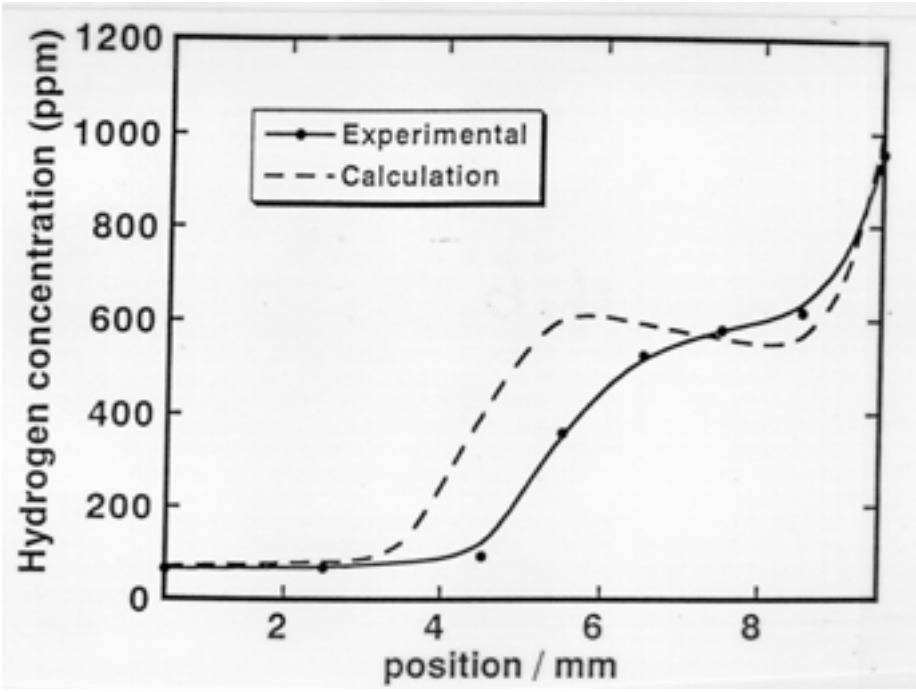

Figure 6. Comparison of experimental and theoretical hydrogen concentration distribution after 24 days of heat treatment for thermomigration. Average temperature is 594K and the magnitude of thermal gradient is 80K/cm.

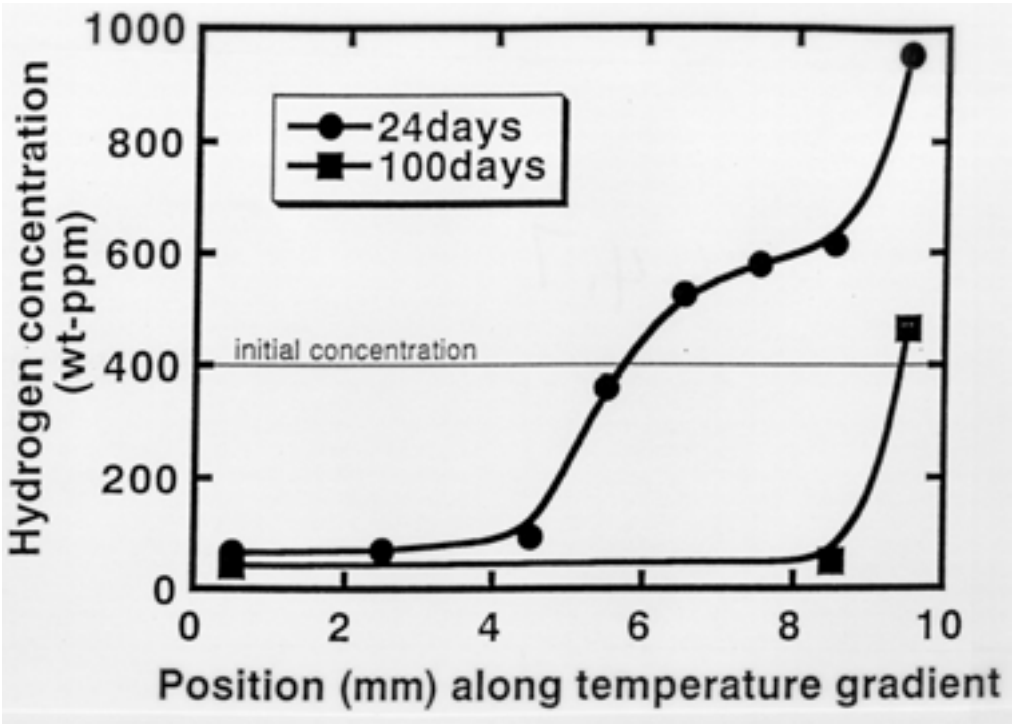

Figure 7. Experimental hydrogen concentration distribution after 24 and 100 days of heat treatment of thermomigration. Average temperature is 594K and the magnitude of thermal gradient is 80K/cm.

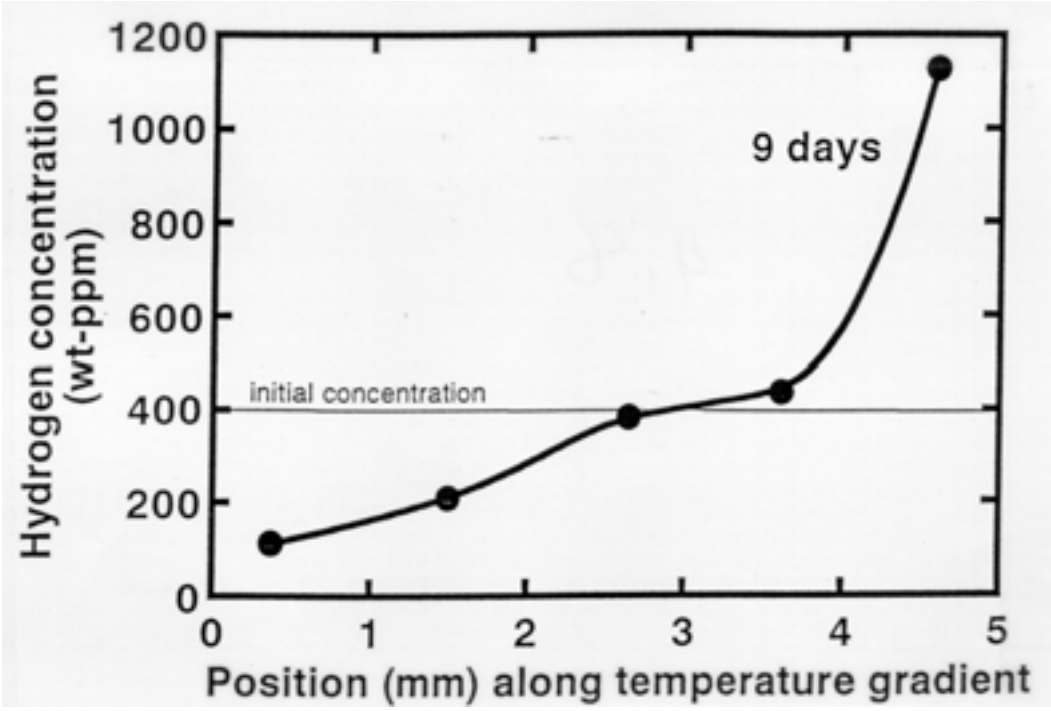

Figure 8. Experimental hydrogen concentration distribution in Type-B specimen after 9 days of heat treatment for thermomigration. Average temperature is 594K and the magnitude of thermal gradient is 80K/cm.

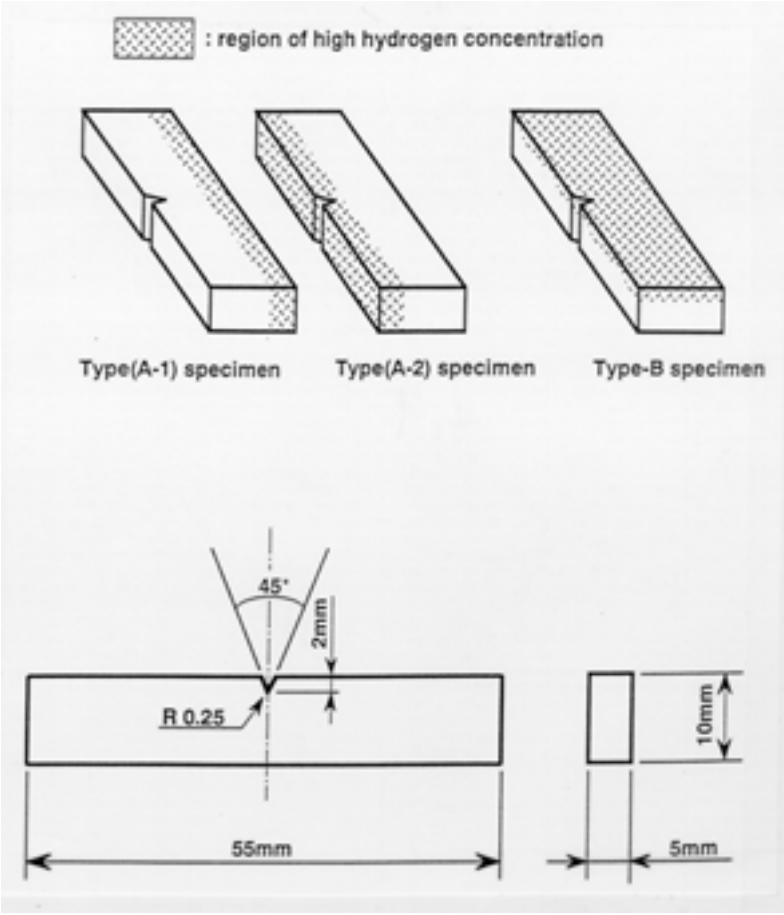

Figure 9. Relation between notch position and hydrogen concentration distribution.

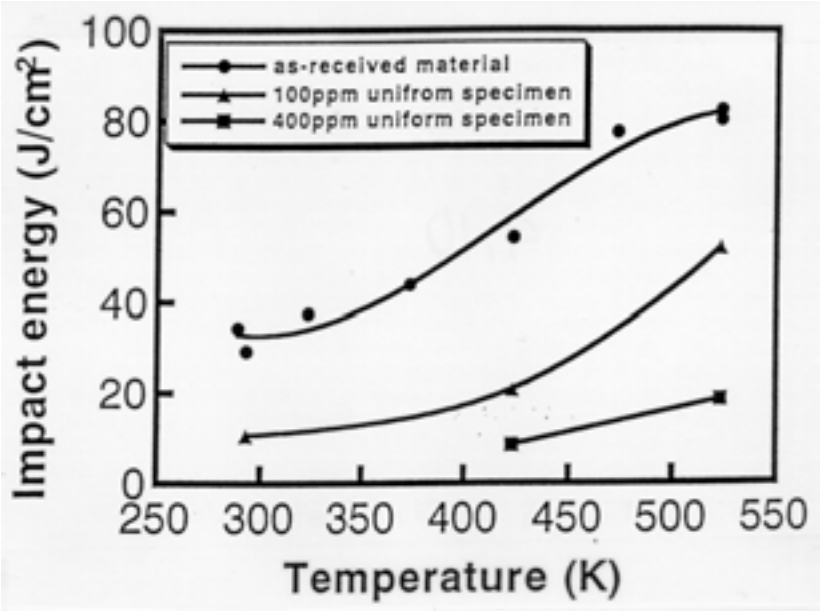

Figure 10. Experimental data of Charpy impact test for specimens with uniform distribution of hydrogen.

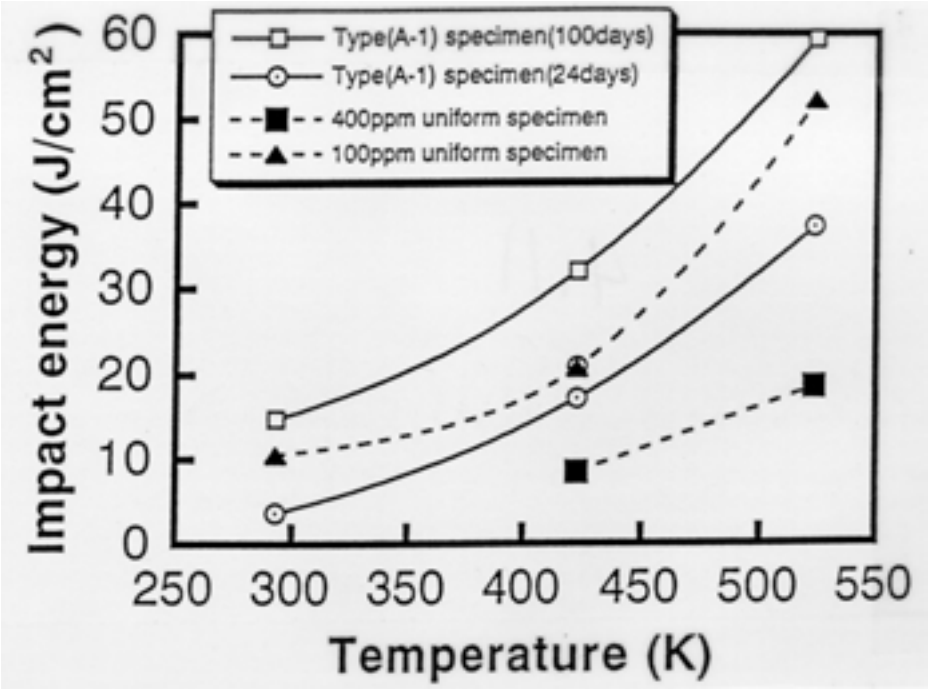

Figure 11. Experimental data of Charpy impact test for specimens with non-uniform distribution of hydrogen.

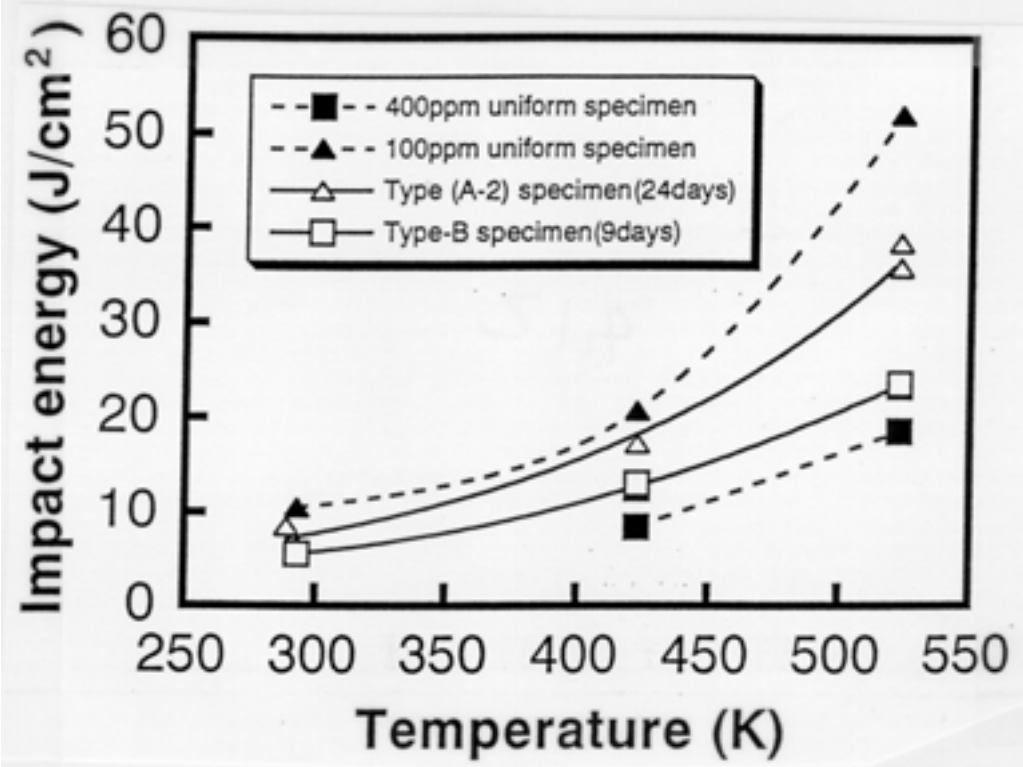

Figure 12. Experimental data of Charpy impact test for specimens with non-uniform distribution of hydrogen.

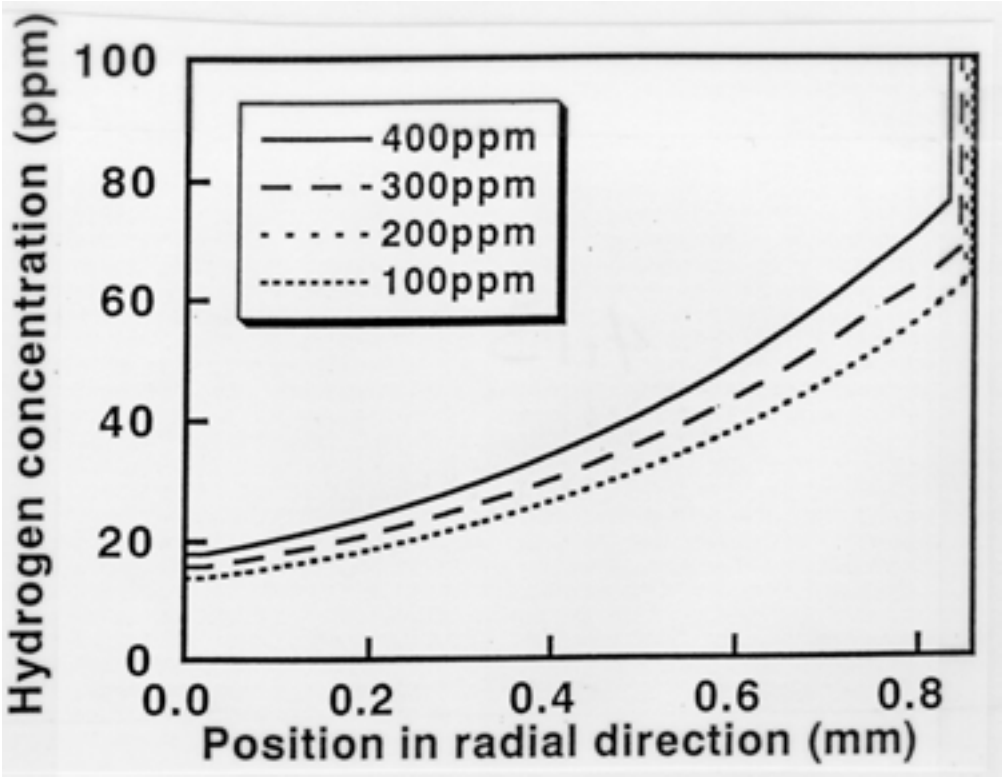

Figure 13. Hydrogen distribution in the radial direction.

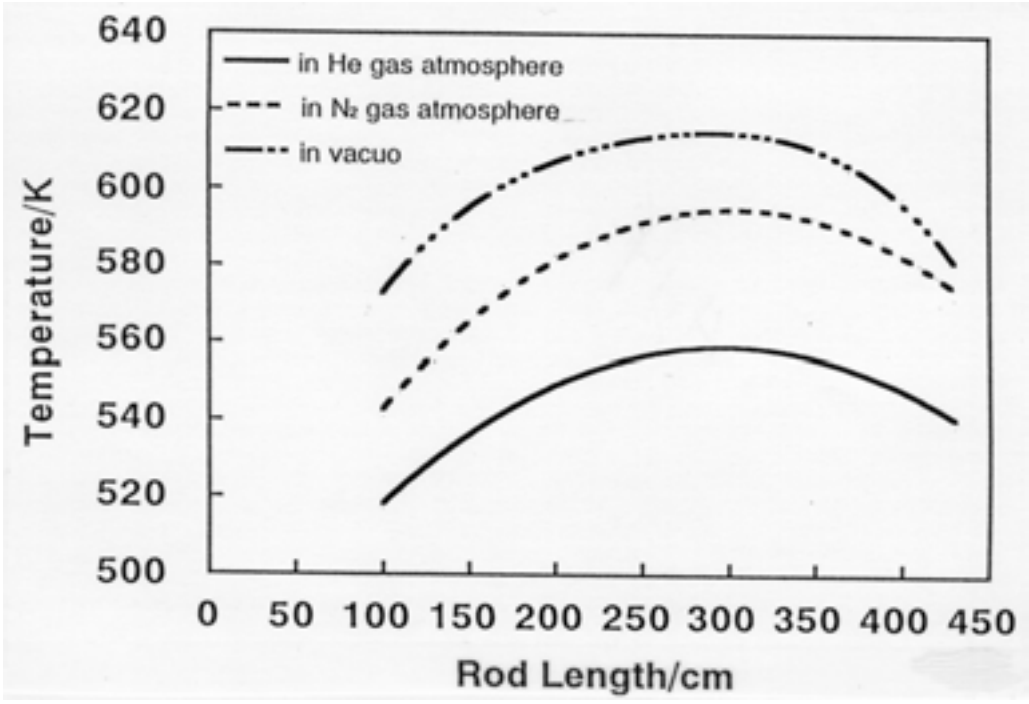

Figure 14. Example of temperature distribution in the cladding in several ambient gases. These data are cited from Figs. 3 to 8 in the references.

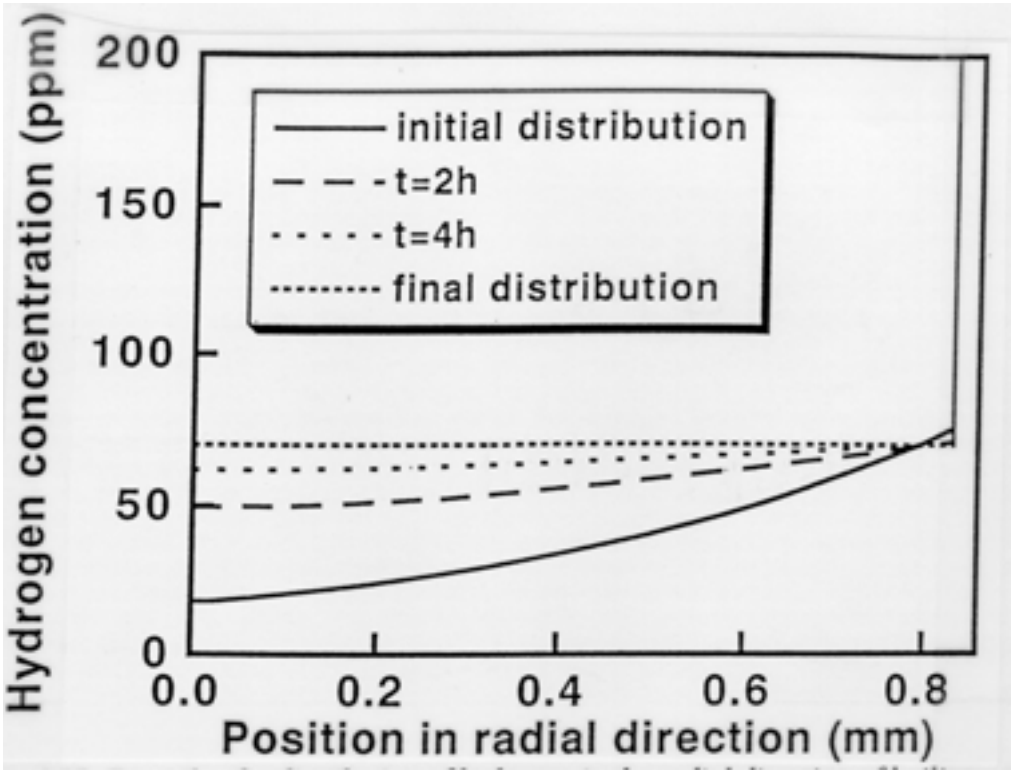

Figure 15. Example of redistribution of hydrogen in the radial direction of boiling water reactor cladding at 573K.

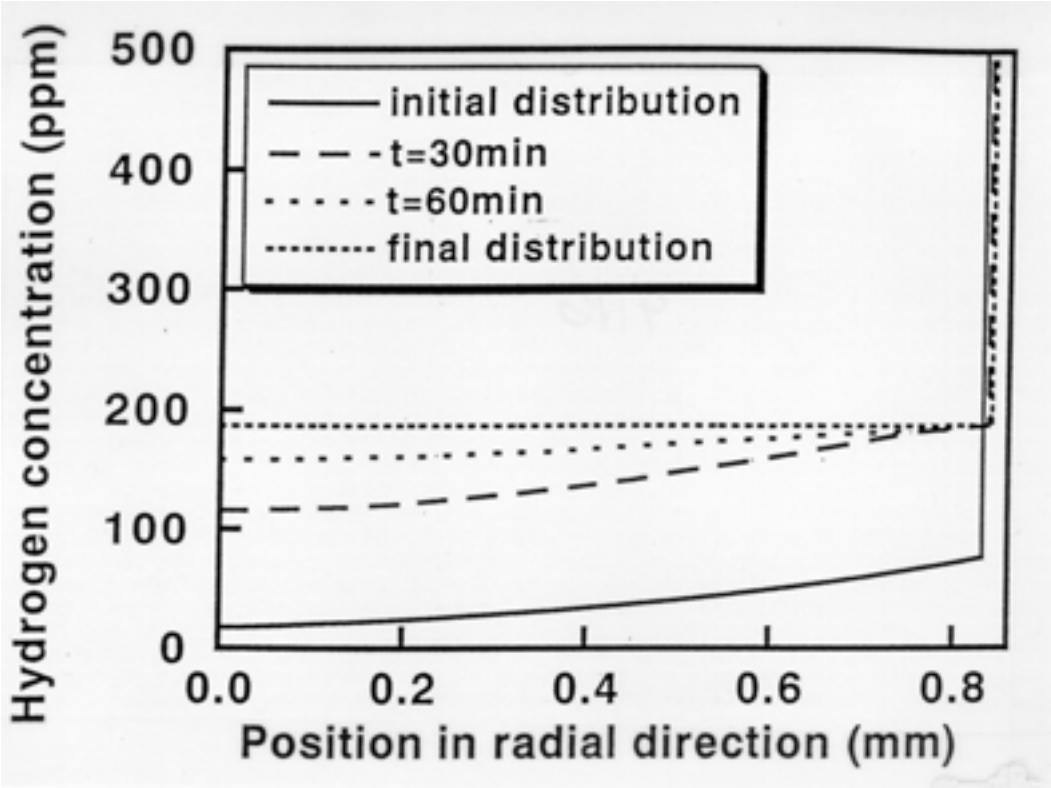

Figure 16. Example of redistribution of hydrogen in the radial direction of boiling water reactor cladding at 673K.

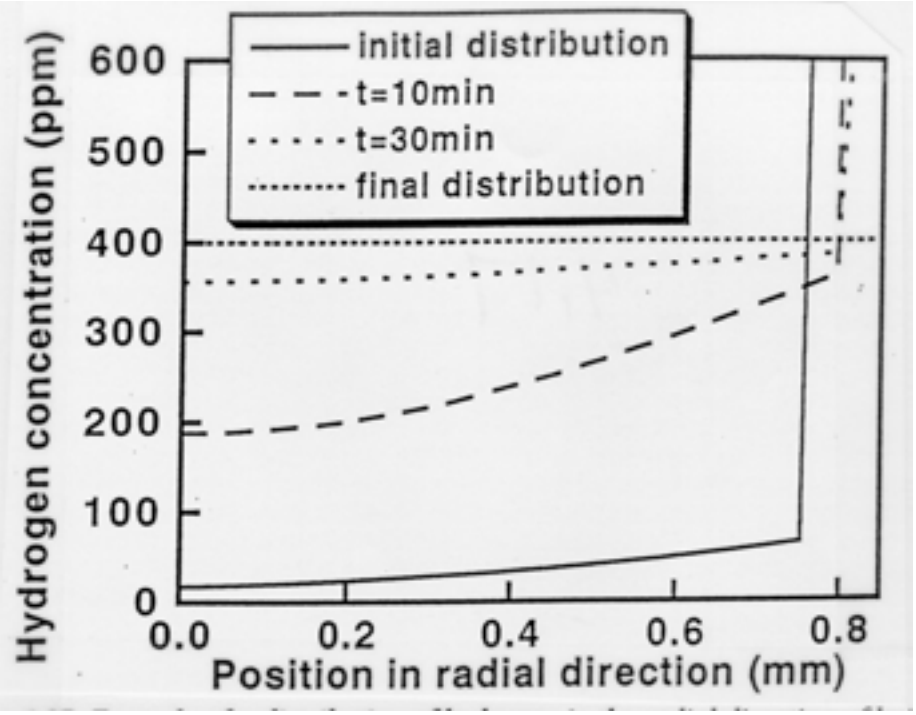

Figure 17. Example of redistribution of hydrogen in the radial direction of boiling water reactor cladding at 753K.

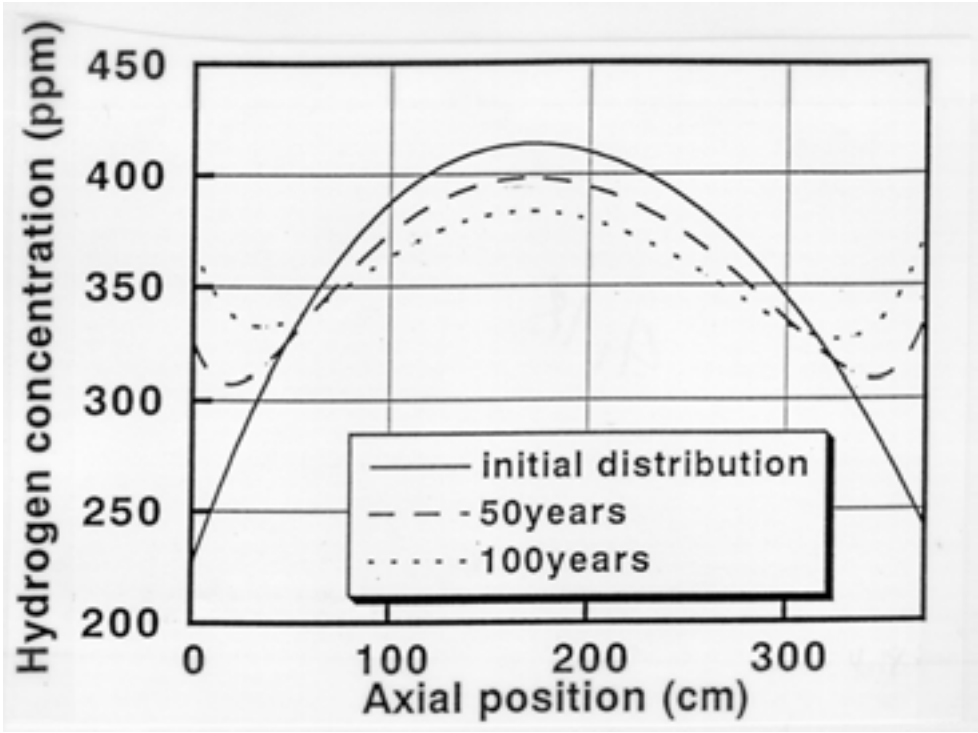

Figure 18. Example of redistribution of hydrogen in the longitudinal direction of boiling water reactor cladding during dry storage.

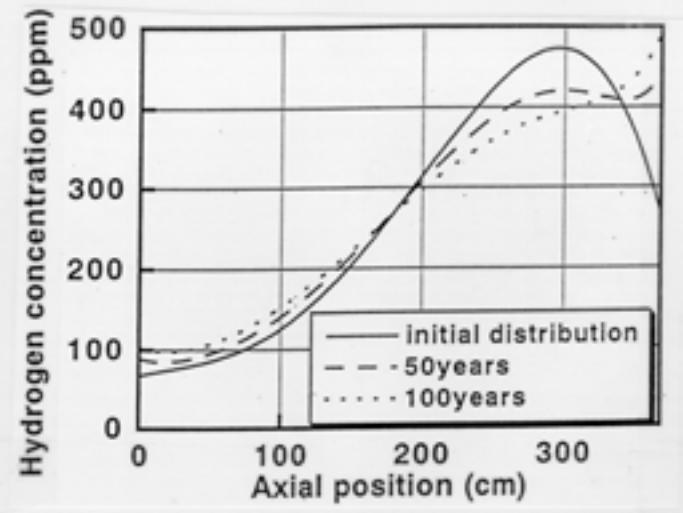

Figure 19. Example of redistribution of hydrogen in the longitudinal direction of pressurized water reactor cladding during dry storage

Table 2. Summary of Data of Charpy Impact Test

specimen	temperature (℃)	impact energy (J/cm²)
as-received material	RT	29. 2
〃	〃	34. 3
〃	50	37. 4
〃	100	43. 9
〃	150	54. 3
〃	200	77. 3
〃	250	82. 1
100wt-ppm uniform specimen	RT	10. 5
〃	150	20. 6
〃	250	52. 0
400wt-ppm uniform specimen	150	8. 4
〃	250	18. 8
type(a-1) specimen 24 days	RT	3. 6
〃	150	17. 1
〃	〃	20. 8
〃	250	37. 1
type(a-1) specimen 100 days	RT	14. 8
〃	150	31. 9
〃	250	59. 3
type(a-2) specimen 24 days	RT	8. 5
〃	〃	6. 4
〃	150	17. 2
〃	250	38. 3
〃	250	35. 7
type(b) specimen 9 days	RT	5. 6
〃	150	12. 5
〃	〃	13. 0
〃	250	23. 3
〃	〃	23. 5

REFERENCES

[1] BLACKBURN, D.E., et al., Maximum Allowable Temperature for Storage of Spent Nuclear Reactor Fuel, HEDL-TME-78-37, Hanford Engineering Development Laboratory (1978).

[2] EINZIGER, R.E., et al., High temperature postirradiation materials performance of spent pressurized water reactor fuel rods under dry storage conditions, Nucl. Technol. **57** (1982) 65.

[3] JOHNSON, A.B., Jr., and GILBERT, E.R., Technical Basis for Storage of Zircaloy-Clad Spent Fuel in Inert Gases, PNL-4835, Pacific Northwest National Laboratory, Richland, Washington (1983).

[4] PEEHS, M., and FLEISH, J., LWR spent fuel storage behavior, J. Nucl. Mater. **13** (1986) 190.

[5] CHIN, B.A., et al. Deformation and Fracture Map Methodology for Predicting Cladding Behavior During Dry Storage, PNL-5998, Pacific Northwest National Laboratory, Richland (1986).

[6] LEVY, I.S., et al., Recommended Temperature Limits for Dry Storage of Spent Light Water Reactor Zircaloy-Clad Fuel Rods in Inert Gas, PNL-6189, Pacific Northwest National Laboratory, Richland (1987).

[7] SAEGUSA, T., et al., Experimental studies on safety of dry cask storage technology of spent fuel: allowable temperature of cladding and integrity of cask under accidents, J. Nucl. Sci. Technol. **33** (1996) 250.

[8] YAMAKAWA, H., et al., Establishment of Cask Storage Method for Storing Spent Fuel: Evaluation on Heat Transmission Characteristic of Storage Cask, CRIEPI Rep. U92038, CRIEPI (1992).

[9] KERNS, J.J., Terminal solubility and partitioning of hydrogen in the alpha phase of Zr, Zry-2 and Zry-4, J. Nucl. Mater. **22** (1967) 292.

[10] SAWATZKY, A., Hydrogen in Zircaloy-2; its distribution and heat of transport, J. Nucl. Mater. **2** (1960)321.

[11] MARKOWITZ, J.M., The thermal diffusion of hydrogen in alpha-delta Zircaloy-2, Trans. Met. Soc. AIME, **221** (1961) 819.

[12] SAWATZKY, A., and VOG, E., Mathematics of the thermal diffusion of hydrogen in Zircaloy-2, Trans. Met. Soc. AIME. **227** (1963) 917.

[13] SAWATZKY, A., The heat of transport of hydrogen in zirconium alloys, J. Nucl. Mater. **9** (1963) 364.

[14] SAWATZKY, A., and WILKINS, B.J.S., Hydrogen solubility in zirconium alloys determined by thermal diffusion, J. Nucl. Mater. **22** (1967) 304.

[15] MOROZUMI, S., et al., Effects of alloying elements and cold work on the redistribution of hydrogen in zirconium under a temperature gradient, J. Nucl. Mater. **33** (1969) 261.

[16] SUGISAKI, M., et al., Thermal diffusion of tritium and protium in alpha phase of zirconium, Fusion Technol. **14** (1988) 723.

[17] HASHIZUME, K., et al., Temperature dependence of heat of transport of hydrogen in zirconium, Defect and Diffusion Forum **95-98** (1993) 323.

[18] KEARNS, J.J., Dissolution kinetics of hydride platelets in Zircaloy-4, J. Nucl. Mater. **27** (1968) 64.

Behaviour of materials in spent fuel storage facilities

K. Agarwal, V. Kain, S. Anantharaman, E. Ramadasan, M. Chandra, C.K.K. Nair, A.K. Sengupta, H.R. Pimparkar, S.S. Shinde, P. Seetharamaiah

Bhabha Atomic Research Centre, Mumbai, India

Abstract. India participated in IAEA CRP on "Irradiation Enhanced Degradation of Materials in Spent Fuel Storage Facilities" during 1993-1996. The experimental programme included study of corrosion behaviour of fuel materials and materials of fuel storage facilities related to aluminium-clad fuel from research reactors and Zircaloy-clad power reactor fuel stored in spent-fuel storage facilities (SFSF). An attempt was also made to study the behaviour of spent fuel during dry storage. This paper highlights the results of various coupon studies, electrochemical potential experiments, metallurgical examination of a SS tray used for PHWR fuel storage, pitting behaviour of materials in chloride environments, out-of-pile fuel-clad compatibility tests using SIM fuel in dry storage, and estimation of microbial species in pools.

1. Introduction

Nuclear fuels are used in reactors to generate energy using different types of fuels. While in India CANDU-type PHWR using natural UO_2 fuel clad with Zircaloy-2 are the mainstay of nuclear power programme (apart from two BWRs),other countries use PWRs and BWRs also, which use enriched UO_2 fuel clad with Zircaloy-2/Zircaloy-4. In addition to these, AGR using UO_2 fuel clad in SS and Magnox reactors using metallic uranium fuel clad with magnesium alloy are also used in some countries. A large number of research reactors use aluminium-uranium intermetallic, oxide dispersion, or metallic uranium fuel and are generally clad with aluminium alloys. In India, the research reactors CIRUS and DHRUVA use metallic uranium fuel and high-purity aluminium, Alloy 1S, for fuel cladding.

After a certain level of burnup, the fuel is removed from the power/research reactors and placed in wet storage. Typical burnup levels are about 40,000 to 60,000 MWd/t of uranium for PWRs and about 20,000 to 50,000 MWd/t of uranium for BWRs. The CANDU-type PHWRs have a typical burnup level of about 7000 MWd/t of uranium. Spent fuels are stored in at-reactor (AR) storage pools for a few months and then transferred to away-from-reactor (AFR) wet/dry storage facilities, where the fuel is stored until subjected to reprocessing or permanent disposal. The predominant mode of storage is wet storage. For the purpose of this study, two SFSFs, namely Trombay Pool and Tarapur Pool, have been used. The Trombay Pool stores metallic uranium fuel clad with aluminium 1-S from research reactors, whereas the Tarapur Pool stores Zircaloy-clad natural UO_2 fuel from power reactors.

The SFSFs use demineralized water, and the capacities of the pools vary with anticipated requirements from site to site. Generally, continuous on-line ion exchange columns are used for water purification to keep the specific conductivity of the water less than 1 to 5 μS/cm. The pools are designed to provide cooling by heat exchangers, if the temperature exceeds about 40^{o}C. These pools are built in covered buildings with suitable ventilation systems. The spent fuels are stored either in aluminium or SS racks. The pool walls and floor are made of concrete and in some of the cases are lined with Type 304/304 L SS. The other hardware and utilities used in fuel pools are also made of SS (e.g., piping, lighting, fuel grapplers, and cask impact pads).

2. General and localized corrosion

Nuclear fuels are stored under water after they are burned in the reactor to produce power. This storage lasts until they are reprocessed or their decay heat allows them to be transferred to dry storage facilities. Corrosion has been identified as one of the factors that decides the life of the SFSF and also of the fuel stored within. The possible corrosion processes are general corrosion, crevice corrosion, pitting corrosion, and stress corrosion. The materials of concern to India are:

- fuel

    (a) Zircaloy-2-clad UO_2
    (b) aluminium-1S-clad uranium metal.

- fuel-handling tools made of Type 304 SS.

- fuel pool liners made of welded Type SS 304L plates. These are welded onto the mild steel framework embedded in concrete.

- services such as piping, ion exchanger, and ventilation ducts.

Under this programme, experiments were initiated to assess the corrosion and condition of the fuel stored in pools.

2.1. Uniform corrosion (general corrosion)

To measure the extent of general corrosion in SFSFs, corrosion coupons of different materials were made and assembled in racks. These racks were made and assembled according to the procedure given in ASTM standard G1-72.

The six racks for corrosion coupons, represented in Fig. 1, were fabricated. The racks were made, weighed, and assembled, using Teflon spacers for insulating coupons. The coupon racks were installed in Trombay and Tarapur Pools at a depth of about 1.5 m and about 1.5 m away from the wall during the beginning of 1995 (maximum radiation levels, 1000 R/h). The coupons were made of 1S-Al, 57-S Al, Zircaloy-2, Type 304 SS, Type 304L SS, and Type 304L SS welded. Five of each type of coupon were provided in one rack. The six racks are installed for studies after 1, 3, and 10 years of residence in pool water (2 racks withdrawn at the end of each exposure period). One set of racks was installed near stored fuels and the other set away from the fuel to compare the corrosion effect with and without radiation. The racks are identified as A, B, C, D, E, and F. The corrosion racks A and B were removed after 1 year, and racks E and F were removed after 3 years. Coupons were cleaned and weighed.

The specimens were subjected to visual examination using a stereomicroscope up to a magnification of 400X and weighed using a semi-micro balance. Selected samples were subjected to evaluation of pit depth and pit density, using a metallurgical microscope, at a magnification up to 1000X. Some of the coupons were cut into two halves to observe the depth of corrosion attack. Afterwards, the two halves were kept together and photographed. Fig. 2 shows adjacent sections, both on the flat face and in cross section.

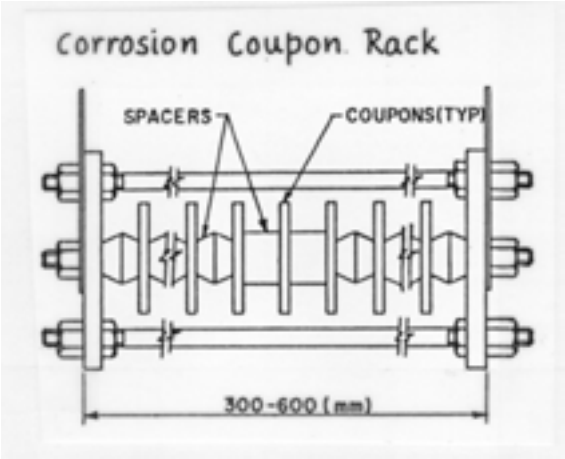

Figure 1. Assembly of corrosion coupons.

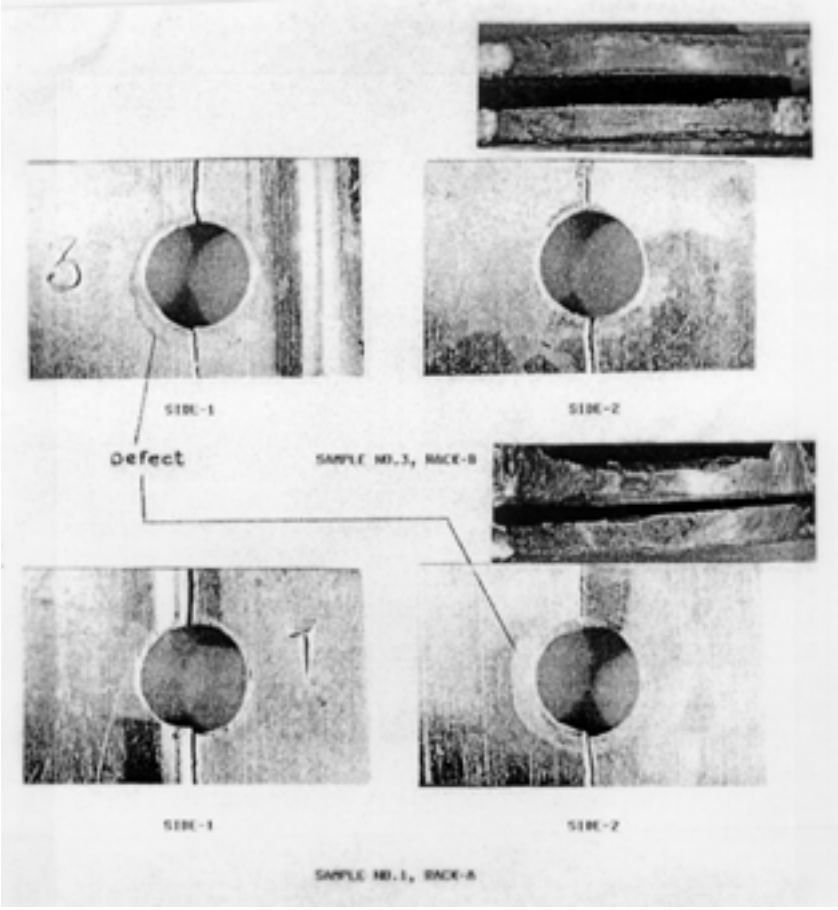

Figure 2. Damage at the edge of the hole in the aluminium corrosion coupons from the test racks and their cross sections at the midpoint.

2.1.1. Results

Visual examination revealed that the anodized aluminium coupons had light pitting sparsely distributed, with shallow pits on the concave as well as the convex side of the coupon. The average pit density was 1348/cm^2. The pit depth varied from 4 to 12 μm. Pit diameter varied from 10 to 40 μm.

The as-fabricated (non-anodized) material, however, revealed evidence of severe corrosion. There was deep and severe pitting, with the pits joining together to form deep corrosion patches. Because the pits were coalesced and large, pit density was not estimated. There were white and powdery corrosion products covering the coupon surfaces. The pit depths varied from 20 to 40 μm. The details are given in Fig 2.

Visual examination showed negligible corrosion on Zircaloy-2 after 3 years in the SFSPs. The surfaces were bright and had no deposits. The weight losses were less than 0.04%, indicating corrosion rates of 2.5 x 10^{-5} to 2.5 x 10^{-4} mpy (1 mpy = 25.4 μm/y).

Visual examination showed negligible corrosion effects on the coupons of Type 304 SS and Type 304L SS plates. Weight changes were positive, but negligible, in the range of 1.1 x 10^{-5} to 3.1 x 10^{-5} mpy for Type 304, and the Type 304L coupons showed corrosion rates of 5.7 x 10^{-6} to 2.2 x 10^{-5} mpy, which are negligible.

The welded Type 304 SS coupons were also seen to have undergone negligible, visible, corrosion damage. There was a patch with a bluish-brown colour, typical of an oxidized region, adjoining the weld bead; this patch appeared to be the result of the fabrication process. The weight changes indicated very low negative change (average 0.009%), indicating a corrosion rate of +5.2 x 10^{-7} to –5.75 x 10^{-5} mpy, which is insignificant.

Conclusions are as follows:

(1) The aluminium crevice corrosion coupons have shown severe pitting corrosion on either surface after 3 years inside the pools.

(2) The as-received material has shown more severe pitting than the anodized material under identical conditions of exposure.

(3) The aluminium test coupons from the racks have shown a low but insignificant damage from corrosion at the edge of the hole. There is no appreciable effect from radiation, and the material of the spacer has not caused any detectable damage.

2.2. Crevice corrosion (crevice bent beam method)

To study the crevice corrosion of materials in SFSFs (e.g., storage trays and liners), the standard type of CBB specimens were prepared, autoclaved, installed in the holders, and placed inside the fuel pools at Trombay and Tarapur in early 1995 at various locations (near fuel and away from fuel). The specimens of aluminium, Zircaloy, and SS in as-received and autoclaved conditions were used. The details of the assembly are given in Fig. 3.

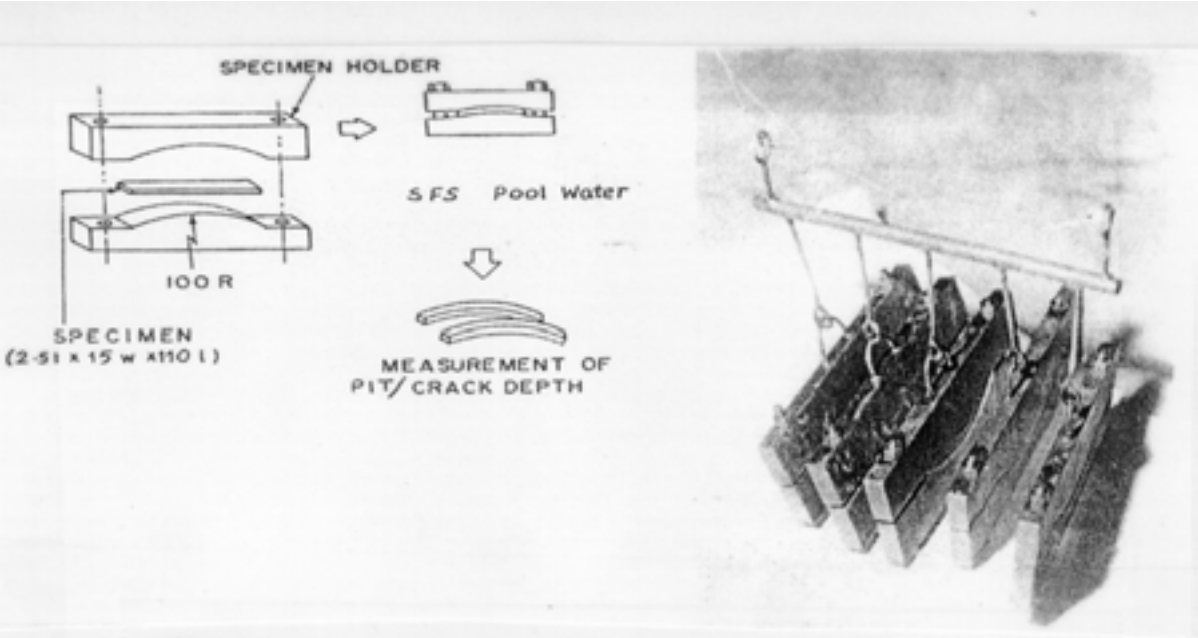

Figure 3. Crevice bent beam test assembly.

The samples in each CBB holder are as follows:

A. aluminium-IS (finished with 120 grit emery paper)
B. aluminium-IS (autoclaved at 150^{o} C for 12 days)
C. Zircaloy-2 (as received)
D. Zircaloy-2 (autoclaved at 400^{o}C in steam for 3 days)
E. Type 304L SS (as received)
F. Type 304 SS (sensitized).

2.2.1. pH measurement

The pH of samples of CBB assemblies at the crevice locations was measured after every 2 months and was found to decrease drastically from 5.5 to 2 to 3 in 6 months. This change suggests that crevice effects were active.

2.2.2. Visual observations

The samples were removed and examined periodically using an optical stereomicroscope up to 400X. There was severe pitting in aluminium samples after 6 months, but Zircaloy and SS samples did not show any pitting during the same period. The photographs given in Figs. 4 through 5.6 show the surface conditions of the exposed strip samples and some of the pit profiles.

2.2.3. Conclusion

This experiment illustrates that, in storage pool conditions, the water chemistry inside the crevice plays an important role in corrosion behaviour of materials and is different from water chemistry of the pool. The Trombay Pool stores aluminium-clad fuel from research reactors, so the crevice may operate between the fuel-clad surface and the storage rack and may

endanger the cladding and fuel. The other interpretation of results shows that autoclaved aluminium was more resistant to localized corrosion than the emery-polished aluminium sample. But possibly the galvanic couple of aluminium with the SS holder might have accelerated the localized corrosion.

2.3. Potential measurements in spent-fuel storage ponds

Electrochemical potential (ECP) is an important parameter that indicates the combined effects of various chemical constituents and the environment: temperature, pH, and surface films on the materials (which form in the particular operating conditions). A particular material-environment would always give rise to a particular potential, and conductive solutions result in stable values of potential. Potential is measured with respect to a reference electrode, e.g., saturated calomel electrode (SCE), and its units are mV. To illustrate the significance of potential vis-a-vis corrosion, two experiments (i.e., in situ and out-of-pool) measured potential. Proper precaution has been taken to avoid Cl^- contamination of the pool water from immersion of the SCE.

2.3.1. In situ potential measurements

The ECP was measured in the spent-fuel storage pool at Trombay using as-received samples of Type 304 SS, aluminium-1S, and Zircaloy-2. The reference electrode used was SCE, and the sample was kept at a fixed distance of 25 mm from the electrode. The ECP was measured with a digital multimeter having high input impedance. ECPs were measured at the depths of 1 and 5 m. The measured potentials are listed in the Table 1. The potential of aluminium is in the positive values in contrast to (-)500 to(-)1000 mV (SCE) generally reported in literature. The experimental set up is given in Fig. 7.

TABLE 1. IN SITU ELECTROCHEMICAL POTENTIAL MEASUREMENTS ON ALUMINIUM, ZIRCALOY-2, AND TYPE 304 STAINLESS STEEL IN THE TROMBAY POOL

Rack No.	Time (h) (Cumulative)	Potential, mV (SCE)					
		Al		Zircaloy- 2		Type 304 SS	
		Top	Near Fuel	Top	Near Fuel	Top	Near Fuel
1.	Upon immersion	107	160	-35 to -40	-110	-115	49
2.	24	312	115	-40	-124	-	-
3.	27	-	-	-50	-78	-	-
4.	48	382	280	-	-	-	-
5.	51	255	185	-	-	-	-
6.	100	-	-	-	-	-	-5 to -10

2.3.2. Out-of-pool potential measurements

The SFSFs contain demineralized (DM) water, which has very low conductivity. The pool water has a near-neutral pH (6.0) at ambient temperature. The polished samples (up to 120-grit emery papers) were cleaned in distilled water and dried. The ECP was measured by immersing the samples and the reference electrode in pool water. Potentials were measured soon after immersion in the solution and then after 5 minutes. Water from various locations was used from Trombay and Tarapur pools. The measured potential values are given in Table 2.

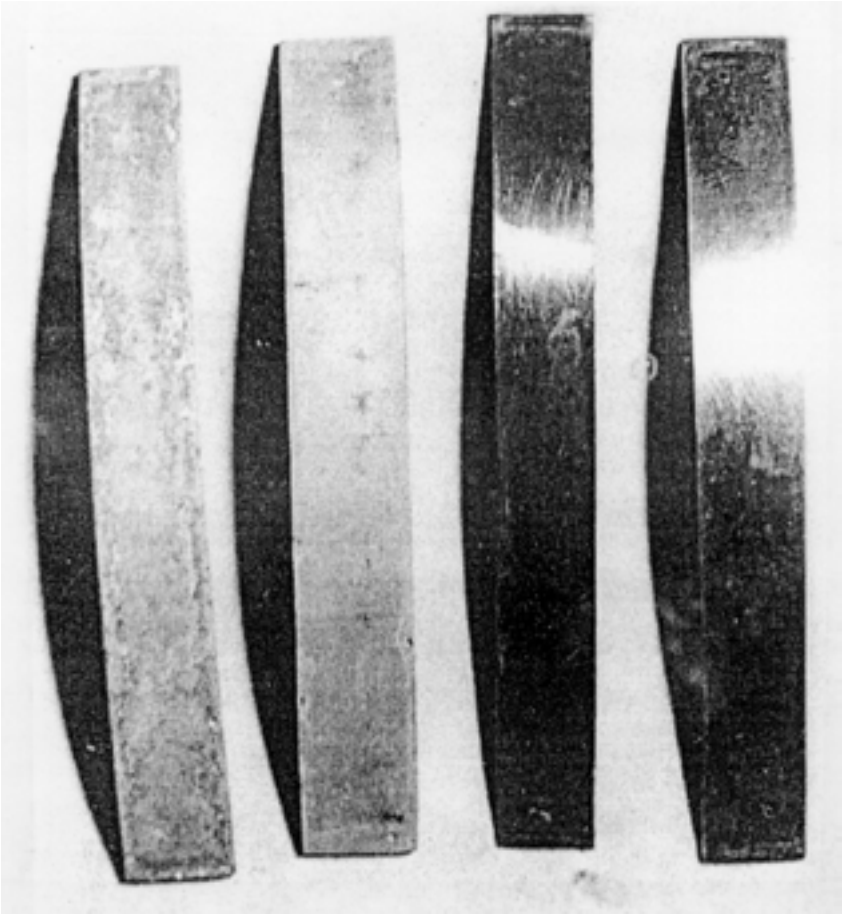

Figure 4. Photographs of aluminium as-received, aluminium oxidized, Zircaloy-2, and stainless steel samples after 1 year of crevice bent beam studies.

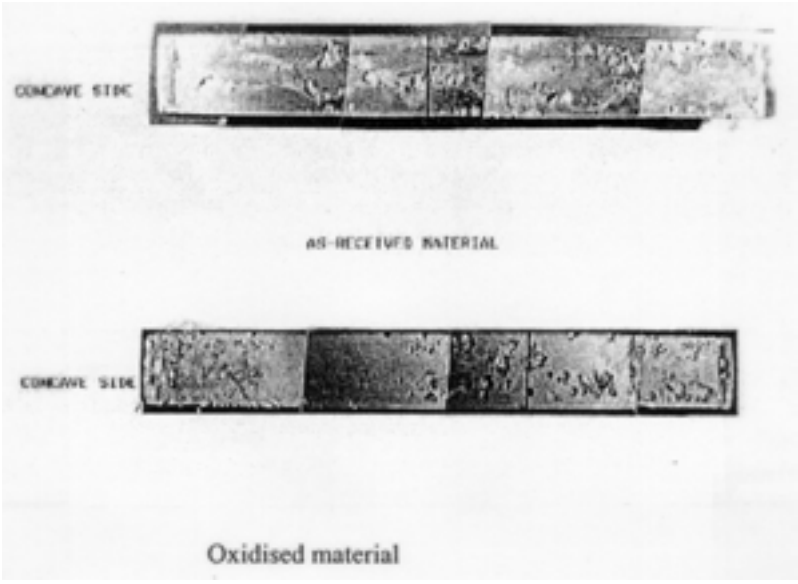

Figure 5. Stereo-photomicrographs of the surfaces of aluminium strips tested for crevice corrosion.

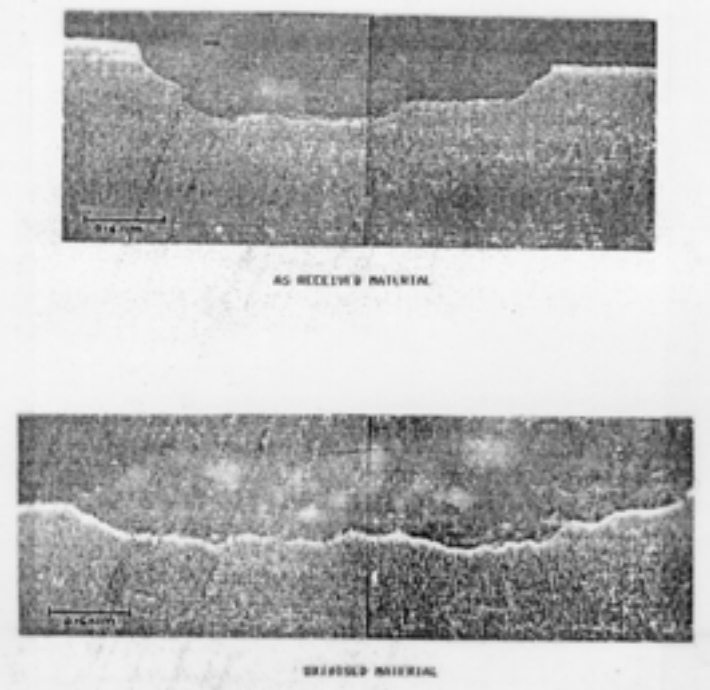

Figure 6. Profiles of the pits on the aluminium strips.

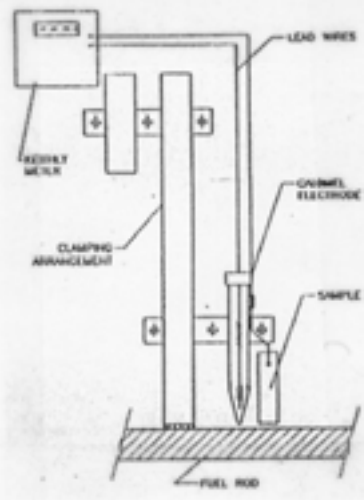

Figure 7. Set up for in situ electrochemical potential measurements.

TABLE 2. ELECTROCHEMICAL POTENTIAL MEASUREMENT RESULTS

RACK NO.	Materials and heat treatments	ECP (mV vs. SCE) in water from Tarapur Pool		ECP (mV vs. SCE) in water from Trombay Pool	
		Instantaneous value	5 min after immersion	Instantaneous value	5 min after immersion
1.	Type 304L SS Annealed	-225 to -240	-170 to -175	-230 to –255	-175 to -190
2	Type 304L SS Sensitized	-215 to -240	-165 to -175	-225 to –255	-170 to -185
3.	Type 304 SS Annealed	-230 to -250	-170 to -185	-200 to –275	-170 to -190
4.	Type 304 SS Sensitized	-230 to -235	-175 to -190	-175 to –255	-170 to -190
5.	Zircaloy - 2	-210 to -245	-170 to -185	-210 to –250	-170 to -195
6.	Aluminium	-960 to -1000	-810 to -840	-860 to -1000	-700 to -810

In addition, potential was measured for sensitized Type 304 SS samples in distilled water in the laboratory. The potential was -225 mV (SCE) soon after immersion and -180 mV (SCE) after 5 minutes. This potential shifted to -75 mV (SCE) after immersion for 2 hours in distilled water. This difference indicates that in low-conductivity solutions, equilibrium is not achieved between the material surface and the ionic species present in the environment, and the rate of reaction is changing with time.

General corrosion rates of materials cannot be determined by ECP measurements alone because of various extraneous factors such as oxide films. However, noise analysis in ECP or current values (electrochemical potential noise--EPN/ electrochemical current noise--ECN) can provide a good correlation with corrosion. In this study, only ECP measurements were attempted, with the intention of incorporating EPN/ECN in future.

2.4. Water Analysis

Typical chemical analyses of water samples from the Tarapur and Trombay pools are given in Table 3 from various locations in the pools. The pH, iron, chromium, nickel, and conductivity values are close to each other in the two pools except for specific activity from the different fuel types stored in the two pools. The chloride concentrations are also higher at middle locations in the pools.

3. Post-irradiation examination studies on spent-fuel

To find the effect of wet storage on spent fuel, PIE results of over 200 fuel elements carried out in the past 20 years were reviewed. These elements comprised:

- BWR fuel elements
- PHWR fuel elements
- experimental fuels irradiated in a pressurized water loop of a research reactor
- metallic uranium fuel elements from research reactors.

TABLE 3. RESULTS OF ANALYSIS OF POOL WATER SAMPLES FROM TARAPUR AND TROMBAY POOLS

Location	α activity (dps/5ml)	γ activity (dps/5ml)*	pH	Cl^- (μg/ml)	Sp. cond. (μs/cm)	Fe (μg/ml)	Cr (μg/ml)	Ni (μg/ml)	Zry (μg/ml) #
Tarapur Pool									
Centre bottom	-	< 50	5.53	0.94	7.35	0.26	2.7	0.04	18.8
Southeast corner bottom	7	< 50	5.75	0.48	3.43	0.20	2.7	0.04	0.2
Centre middle	20	< 50	5.68	2.40	13.25	0.21	2.7	0.04	17.6
Centre top	22	< 50	5.49	0.43	3.71	0.20	2.7	0.04	15.6
Trombay Pool									
Centre top	-	< 50	5.80	0.37	3.68	0.32	3.6	0.07	--
Corner bottom	5	430	5.93	0.20	2.67	0.17	2.5	0.03	--
Centre middle	81	580	5.80	0.68	4.11	0.23	2.8	0.04	--
Centre bottom	352	315	5.95	0.28	3.47	0.35	3.8	0.07	--

* Only fission product activity detected was from ^{137}Cs.
# Tarapur pool stores zircaloy-clad power reactor fuel; Trombay pool stores aluminum-clad metallic fuel from research reactor

TABLE 4. SUMMARY OF POST-IRRADIATION EXAMINATION FINDINGS

RACK NO.	Type of fuel	Number examined	Cause of failure
1.	Experimental Zry-2-clad UO_2	5	Faulty hanger rod design; clad abrasion led to leaks
2.	Experimental Zry-2-clad MOX	1	High moisture content in fuel pellets
3.	EXPERIMENTAL ZRY-2-CLAD MOX CLUSTERS	4	No failure
4.	Power Reactor BWR, Zry-2-clad UO_2	18	(i) hydriding at end plug-weld region, (ii) PCI, (iii) SCC, and (iv) fretting
5.	Power Reactor PHWR, Zry-2-clad UO_2	3 bundles, 57 elements	(i) fretting, (ii) end plug-weld failure, and (iii) primary hydriding
6.	Research Reactor DHRUVA, both prototype and actual Al-1S-clad U metal	140 elements	Non-uniform growth/ shrinkage, bowing, blistering, vibration wear, and fretting

The fuels comprised different categories of material, dimensions, and burnups (e.g., mixed oxides--MOX clad in Zircaloy-2, UO_2 clad in Zircaloy-2, uranium metal clad in aluminium). Types of cladding failures included pellet-clad interaction (PCI)/SCC, fretting, and hydriding in Zircaloy-2 cladding. However, all could be attributed to reactor service. These elements could be handled and transported in the defected condition and could withstand the associated strains. The summary of the PIE findings is given in Table 4.

4. Stress corrosion cracking

The following observations are important to evaluate the possibility of SCC of Zircaloy cladding during spent-fuel storage. First, in connection with dry storage of spent fuel, it has been demonstrated that cladding temperatures up to at least 400°C can be tolerated without SCC causing cladding breach. As long as the probability of in-reactor failure was <1%, which is the case for the vast majority of LWR fuel rods, >99% of the remaining unfailed fuel will enter the storage facility with incipient cracks <20% of clad-wall thickness. A model (SCCIG developed for the Electric Power Research Institute--EPRI) applied to dry storage conditions showing fail/no fail lines is shown in Fig. 2. With realistic iodine concentrations representative of the majority of rods (5×10^{-5} -----> 5×10^{-4} kg/m^2) and a 20% radial wall crack, Zircaloy cladding can be safely stored up to 1000 years, because these cracks would not propagate beyond 60% wall thickness in a 1000-year time frame.

Second, during wet storage, temperatures are much lower (ambient to 60°C, maximum), and crack propagation rates would still be lower. Therefore the 1000-year no-fail model is also applicable to wet storage. In addition, during wet storage, stresses would relax, because creep, more fission products, thermal expansion, and related factors contributing to stresses would not be present. Additional stresses imposed by power ramps also would not be available. Therefore, stresses to cause failure would not be available during wet storage. However, criticality accidents in storage, if they occur (which is a remote possibility), could provide conditions for SCC (i.e., chemistry, stress, and temperature). SFSFs are designed to preclude criticality events. Also, although significant radiation is available during initial storage periods, it is not likely to be sufficient to dissociate CsI to release free iodine to initiate

5. Metallurgical examination of an AISI type 304 stainless steel tray used to store spent pressurized heavy-water reactor fuel in tarapur pool for 10 years

AISI Type 304 SS trays have been in use for over 10 years in the Tarapur Pool for storing power reactor spent-fuel assemblies. To assess the performance of these trays and to evaluate their durability, one of the trays was removed for detailed metallurgical evaluation. These trays hold 11 fuel assemblies each and are stored in the pool in stacks of 20 trays. To assess the tray to the severest conditions in the pool, such as load on the tray and radiation dose, the tray at the bottom of one of the stacks, which had other stacks surrounding it, was chosen for examination.

The tray was thoroughly washed and decontaminated at the Tarapur facility and was cleaned of loose contamination. An unused tray of equal vintage was also chosen for detailed evaluation for the sake of comparison. The two trays were cut into smaller pieces, for ease of transportation and handling, for metallurgical examination. The pieces were chosen to provide the following regions:

- the weld region joining the channel and the stiffener
- the weld region joining the channel and the angles
- the angle with the weld region joining the spacer.

A macro view of the pieces put together is given in Fig. 8. The pieces were thoroughly cleaned, firstly using detergent and water and subsequently using acetone, then dried in hot air. The pieces were subjected to visual examination using the naked eye as well as under a stereomicroscope at higher magnifications.

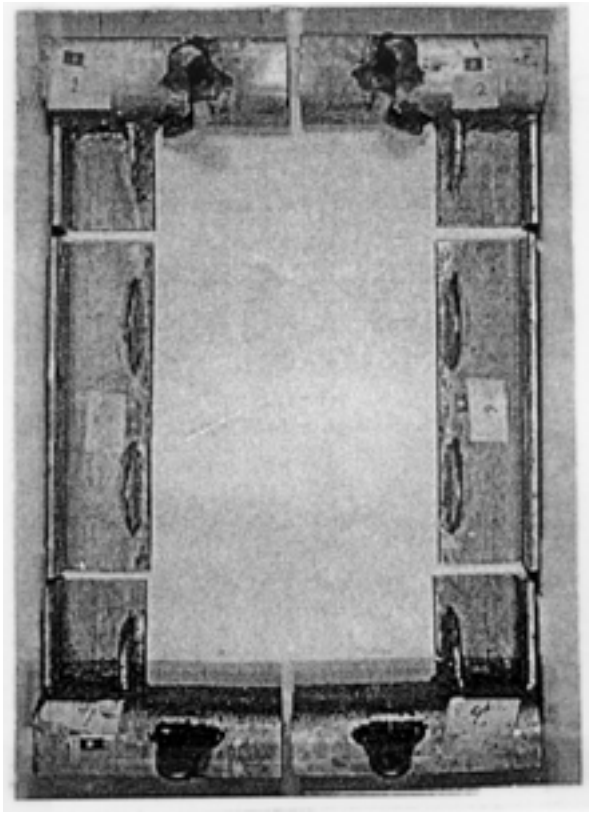

Figure 8. Macro view of the pieces cut from the used tray put together, indicating their positions.

5.1. Metallography

The metallographic specimens were selected carefully to include the weld regions having possibility of crevice formation and the sections of the surface of the angle portion that was in contact with the pool bottom surface. The specimens were mounted in Bakelite and prepared for metallographic examination by grinding, polishing, and electrolytic etching with oxalic acid to reveal the microstructure.

5.2. Results

Visual examination revealed that, whereas the unused tray material had a shining and uncorroded surface, the used tray had a dull surface, with evidences of pitting corrosion on the surface. The pits were light and sparsely distributed, generally on the surface. However, at and surrounding the weld regions (Fig. 9), the pit density was higher.

Microstructural details revealed that the pits were shallow and the depth was less than 150 μm. The pit density was more at and around the weld regions. The extent of pitting corrosion was not severe enough to affect the structural integrity of the tray. Though there are sharp crevices (Fig.10), there was no evidence of crevice corrosion in any of the weld regions. The heat-affected zones (HAZs) adjacent to the welds showed sensitization (Fig. 11) to some extent, but there was no evidence of IG attack, using the ASTM A-262 Practice A Test.

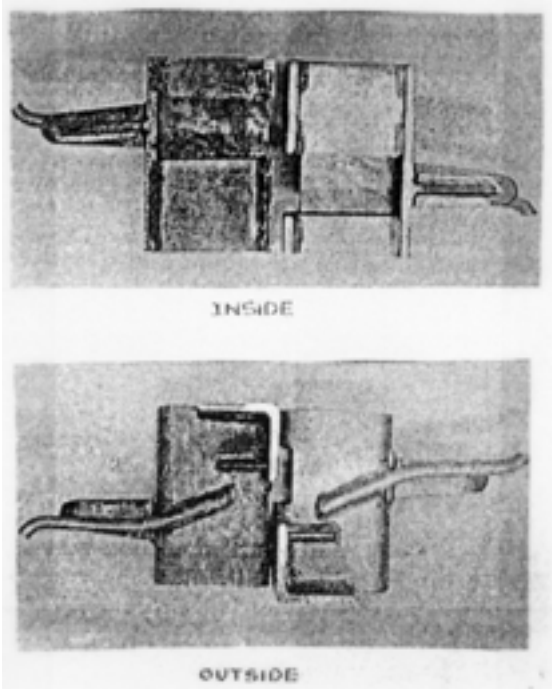

Figure 9. Weld and surrounding locations on the used tray (2), showing corrosion effects, and the unused tray (2a), showing the shiny surface.

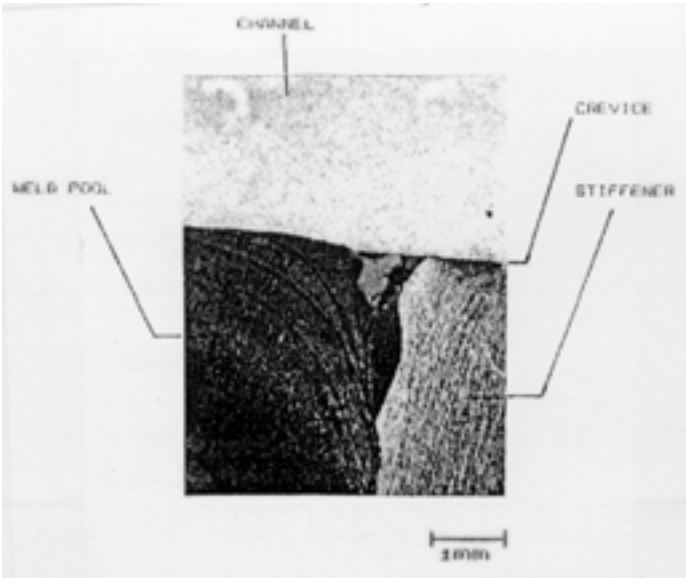

Figure 10. Microstructure of the weld and the crevice region of the stiffener weld, with no evidence of crevice corrosion.

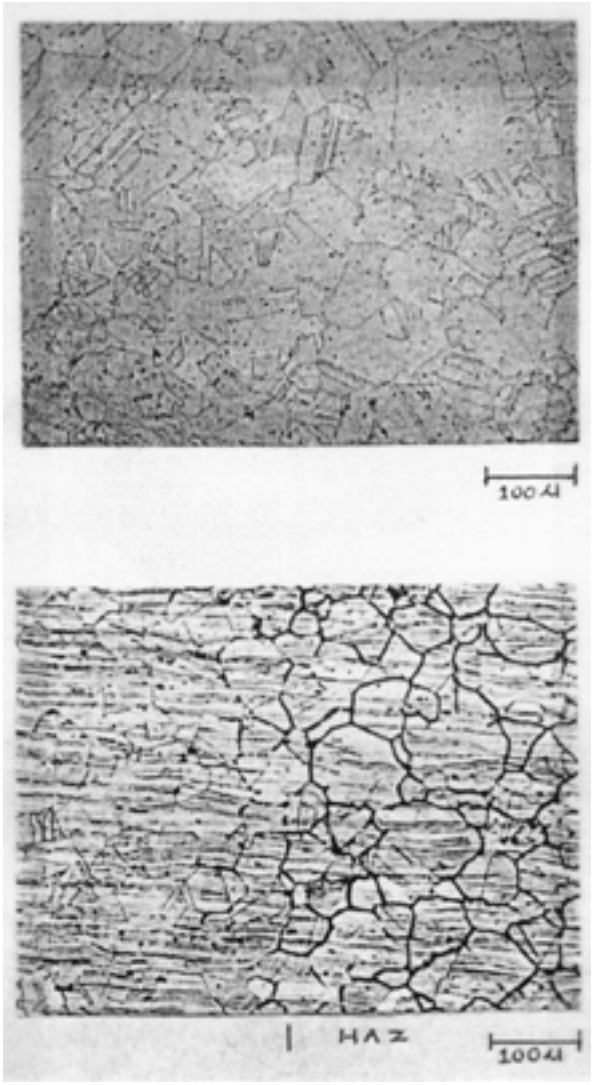

Figure 11. Microstructure of the stiffener: (a) general microstructure showing absence of sensitization away from the heat-affected zones (HAZs), (b) microstructure at HAZ showing sensitisation.

5.3. Conclusions

The AISI Type 304 SS tray, used for storage of spent power reactor fuel in the Tarapur Pool for over 10 years, showed the following characteristics:

- evidence of light and shallow pitting corrosion on the surface, with the pit density increasing around the HAZs. The severity of pitting was not detrimental enough to affect the structural integrity of the tray.

- no evidence of either crevice corrosion, SCC, or IG attack anywhere on the tray. Even the sensitized regions in the HAZs showed no aggravated attack.

Based on these findings, the trays of this category can be safely used for continued storage of spent PHWR fuel in the pool for another 10 years.

6. Behaviour of AISI type 304L stainless steel, zircaloy-2, and Al-1S in water containing chlorides

Every effort is made to remove chloride from SFSF water; however, at certain locations, chloride ion concentrations may build up from limited flow conditions. As mentioned earlier, SS components in the Tarapur Pool experienced pitting damage after 10 years of use. In view of this, some laboratory experiments have been carried out to ascertain the influence of chloride ions on the anodic polarization behaviour vis-à-vis the pitting tendency of Type 304L SS, Zircaloy-2, and Al-1S samples having various heat treatment and surface conditions in DM water at 30°C containing chloride ions in the range of 100 to10,000 ppm. The experiments have been carried out potentio-statically, using a conventional 3-electrode system with SCE as the reference and pure platinum as the auxiliary electrode, at a scan rate of 20mV/min. Metallographically polished samples have been used in each experiment, and surfaces were examined after the polarization test.

The components, in wt%, of the materials are as follows:

- Type 304 SS—0.05 carbon, 18.1 chromium, 8.2 nickel, 1.5 manganese, 0.5 silicon, 0.04 phosphorus, 0.05 sulphur, and the rest iron

- Aluminium-1S—0.05 copper, 0.05 manganese, 0.1 zinc, 0.04 iron, 0.3 silicon, 20 ppm boron, and the rest aluminium (no magnesium and no chromium)

- Zircaloy-2—1.5 tin, 0.15 iron, 0.05 nickel, 0.1 chromium, and the rest zirconium.

Figs. 12 and 13 show anodic polarization curves obtained for mill annealed and sensitized (675^{o}C/1 h) SS samples, respectively, at various chloride ion concentrations. It appears that tendencies for pitting attack exist in the potential range of –100 to +400 mV (vs. an SCE), depending on heat treatment and chloride ion concentration. Susceptibility to localized/pitting attack would be higher for sensitized samples for a particular chloride ion concentration. This finding is in agreement with the observation made on SS components in the Tarapur Pool. No experiments have been carried out for detailed study of pitting behaviour of SS in water from the Trombay Pool.

Figs. 14 and 15 show anodic polarization behaviour obtained on aluminium samples under different surface conditions in similar experimental conditions. Anodic polarization behaviour of mechanically polished samples (Fig. 14) in DM water indicated that pitting potential may decrease with the increase of chloride ion concentration. Therefore, chloride ion concentrations in SFSFs should be strictly controlled. Preoxidized/autoclaved aluminium samples showed slightly different behaviour, with marginal change in the susceptibility to pitting attack.

Fig. 16 shows anodic polarization behaviour of Zircaloy-2 samples in Cl- containing DM water. Although there is a sudden increase in current values at about 200 mV, no pits were observed in the specimen, perhaps because of short exposures in the solution at oxidizing potentials. Detailed study on pitting corrosion of zirconium in chloride solution has been conducted at this centre. The results indicated that the pit nucleation potential for Zircaloy decreases with an increase in chloride ion concentration, and it does not follow the linear relationship with log Cl- in NaCl as well as in HCl solution. Limited studies carried out in the present context are insufficient to make definite conclusions.

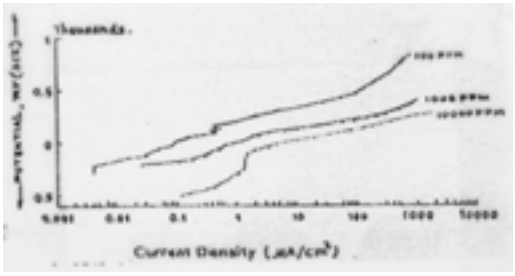

Figure.12. Anodic polarization of mill-annealed Type 304 stainless steel samples in demineralized water containing Cl⁻.

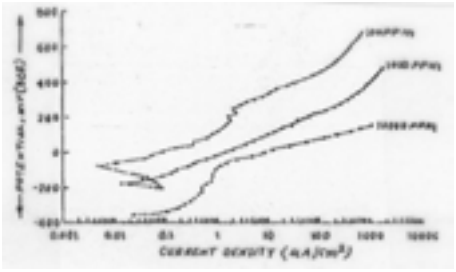

Figure 13. Anodic polarization of Type 304 stainless steel (sensitized) in demineralized water containing Cl⁻.

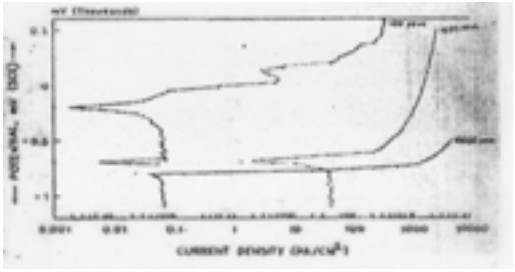

Figure 14. Anodic polarization of mechanically polished aluminium samples in demineralized water containing Cl⁻.

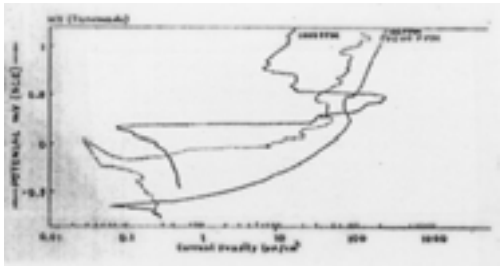

Figure 15. Anodic polarization of pre-oxidized (autoclaved) aluminium samples in demineralized water containing Cl⁻.

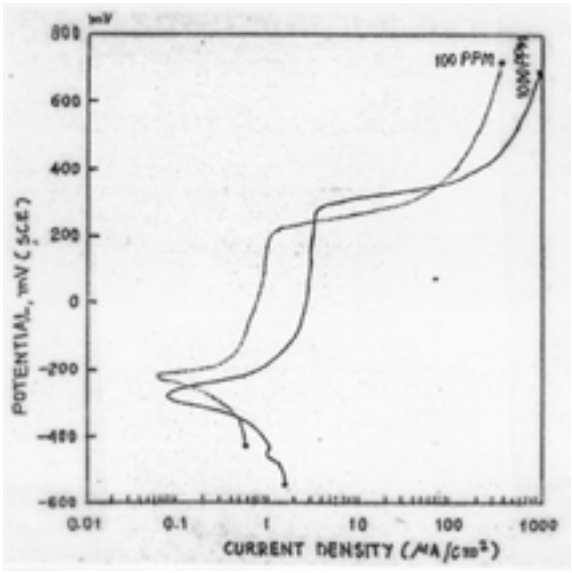

Figure 16. Anodic polarization of Zircaloy-2 in demineralized water containing Cl^-.

6.1. Discussion

Limited experiments carried out in the present study can only indicate that localized corrosion in SS in either mill-annealed or in pre-sensitized condition can occur in DM water containing chloride ions in highly oxidizing environments. Perhaps the presence of ferric ions in combination with chloride enrichment within crevices or under deposits may create a situation that is prone to localized damage as observed in the SS components in the Tarapur Pool. Present studies only emphasis the need to control and monitor chemistry in SFSF water with respect to chloride and other species. HAZs near SS welds may be more susceptible to pitting attack, as shown in Fig. 17.

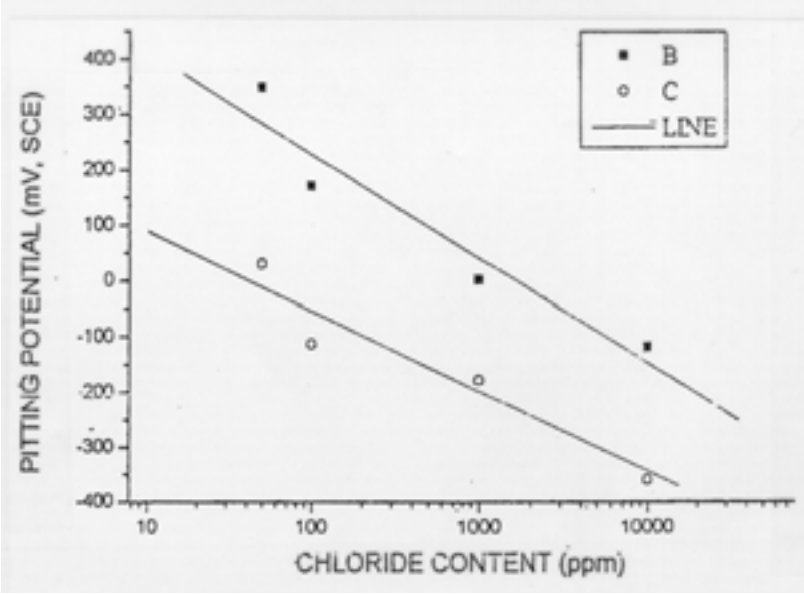

Figure 17. Correlation of the pitting potentials with the concentration of chloride ions for stainless steel (annealed) and stainless steel (sensitized).

Many researchers have attempted to provide a predictive model for the corrosion of these materials. It is not rather difficult to predict uniform corrosion of SS, Zircaloy, and aluminium, but these are of little use, because most failures of the cladding materials or SS lining of SFSFs or under water handling equipment occur from pitting, crevice attack, or IG attack. The existing predictive models do not address some of these issues because the extent of changes in the parameters in the environments is quite uncertain and depend mostly on off-normal conditions, which are very difficult to predict. Hence, attempts to model the localized corrosion phenomena are not included in the report.

7. Estimation of bacterial counts in the water of the spent fuel storage pool

The presence of active microorganisms in pool water can have a profound effect on the biocorrosion of the spent-fuel containers. Microbiologically influenced corrosion occurs as the result of a consortium of microorganisms colonizing on the metal surfaces. The metabolic processes influence corrosion of materials by several ways, such as by destroying the protective coating, producing localized acid environment, creating corrosive deposits, and altering anodic and cathodic reactions. Microbiologically influenced corrosion may result in penetration of the aluminium tubes, leading to contamination of the pool water by fission products and transuraniucs. Studies have been initiated to examine the presence of microbes causing biocorrosion of aluminium in pool water.

7.1. Methodology

Samples of water were collected from different sites such as the top surface and depths of 1 and 4 m of the Trombay Pool. The microbial cells in 100 ml of these samples were collected on millipore membrane filters of 0.45 microns pore size. The bacterial-growth medium contained 1% Tryptone, 1% peptone, 0.5% yeast extract, and 0.5% sodium chloride.

To estimate colony-forming units (CFUs), this medium was plated with1.5% agar. Chloramphenicol and ampicillin were used in the agar media to inhibit bacterial growth and to estimate fungi and other organisms. Cycloheximide was used in the plating media to inhibit growth of all eukaryotic organisms.

The microbes obtained by millipore filtering of the water were then suspended in 20 ml of the medium. Aliquots of the suspensions were immediately serially diluted and plated using the same medium containing 1.5% agar along with different antibiotics such as chloramphenicol, cycloheximide and ampicillin. The plates were incubated at 37^{o}C, and the colonies were counted after 48 hours.

The suspension of the microbes was inoculated in 50 ml of the medium and incubated at 37^{o}C for 20 hours. The culture so obtained was centrifuged at 5000 rpm in a Sorval RC2B centrifuge using a SS34 rotor for 10 minutes. The collected cells were washed twice with sterile distilled water and suspended in sterile distilled water. The cell density was estimated from the A_{600} of the suspension measured in a Varian UV/VISIBLE spectrophotometer.

Aluminium strips were incubated at ambient temperatures with suspensions of the bacterial cells in sterile distilled water at different densities (0 to 10^{8} cell/ml). Conductivity of the cell suspensions was monitored at various intervals.

7.2. Results and discussion

The plates containing ampicillin and chloraphenicol did not have any colonies, while plates containing cycloheximide had a similar number of colonies as the control plates (i.e., plates containing no antibiotic). This finding would suggest absence of eukaryotic cells in the pool water. The total number of bacteria present in 1 ml of water at different locations of the pool is as follows:

- Centre, top surface (0.0-m depth)—248 CFU/ml
- Centre, 1 m below top surface—44 CFU/ml
- Centre, 4 m below—62 CFU/ml

The colonies appeared to be morphologically of three different types - one large colony and two smaller colonies with differing morphology. It would be interesting to identify or characterize these organisms and to study their sensitivity to radiation and bactericidal agents so that suitable remedial measures for their growth can be devised. Further it would be worthwhile to monitor periodically the microbial flora and their density. Aluminium corrosion studies by measuring the conductivity of the cell suspensions at various intervals revealed considerable increase in conductivity. This increase would indicate that the bacteria can cause corrosion in aluminium.

Though the results are preliminary, they show the presence of bacteria in the pool water, which might lead to considerable biofuoling in due course.

8. Dry storage

The economics of water reactor operation can be improved to a large extent by extending burnup via improved fuel utilization and spent-fuel volumes. In examining life-limiting factors at extended burnup, increased fission product mobility and gas release rank as most important. Apart from the extended burnup, the dry storage behaviour of the spent fuel containing several fission products is also important. The extent of degradation in the thermophysical properties of the fuel from the presence of several fission products, its oxidation behaviour, and chemical compatibility with the cladding material are some important aspects of the SIM fuel, which need in-depth study and generation of experimental data so that the spent fuel can be safely stored with a predefined set of storage parameters.

Simulated high-burnup nuclear fuels (SIM fuel) attempt to replicate the chemical state and microstructure of the solid fission products generated in irradiated fuel so that detail experiments can be undertaken without intense radiation fields. The fission products in irradiated fuel have been classified into four groups:

(1) Oxides dissolved in the matrix (strontium, zirconium, niobium, yttrium, lanthanum, cerium, praseodymium, neodymium, promethium, and samarium)

(2) Metallic precipitates molybdenum, technetium, ruthenium, rhodium, palladium, silver, cadmium, indium, antimony, and tellurium

(3) Oxide precipitates rubidium, cesium, barium, zirconium, niobium, molybdenum, and tellurium

(4) Volatile elements krypton, xenon, bromine, iodine, etc.

SIM fuel that has been tested in the present investigation corresponds to the presence of the first three classes of fission products. The composition (fission product inventories) of the SIM fuel was obtained using the ORIGEN code (Oak Ridge Isotope Generation and depletion), based on an average burnup of 7000 MWd/t for PHWRs and without any post-service cooling.

The ORIGEN code formulation was simplified to select only 11 elements as mentioned in Table 5, showing their amounts added. This tabulation represents all major fission products except the volatile fission products. In some cases, elements of similar chemical behaviour are represented by a single element; for example "La" represents itself and the actinide elements "Am" and "Cm."

In the present investigation, the SIM fuel has been synthesized by powder metallurgy to make sintered pellet samples to measure some important properties such as thermal diffusivity, thermal conductivity, coefficient of thermal expansion, hot hardness, and out-of-pile chemical compatibility behaviour with Zircaloy-2 cladding at 400°C for 1000 and 2000 hours. Any changes in property from the presence of the fission product elements were noted by comparing the measured value of the sintered pellets of UO_2, which have undergone the same fabrication procedure as the SIM fuel.

It was observed that thermal conductivity of the SIM fuel is lower than that of UO_2, and both decrease with increase in temperature. The decrease is more at lower temperatures compared to that at higher temperatures. The decrease in conductivity of the SIM fuel compared to that of UO_2 could be attributed to the presence of impurity scattering centres for anhamonic phonon scattering, which is predominantly the heat conduction (phonon conduction) mechanism at lower temperature.

8.1. Out-of-pile fuel-clad chemical compatibility tests

Out-of-pile chemical compatibility of Zircaloy-2 cladding with UO_2-based SIM fuel was tested by heating Zircaloy-2 cladding discs in contact with UO_2-based SIM fuel in a miniature compatibility capsule shown in Fig.19.

TABLE 5. COMPOSITION OF SIMULATED FUEL, (BASED ON THE ORIGEN CODE), CORRESPONDING TO A BURNUP OF 7000 MWD/T

Element	wt%
ZrO_2	0.108
MoO_3	0.102
CeO_2	0.088
Nd_2O_3	0.086
RuO_2	0.076
$BaCO_3$	0.044
La_2O_3	0.032
PdO	0.028
SrO	0.026
Y_2O_3	0.014
Rh_2O_3	0.012
UO_2	99.380

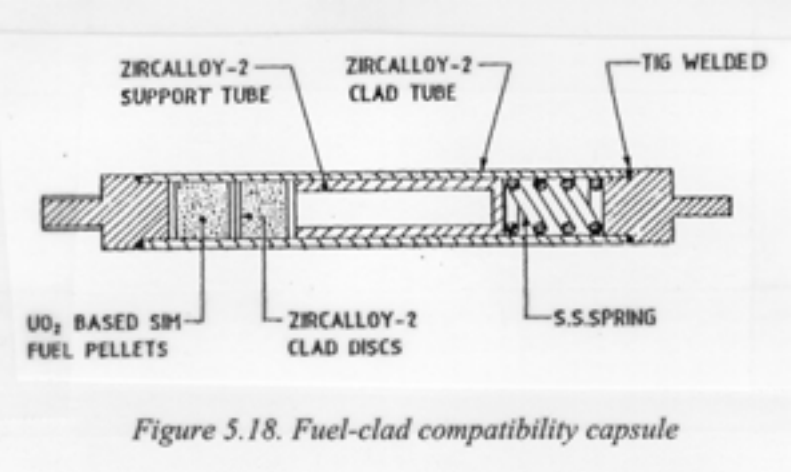

Figure 5.18. Fuel-clad compatibility capsule

Figure 18. Fuel-clad compatibility capsule.

The capsule essentially consists of two sintered pellets of SIM fuel with Zircaloy-2 cladding disks between them. Use of a spring established intimate contact between the pellets and disks. The whole assembly was enclosed in another Zircaloy-2 cladding tube, which was welded at both ends by tungsten inert gas (TIG) welding under helium cover gas. The capsule was filled with helium inert gas; two such capsules were heated at 400°C for 1000 and 2000 hours in an annealing furnace. After the specified heating time, the capsules were cut open to identify any reaction product between the cladding and the fuel. Visual examination revealed no apparent reaction between the fuel and cladding, as they could be easily separated. The cladding disk and tube will be examined metallographically and microhardness will be measured to identify any reaction product at the pellet-clad interface.

9. Degradation of elastomers

The age-related degradation of elastomeric components causes the failure of many components. The elastomer properties are affected by time, temperature, and radiation. The various studies carried out in Canada and India indicated the following ageing mechanisms:

- scission: The process of breaking molecular bonds, typically by ozone attack, UV light, or radiation

- cross-linking: The process of creating molecular bonds, typically by oxygen attack, heat, or curing

- compound ingredient evaporation, migration, mutation, etc.

Of these ageing processes, scission and cross-linking have the major impact on physical property change as given below:

- For scission: i) Increased elongation

  ii) Decreased tensile strength

  iii) Decreased modulus

Cross-linking results in the reverse of the above changes. The rate at which these changes occur is temperature dependent.

Various studies have outlined approximate shelf life of elastomers based on ageing studies, as enumerated in Table 7. As per studies carried out in BARC, the limiting values of cumulative radiation dose on various elastomers are given in Table 8.

TABLE 6. DRYING TEST DATA

Polymer	Age (y)	Hardness (PTS)	Tens. test (PSI)	Mod (PSI)	Elong.	70 h/205°F Compr.
Nitrile	0	70	1800	900	200	75
	31	90	2290	1800	150	80.9
Neoprene	0	70	2150	450	340	57
	31	82	1940	1100	175	73.8
Butyl	0	71	1490	450	350	87
	31	70	1630	550	300	97
Viton	0	75	2010	450	320	37
	26	79	2040	600	310	45
Styreine	0	68	1500	550	200	41
(SBR)	31	77	1400	850	150	47
Urethane	0	73	3200	600	475	93
	30	80	3000	1160	265	103
Silicone	0	70	800	--	85	10
	31	72	825	--	60	12
Acrylate	0	70	1300	470	210	37
	31	64	1360	300	350	45
Ethylene	0	81	1600	685	216	--
	24	79	1680	741	221	--

TABLE 7. APPROXIMATE SHELF LIFE OF ELASTOMERS BASED ON AGEING STUDIES

Polymer	US/Canada (IEEE, y)	India (Dr. Bohra, y)
Fluorocarbons	20	>30
Ethylene/propylene	5-10	>40
Silicone	20	>40
Styreine (SBR)	3-5	5
Neoprene	5-10	2
Butyl	5-10	10
Urethane	3-5	5

TABLE 8. LIMITING VALUES OF RADIATION DOSE ON ELASTOMERS

TEST ITEM (40°C)	Life span (y)	Dose (MRads)
PVC cables	12	50 - 100
HR PVC cables	10	50 - 100
EPR cables	40	130 - 200
XLPE cables	>40	140 - 200
ETFE cables	>40	20 - 40
Vulkene cables	>40	100 - 140
Silicone rubber	>40	30 - 50
Viton	>40	50 - 100
Neoprene rubber	2	50 - 100
Natural rubber	1	50 - 100
EPDM	>30	150 - 200
NBR	10	100 - 150
PTFE	>40	< 2

9.1. Conclusions

(1) For cables, XLPE and EPR are more suitable; for gaskets and `O' rings, EPDM is the best material.

(2) Long-term performance of natural rubber and neoprene rubber at elevated temperatures is very poor.

(3) All the elastomeric materials fail in the same manner (identical failure is hardening followed by cracking and brittleness), from thermal ageing and radiation ageing, except viton, which becomes sticky above 50 MRads.

ACKNOWLEDGEMENTS

The authors thank Shri H.B. Kulkarni, Group Leader, Spent Fuel Handling Section; Dr. P.K. De, Head, Corrosion Science Section; Dr. S. Banerjee, Associate Director and Head, Materials Group; and Dr. K. Balu, Director, Fuel Reprocessing and Nuclear Waste Management Group, for their keen interest and suggestions during the course of work on this CRP.

REFERENCES

[1] AMERICAN SOCIETY OF METALS, ASM Handbook 9th Edition, Vol. 13 (Corrosion) Stress Corrosion Cracking of Stainless Steels.
[2] TRUMAN, J.E., The influence of chloride content, pH and temperature of test solution on the occurrence of stress corrosion cracking with austenitic stainless steel, Corrosion Science **17** (1977) 737.
[3] KUNIYA, J., MASACKA, I., and SASAKI, R. , Effect of cold work on stress corrosion cracking of non-sensitized AISI 304 stainless steel in high temperature oxygenated water, Corrosion-NACE **44** (1988) 21.
[4] AMERICAN SOCIETY FOR TESTING AND MATERIALS, Guide for Conducting Corrosion Coupon Tests in Field Applications, ASTM G4 – 68, ASTM, Philadelphia (1974).

[5] NATIONAL ASSOCIATION OF CORROSION ENGINEERS, NACE Standard TM - 01 – 69, NACE (1976 revised).
[6] AMERICAN SOCIETY FOR TESTING AND MATERIALS, Practice for Preparing, Cleaning, and Evaluating Corrosion Test Specimens, ASTM G1 – 72 ASTM, Philadelphia (reapproved in 1979).
[7] AMERICAN SOCIETY FOR TESTING AND MATERIALS, Methods of Tension Testing of Metallic Materials, ASTM E 8 – 87a , ASTM, Philadelphia.
[8] AMERICAN SOCIETY FOR TESTING AND MATERIALS, Test method for Corrosion Testing of products of Zry, Hafnium and their Alloys in Water at 680°F or in Steam at 750°F and Evaluation of Pitting Corrosion, ASTM G2 – 74, ASTM, Philadelphia.
[9] AMERICAN SOCIETY FOR TESTING AND MATERIALS, Guide for Examination and Evaluation of Pitting Corrosion, ASTM G 46 – 76, ASTM, Philadelphia.
[10] PAJKOSSY, J., and NYIKOS, L., Fast algorithm for differintegration, J. Electroanal. Chem. **179** (1984) 65-69.
[11] CIPOLLINI, N.E., Visual detection of hydrated aluminum oxide by staining with fluorescing and non-fluorescing dyes, J. Electrochem. Soc. **129** (1982) 1570.
[12] PATHAK, B.R., and GODARD, H.P., Equation for predicting the corrosivity of natural fresh water to aluminium, Nature **218** (1968) 893.
[13] OLDFIELD, J.W., and SUTTON, W.H., Crevice corrosion of stainless steel, 1.A mathematical model, Br. Corro. J **13** (1978) 13.
[14] BOYAM, B.M., and RHOADS, J.E., "Elastomer shelflife: aged junk or jewels?," Nuclear Power Plant Ageing (Proc. Int. Symp., Maryland, 1988), U.S. Nuclear Regulatory Commission, Washington, D.C. (1988).
[15] BORA, J.S., Ageing Studies on Elastomeric Components and Materials, Internal Technical Report, BARC, India.
[16] INTERNATIONAL ATOMIC ENERGY AGENCY, Extended Storage of Spent Fuel, Final Report of a Co-ordinated Research Programme on the Behaviour of Spent Fuel and Storage Facility Components During Long Term Storage (BEFAST-II) 1986-1991**,** IAEA-TECDOC-673, IAEA, Vienna (1992).
[17] COX, B., Pellet-clad interaction (PCI) failures of zirconium alloy fuel cladding - a review, J. Nuclear Mat., **172** (1990) 249 – 292.
[18] EINZIGER, R.E., BOSI, D.M., and MILLER, A.K., Zircaloy cladding - tough containment for spent fuel storage, Transaction American Nuclear Society, **38** (1981) 131-133.
[19] BUXTON, G.V., Radiation chemistry of the liquid state (I) water and homogeneous aqueous solutions, in Radiation Chemistry, Principles and Applications (FARHATAZIZ, A.J., and RODGERS, M., Eds.), VCH Publishers Inc., New York (1987) 321-349.
[20] INTERNATIONAL ATOMIC ENERGY AGENCY, Corrosion of Zirconium Alloys in Nuclear Power Plants, IAEA TECDOC-684, IAEA (1993) 82-92.
[21] BURNS,W.G., and MARSH, W.R., Radiation chemistry of high temperature water (300-410°C), Part 1- Reducing products from gamma radiolysis, J. Chem. Soc. Faraday Trans. I **77** (1981) 197-215.
[22] TAKAGI, J., ICHIKAWA, N., and HEMMS, Y., "Evaluation of corrosion environment in BWR primary circuit by water radiolysis model, water chemistry of Nuclear Power Plants (Proc. Int. Conf. 1988), vol. 2, Japan Atomic Industrial Forum, Tokyo (1988) 517-522.
[23] GLASS, R.S., et al., Gamma radiation effects on corrosion-I. electrochemical mechanisms for the aqueous corrosion processes of austenitic stainless steel relevant to nuclear waste disposal in TUFF, Corrosion Science **26** (1986) 577-590.

[24] KRITSKY, G.V., et al., Materials corrosion under spent nuclear fuel storage conditions, Material Reliability in the Back End of the Nuclear Fuel Cycle, TECDOC-421, IAEA (1987) 51-61.
[25] OKAMOTO, H., et al., Evaluation of the integrity of the pool components by the concentration of the corrosion products in the spent fuel storage pool water, Long Term Wet Spent Nuclear Fuel Storage, TECDOC-418, IAEA (1986) 143-150.
[26] ALEXANDROV, A.B., et al., Effect on gamma radiation on metal corrosion under spent fuel storage conditions, Long Term Wet Spent Nuclear Fuel Storage, TECDOC-418, IAEA (1986) 181-1190.
[27] SENGUPTA, A.K., Some Important Thermophysical and Thermomechanical Properties of UO_2 base SIM Fuel, in preparation as BARC Report, India.
[28] KAIN, V., et al., "Corrosion behaviour of materials in spent fuel storage facilities, First National Conference on Corrosion and Its Control-NACE-95 (Proc. Symp., Mumbai, 1995), NACE Int., Mumbai, India. (1995) 1201.
[29] KAIN, V., SHINDE, S.S., and SEETHARAMIAH, P., "Prediction of pitting corrosion tendency of materials during extended storage of spent nuclear fuels," Conference on Corrosion, CONCORN-97 (Proc. Symp., Mumbai, 1997), Mumbia, India (1997).
[30] SINGH, J.L., et al., "Development of ultrasonic testing technique for inspection of irradiated spent fuel storage pool liner weld joints," National Symposium on Non Destructive Examination – NDE-94, National Seminar on Non-Destructive Evaluation Techniques (Proc. Symp., Mumbai, 1994), Mumbai, India (1994).
[31] KAIN, V., et al., Environmental degradation of materials during wet storage of spent nuclear fuels," J. of Materials Engg. And Performance **9** (2000) 317.
[32] PALIT, G.C., and GADIYAR, H.S., Pitting corrosion of Zry in chloride solution, Corrosion **43** (1987) 140.

Radiation effects and the modelling of the corrosion of nuclear waste disposal containers

F. King, B.M. Ikeda, D.W. Shoesmith

Atomic Energy of Canada Ltd, Whiteshell Laboratories, Pinawa, Manitoba, Canada

Abstract. Gamma radiation emitted by used fuel, or other forms of radioactive waste, may affect the corrosion behaviour of nuclear waste disposal containers. The extent of these effects must be taken into account in models designed to predict container lifetimes. In Canada, two materials have been considered as candidate container materials, dilute titanium alloys and oxygen-free copper. The impact of γ-radiation on the crevice corrosion of Grade-2 (commercially pure) Ti has been studied using a coupled electrochemical technique. The effect of irradiation on the corrosion potential of Cu has been studied under conditions designed to simulate those in a disposal vault. The results of these experimental studies are described, along with a review of the relevant literature describing possible effects of γ-radiation on the absorption of hydrogen by Ti and the pitting, stress corrosion cracking and microbially influenced corrosion of Cu. Methods for including the effects of γ-radiation in predictive container failure models are discussed. It is concluded that, at the dose rates expected in a Canadian disposal vault, there are no deleterious effects of γ-radiation on the corrosion behaviour and predicted lifetimes of Ti or Cu containers.

1. Introduction

The only radiation source likely to affect the lifetimes of nuclear fuel waste disposal containers is γ-radiation, produced by the decay of radionuclides within the fuel. The magnitude of the radiation field at the container surface will depend on the nature and age of the waste form, and the material and wall thickness of the container. Irradiation of the container surface and the surrounding environment may have a number of effects on the corrosion behaviour of the container: (i) radiolysis of the aqueous and vapour phases to produce oxidizing and reducing radical and molecular radiolysis products, (ii) interaction with semiconducting oxide films, and (iii) reduction in the number of viable microbes at or near the container surface.

Two classes of alloy have been considered as container materials for the disposal of used nuclear fuel in Canada. Dilute titanium alloys, specifically Grade-2 (commercially pure), Grade-12 (0.8 wt% nickel, 0.3 wt% molybdenum) and Grade-16 (0.04 to 0.08 wt% palladium), were chosen for study because of their excellent behaviour in saline conditions, similar to those expected in a Canadian disposal vault. Copper, in particular those alloys with copper contents >99.3 wt% such as the oxygen-free, phosphorus-deoxidized, and tough-pitch alloys, were chosen because of their thermodynamic stability under the anoxic conditions expected to prevail in the disposal vault in the long term.

Following an introduction to the Canadian disposal concept, this paper describes the impact of γ-irradiation on the corrosion behaviour of these two classes of alloy. Techniques for modelling the effect of radiation will also be discussed for each material.

2. Canadian concept for disposal of used nuclear fuel

The Canadian concept calls for the disposal of used nuclear fuel in corrosion-resistant containers in a disposal vault located 500 to 1000 m underground in the granitic rock of the Canadian Shield [1]. Fig.1 illustrates two conceptual vault layouts: in one the containers are placed in boreholes drilled in the floors of rooms and in the other within the disposal rooms themselves. In both cases, the containers are surrounded by, and the disposal rooms sealed with, compacted clay-aggregate buffer and backfill materials [2,3].

While no final choice of container has been made, several options for both the material and design of container exist. Fig.2 shows a number of container designs proposed [2,3]. As well as having different corrosion-resistant outer shells, the designs differ in the internal support structures, required to withstand the hydrostatic loads at the vault depth (between 5 and 10 Mpa for vault depths of 500 to 1000 m, respectively). In the packed-particulate design, the load is supported not by the outer corrosion-resistant shell, but by the particulate material and internal structure in which the fuel bundles would be placed. If the container is required to withstand hydrostatic pressures from future glaciation events (up to 40 Mpa for a 2- to 3-km-thick icesheet), a more-robust design will be required. The dual-shell concept includes an inner 6.5-cm-thick carbon-steel liner to withstand stresses from glacial loading.

The nature of the corrosive environment within the vault is expected to change with time (Fig. 3) [4]. Initially, O_2 trapped within the pores of the buffer and backfill materials and the decay heat from the waste will produce warm, oxidizing conditions within the vault. The trapped O_2 will be consumed by corrosion of the container and in redox reactions with Fe(II)-containing minerals in the crushed rock used as part of the backfill. Radiolysis of water in the surrounding environment is the other potential source of oxidants for corrosion. The concentration of radiolysis products will decrease, however, as the activity of the fuel inside the container decays. At the same time the container will be cooling, so that vault conditions will become cool and anoxic and remain so indefinitely. The transition from warm, oxidizing to cool, anoxic conditions is expected to occur within 500 to 1000 a after vault closure.

Apart from temperature and the availability of oxidant, the other important environmental parameters that affect the corrosion behaviour of the containers are the chloride concentration and the mass-transport conditions. Deep Canadian Shield groundwaters are saline with $[Cl^-]$ typically in the range from 0.1 to 1 $mol \cdot dm^{-3}$ at the proposed vault depth [5]. Mass transport within the vault is restricted primarily to diffusion because of the low hydraulic conductivity ($<10^{-12}$ $m \cdot s^{-1}$) of the compacted buffer and backfill materials [2,3]. Effective pore-water diffusion coefficients in these materials are approximately 100 times lower than in bulk solution [6]. In addition, adsorption of positively charged solutes by the cation-exchanging clay will retard the transport of species, especially of radionuclides away from failed containers [2,3,6].

Because of the nature of used CANDU® fuel and the design of the containers, the predicted γ -radiation field at the surface of the container is expected to be quite small. For the 6.35-mm-thick titanium packed-particulate container (Fig. 2a), the initial surface dose rate for the reference 10-a-cooled fuel is ~52 $Sv \cdot h^{-1}$ [2]. In fact, the used fuel that will eventually be disposed of will be older, with a mean age of perhaps 20 to30 a. Fig. 4 shows the predicted dependence of the initial dose rate on the age of the fuel, based on a mean half-life of 30 a, equivalent to that of ^{137}Cs, the major γ-emitter in the used fuel. The same decrease in activity will occur after disposal, and the impact of γ-radiation should be insignificant after a period of

300 a, equivalent to ten half-lives of ^{137}Cs (Fig. 4). The compacted buffer material surrounding the container will also be irradiated. Fig. 5 shows the predicted dose rate as a function of distance into the buffer material for the initial container-surface dose rate of 52 Sv·h^{-1}. The initial surface dose rate is also dependent on the container design.

Because of the extra shielding afforded by the thicker and denser container wall, the dose rate for a 25.4-mm-thick copper packed-particulate container (Fig. 2b) is ~11 Sv·h^{-1} for the same 10-a-cooled fuel. For the copper/carbon-steel dual-wall container design (Fig. 2c), the surface dose rate becomes almost insignificant in terms of the impact on radiolysis (~0.2 Sv·h^{-1}).

Because of the evolution of vault conditions, the corrosion behaviour of the containers is also expected to change with time [4]. In general, the severest corrosion (both localized and uniform) will occur during the aggressive warm, oxidizing period. As conditions become cooler and anoxic, corrosion should slow down and become more uniform in nature. During the warm, oxidizing period crevice corrosion is possible for titanium (the extent varying for the different alloys), with uniform corrosion predominating in the long term once any propagating crevices have repassivated. Hydrogen-induced cracking (HIC) is also possible, as a result of the hydrogen absorbed during crevice corrosion and, more slowly, during uniform corrosion. For copper, uniform corrosion is expected to be the predominant form of corrosion. Once all the trapped O_2 has been consumed and the concentration of radiolytically produced oxidants becomes insignificant, however, corrosion should cease, because copper is thermodynamically stable in O_2-free H_2O. Localized corrosion, in the form of pitting or underdeposit corrosion, may occur during the warm, oxidizing period and the possibility of microbially influenced corrosion (MIC) at any time must also be taken into account [7]. SCC of copper must also be considered, although, for a variety of reasons, the possibility of container failure by SCC is remote [8].

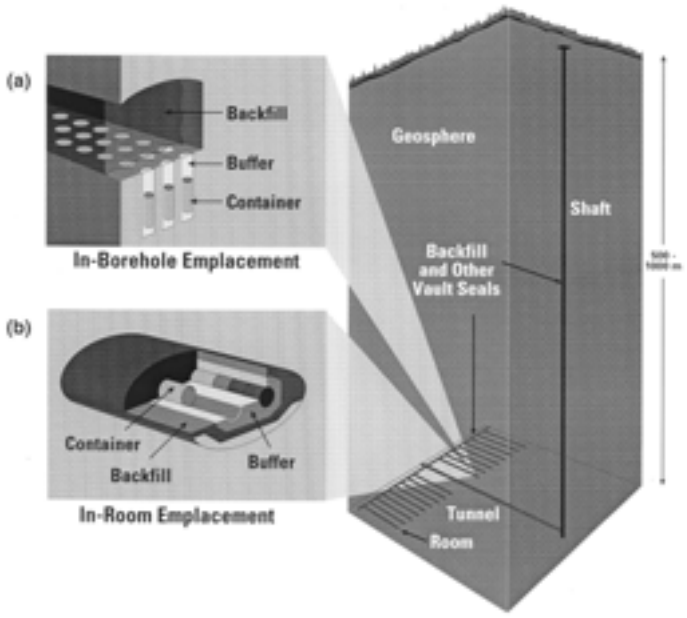

Figure.1. Two possible vault configurations for the disposal of nuclear waste in Canada: (a) borehole emplacement, and (b) in-room emplacement.

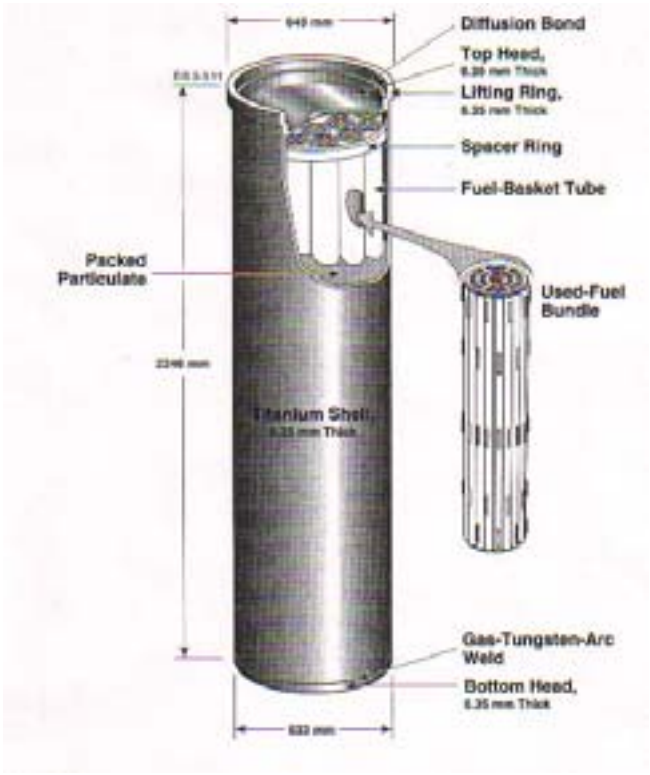

(a) Ti-shell packed-particulate container

Figure 2. Various container designs proposed for the disposal of nuclear fuel waste in Canada: (a) titanium-shell packed-particulate container, (b) copper-shell packed-particulate container, and (c) copper-shell dual-wall container with carbon-steel inner liner.

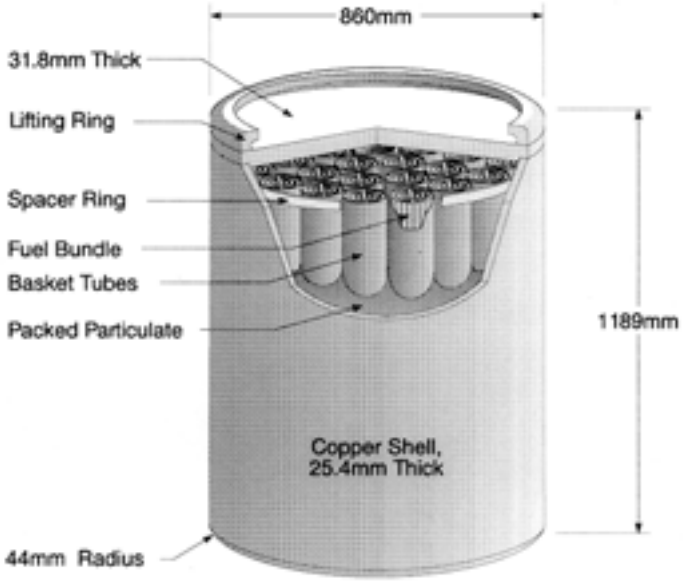

(b) Cu-shell packed-particulate container

Figure 2. Various container designs proposed for the disposal of nuclear fuel waste in Canada.

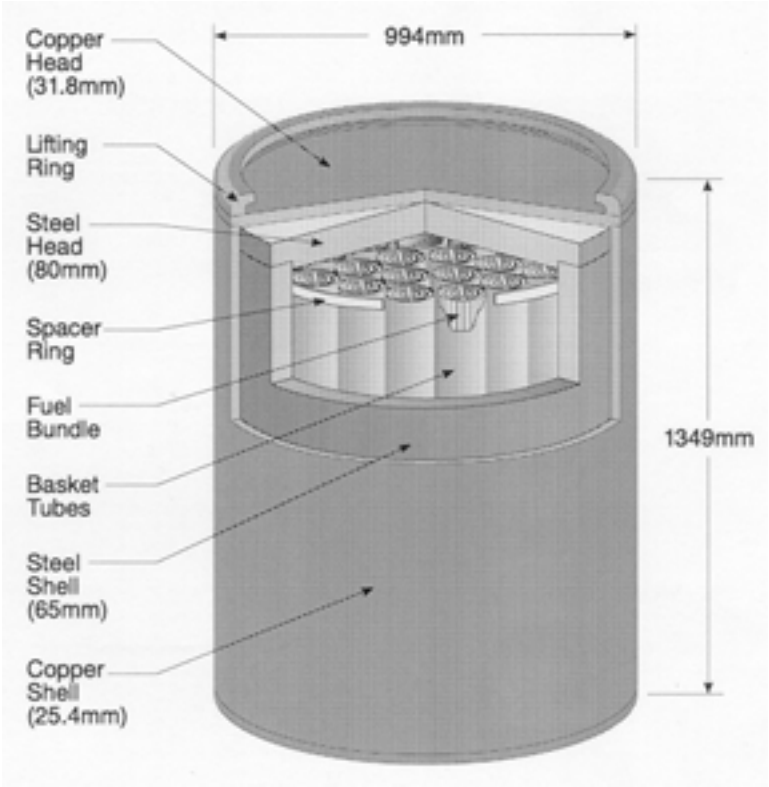

(c) Cu-shell dual-wall container with C-steel inner liner.

Figure 2. Various container designs proposed for the disposal of nuclear fuel waste in Canada.

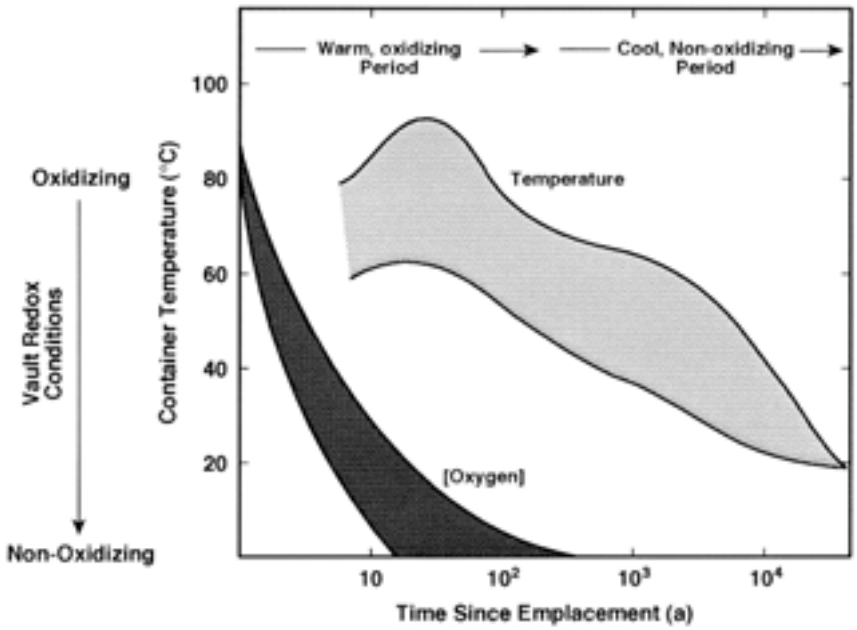

Figure 3. Expected evolution of environmental conditions within a Canadian nuclear waste disposal vault illustrating the change from warm, oxidizing to cool, anoxic conditions.

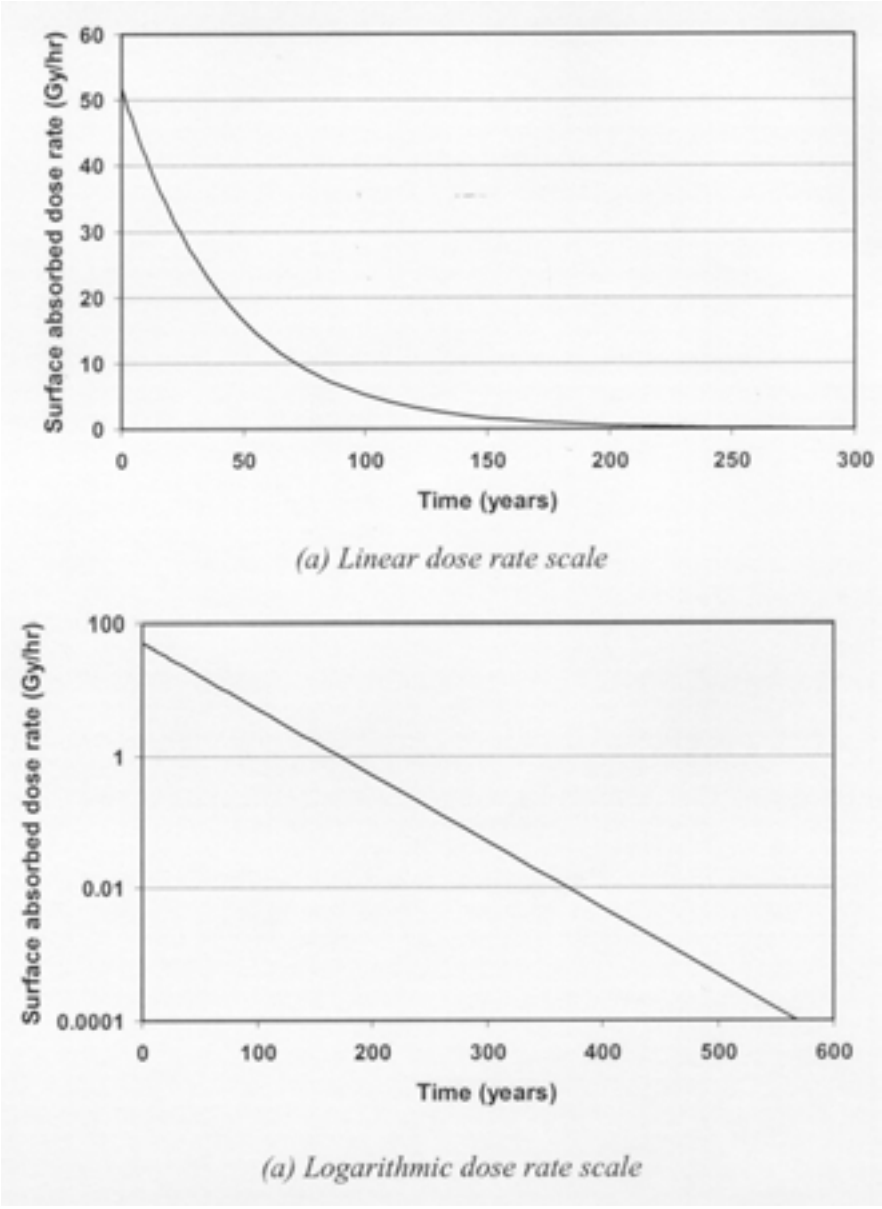

Figure 4. Expected time dependence of the dose rate at the surface of a titanium-shell packed-particulate container with 72 used, 10-a-cooled CANDU fuel bundles.

3. Radiation effects on titanium containers

3.1. γ-radiation effects on titanium corrosion

Crevice corrosion has been studied using a galvanic coupling technique in which a creviced coupon is connected to a large planar cathode (Fig. 6) [9]. The potentials of the creviced coupon (E_{CREV}) and the coupled current (I_{CREV}) passing between the creviced anode and planar cathode are recorded simultaneously. The coupled current is a measure of the rate of O_2 reduction on the planar cathode and is proportional to the total amount of crevice corrosion. Most of the titanium dissolution within the crevice is driven by the reduction of protons inside the occluded region (Fig. 7).

Only preliminary data on the effects of radiation on the crevice corrosion is available for Grade-2 titanium [9-11]. The effects appear to depend on the ability of the material to sustain

crevice propagation, which, in turn, is a function of the alloy processing. Thus, for a very susceptible material (low iron and nickel content, large-grain microstructure) that undergoes full activation within the crevice (i.e. extensive rapid propagation over the majority of the creviced area), the presence of a radiation field appears only to slow the rate of propagation without apparently causing repassivation. This finding is suggested by the observed decrease in I_{CREV} when the γ-field is introduced (Fig. 8). This decrease is accompanied by a negative shift in E_{CREV}. For a fully activated material undergoing active corrosion within the crevice, these shifts indicate a decrease in the active propagation rate but no tendency to repassivate (Fig. 9). Whether this decrease in propagation rate is accompanied by an increase in pH within the crevice is not known. That the presence of radiation leads to overall lower crevice propagation rates is shown by comparing the rates derived from the corresponding coupon weight changes. In the absence of irradiation, the mean rate of crevice corrosion in 0.26 mol·dm^{-3} NaCl at 100°C is 180 μm·a^{-1}. Irradiation at an absorbed dose rate of 4.2 Gy·h^{-1} in 1 mol·dm^{-3} NaCl resulted in a rate of just 38 μm·a^{-1} for the same exposure period of ~860 h.

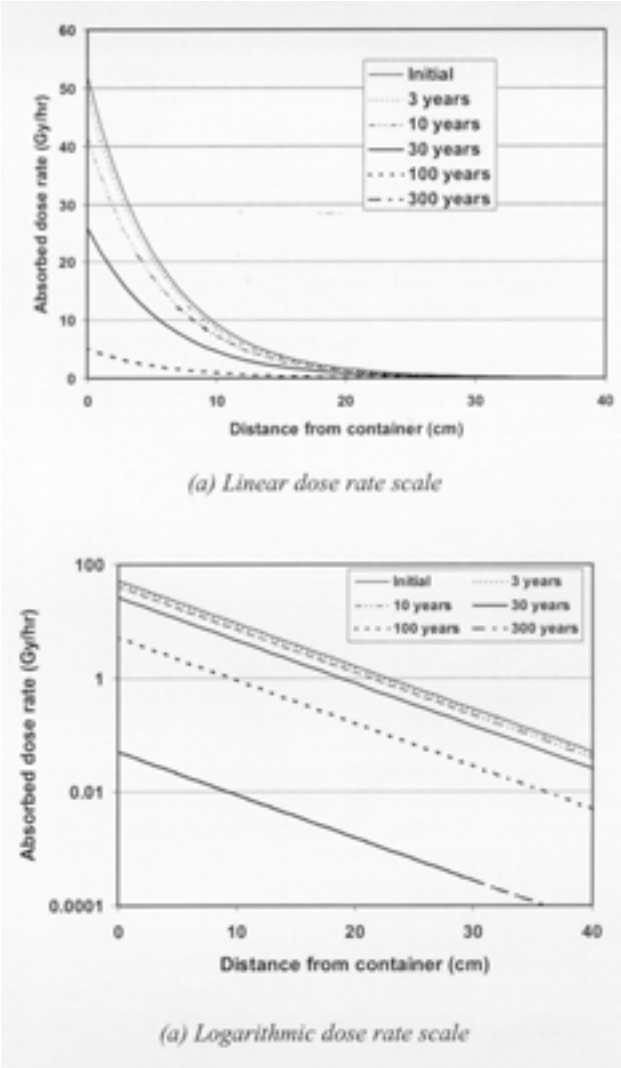

Figure 5. Estimated spatial dependence of the dose rate for a titanium-shell packed-particulate container with 72 used, 10-a-cooled CANDU fuel bundles.

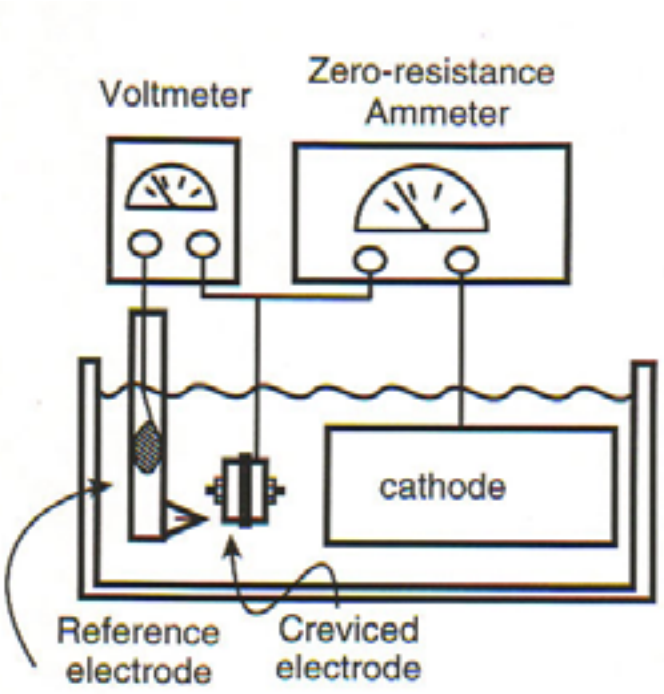

Figure 6. Experimental arrangement used to measure the coupled current and crevice potential during crevice corrosion experiments.

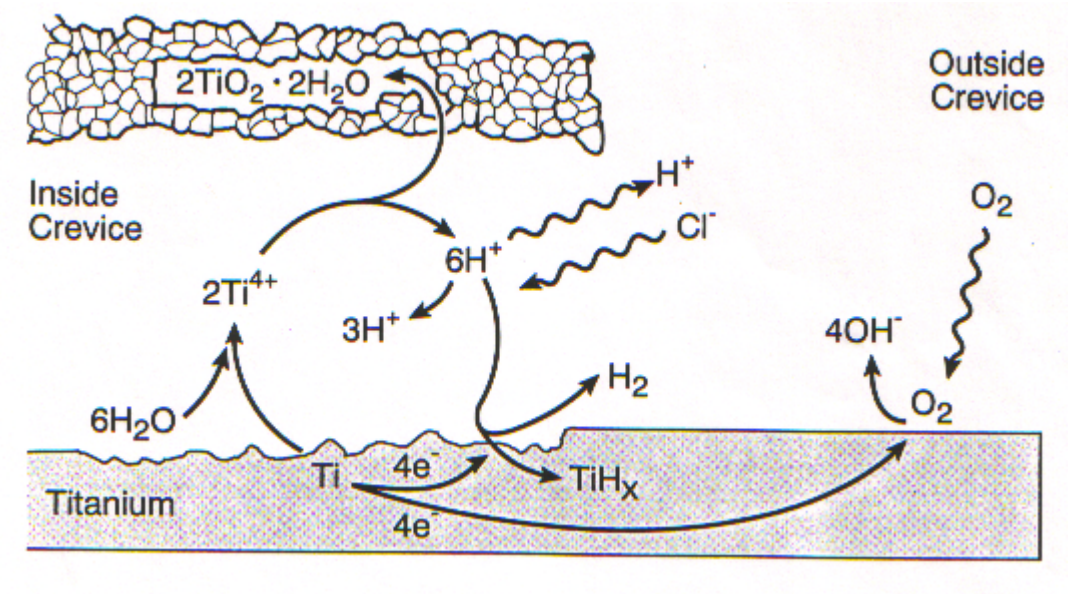

Figure 7. Chemical and physical processes involved in the crevice corrosion of titanium.

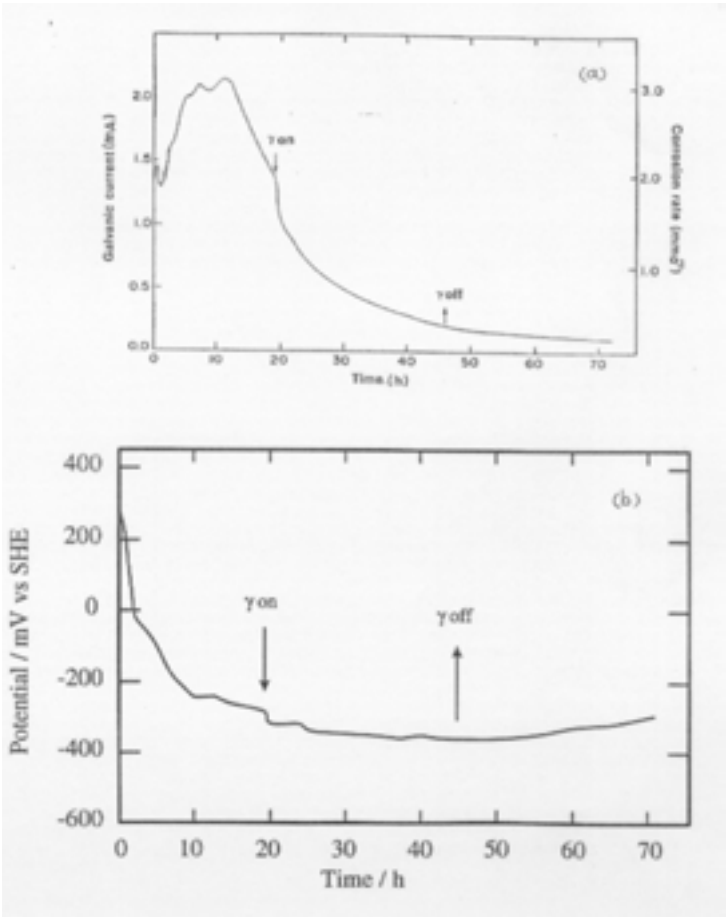

Figure 8. Effect of radiation on the crevice corrosion behaviour of susceptible Grade-2 titanium: (a) variation of the coupled current (I_{CREV}) and (b) of the crevice potential (E_{CREV}). Dose rate ~100 Gy·h^{-1}.

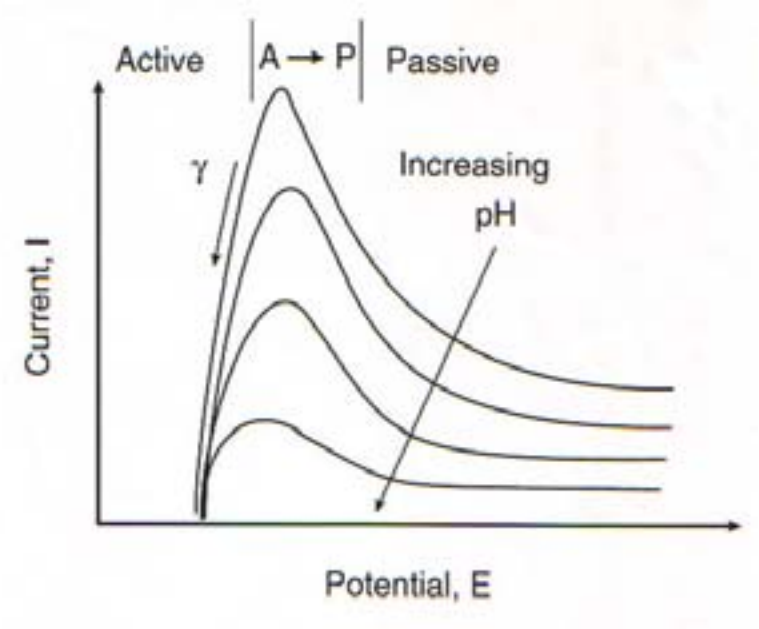

Figure 9. Current/potential curves as a function of pH demonstrating the effect of radiation for susceptible Grade-2 titanium.

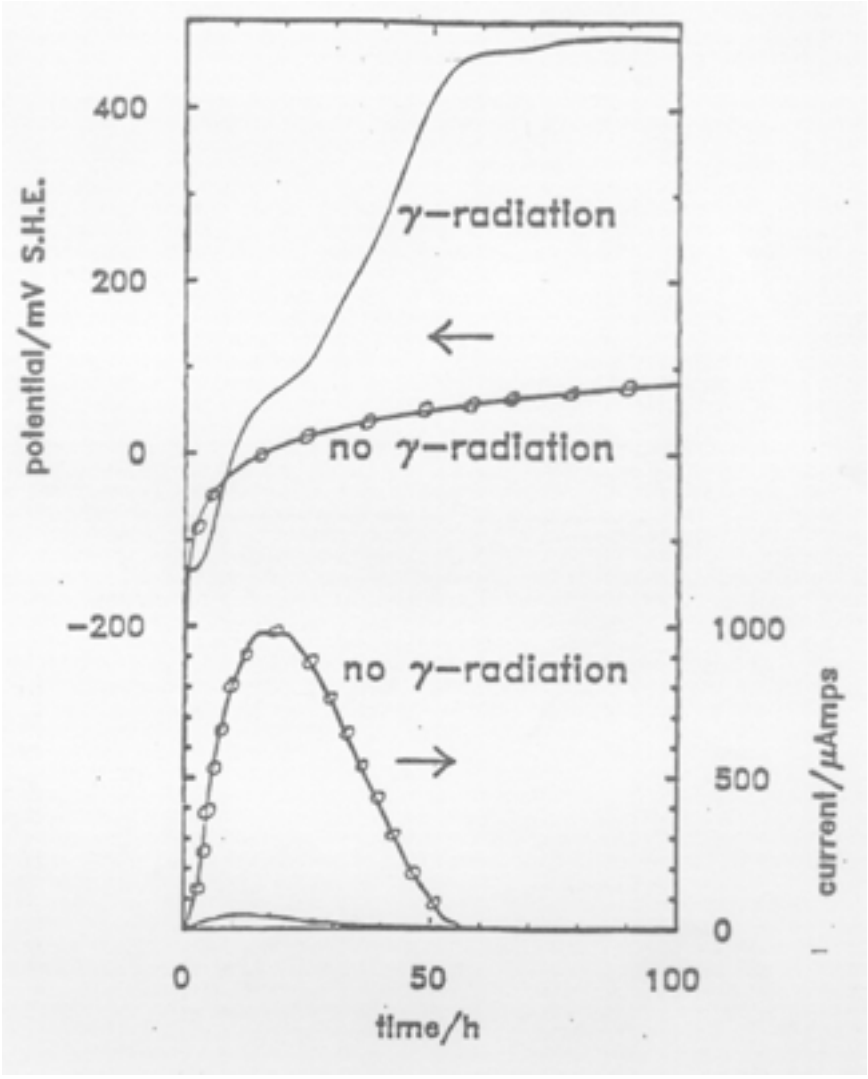

Figure 10. Effect of radiation on (a) the crevice potential and (b) the coupled current for a repassivating crevice condition for Grade-2 titanium: - - - - - no radiation, ——— irradiated

If the Grade-2 titanium material is less susceptible to crevice corrosion (i.e. a high iron/nickel content, increased β phase, smaller-grain size), the effect of radiation is much more significant. In the *absence* of a γ-field, substantial propagation is obtained (high I_{CREV}) but the crevice potential never achieves the negative potentials (~-0.30 V_{SHE}), which indicate full activation of the more susceptible Grade-2 titanium specimen discussed above (dashed curves, Fig. 10). This behaviour suggests that crevice propagation is confined to individual pits within the crevice, which never coalesce to give general activation. In addition, I_{CREV} drops to zero, suggesting crevice repassivation, long before all of the O_2 in the sealed pressure vessel is consumed. This failure to fully activate and to repassivate rapidly appears to be attributable to the catalysis of proton reduction on iron-containing intermetallics (possibly also containing trace quantities of nickel) within the crevice. (This kind of behaviour is optimized in Grade-12 titanium in which 0.8 wt% nickel is added to optimize the catalytic reduction of H^+).

When this material is irradiated from the beginning of the experiment (solid curves, Fig. 10), the activation of the crevice corrosion process is even more inhibited (lower I_{CREV}), and when repassivation occurs, a much more positive potential is achieved. These effects suggest that the radiolytic production of oxidants within the crevice inhibits the local activation events, possibly by enhancing oxide repair at the initial breakdown sites. Alternatively, it is possible that radiolytically produced reductants catalyse the proton reduction on the intermetallics to an even greater extent than in the unirradiated experiment, thereby causing repassivation before significant local site propagation can occur. The more positive value of E_{CREV} in the presence of γ-radiation may indicate a direct effect on the composition and/or structure of the film formed when the crevice repassivates. Kim and Oriani [12] have observed a change in the film composition and structure on Grade-12 titanium in the presence of high γ-radiation fields (1.5×10^3 Gy·h^{-1}) in brine solutions. Irradiation produced less defective films containing more anatase (as opposed to rutile) than films formed in the absence of radiation.

The presence of γ-radiation could also affect the rate of hydrogen absorption by titanium since radiolysis produces hydrogen and H_2. The rates of proton reduction and hydrogen absorption in the crevice during crevice corrosion are so high that additional hydrogen absorption from radiolytically produced hydrogen will be negligible. However, because γ-radiolysis tends to inhibit crevice initiation and propagation, it will limit the overall duration of crevice propagation, and hence the amount of hydrogen absorbed by Grade-2 titanium. This latter effect will be much more significant than any additional small amounts absorbed because of radiolytic production of hydrogen while the crevice is still active.

Under passive, non-crevicing conditions, the oxide acts as a barrier to hydrogen absorption and the effect of γ-radiation on the nature of the film is likely to be the most significant effect of radiation. Kim and Oriani [12] observed lower hydrogen pick-up rates in the presence of radiation on Grade-12 titanium, indicating the formation of a more protective barrier. Interestingly, these authors observed a measurable hydrogen pick-up rate in the absence of radiation (usually a very difficult parameter to measure). These observable rates may indicate only partial passivation in the concentrated brine solutions used, or could suggest that Ti_2Ni intermetallics in or near the passive layer act as windows for hydrogen absorption in the Grade-12 material.

In contrast, Ikeda et al. [11] saw no evidence for hydrogen absorption by either Grade-2 or Grade-12 titanium after extended exposure to irradiated saline solutions at 100°C and 150°C ([Cl^-] = 0.97 mol·dm^{-3}, ~5 Gy·h^{-1}, =5 a exposure). Westerman et al. [13,14] report significant hydrogen pick up by both materials in basaltic groundwaters and brines at dose rates of 10^4 Gy ·h^{-1} at temperatures of 250°C and 150°C, respectively. Less hydrogen absorption occurred at an absorbed dose rate of 100 Gy·h^{-1}, suggesting a dose-rate dependence. Consequently, there appear to be some indications of higher absorption rates in the presence of radiation, but only at high temperatures and high dose rates.

3.2. Modelling γ-radiation effects for titanium containers

For the crevice corrosion of Grade-2 titanium, our experiments indicate that radiation influences all the steps involved in crevice corrosion: (i) initiation, (ii) propagation, and (iii) repassivation. No such studies have been performed for either Grade-12 or Grade-16 titanium. These alloys are significantly more crevice-corrosion resistant than Grade-2 titanium. Crevice corrosion does initiate on Grade-12 titanium, but the extent of propagation is limited before repassivation occurs. For Grade-16 titanium, although indications of initiation can be

observed, the material repassivates almost immediately and does not propagate. The discussion below is limited to the Grade-2 material. The effects of γ-radiation on the crevice corrosion of Grade-12 and Grade-16 titanium, and the way in which they would be modelled, would be quite different.

In the current model for the crevice corrosion of Grade-2 titanium, it is assumed that initiation occurs rapidly on all containers [2]. Consequently, having to predict the notoriously unpredictable initiation event is avoided. Even in demonstrating an effect of irradiation on initiation was successful, however, a statistically meaningful set of data would be needed before introducing a lower probability for initiation, because the effect of irradiation depends upon the material properties.

Instead of trying to predict initiation, the crevice-corrosion model predicts the rate and extent of propagation [2]. The rate data used in the model were measured in the presence of a radiation field. Hence, the effects of radiation are empirically included in the propagation rates. To improve the model, it would be necessary to take into account the dose-rate dependence of the propagation rate. The rate of crevice corrosion could be measured either electrochemically or from the total weight change of the crevice-corroded specimen. In addition, the mode of crevice propagation, i.e. the spatial distribution of penetration sites within the creviced area, might also depend on the dose rate, and would need to be studied using the same metallographic and image-analysis techniques used to study propagation modes on unirradiated coupons.

The most significant factor limiting the extent of crevice propagation is the ability of the material to repassivate. If a correlation could be determined between the γ-dose rate and the time for the crevice to repassivate, it might be able possible to place limits on the extent of propagation and, hence, penetration depth for a given dose rate under vault conditions.

The effect of γ-radiation on hydrogen absorption appears to be a little easier to model. Failure by HIC is deemed to occur when the absorbed hydrogen concentration reaches a threshold value of ~500 $\mu g \cdot g^{-1}$ [4,15]. Calculation of the failure time by HIC then requires determination of the hydrogen absorption rate. Our experimental evidence suggests that, under crevice-corrosion conditions, the rate and extent of hydrogen absorption will be lower in a radiation field because of crevice repassivation by oxidizing radiolysis products and/or by catalysis of proton reduction inside the crevice. These effects could be accounted for by using a modified hydrogen absorption rate and a shorter period of hydrogen absorption. For passive surfaces, it is not clear that the rate of hydrogen absorption will be modified by γ-radiation at the absorbed dose rates expected in a Canadian disposal vault. Increased rates of hydrogen absorption might occur at higher dose rates ($>10^3$-10^4 $Gy \cdot h^{-1}$) and could similarly be modelled by increasing the value for the hydrogen-absorption rate used in the model.

4. Raditaion effects on copper containers

4.1. γ-radiation effects on copper corrosion

Irradiation could affect the corrosion behaviour of copper in a number of ways. The production of radiolytic oxidants could enhance the rate of uniform corrosion. Irradiation of semi-conducting Cu_2O films or the formation of differential radiolytic-oxidant concentration cells within porous corrosion-product films might increase the susceptibility to localized forms of attack (pitting or underdeposit corrosion) [16]. The production of aggressive species

by solution- or gas-phase radiolysis could increase the risk of SCC [8]. Finally, irradiation will have an effect on the viability of microbes around the container, and the consequent possibility of MIC [17].

Fig. 11 shows the mechanism proposed for the uniform corrosion of copper in compacted buffer material [16]. The only oxidant included in this mechanism is the O_2 trapped in the pores of the buffer initially. Measurements of the corrosion potential (E_{CORR}) of copper electrodes with and without irradiation suggest that dose rates higher than those expected in a Canadian disposal vault are required for any effect of γ-radiation to be observed. An increase in the concentration of oxidants would produce an anodic (positive) shift in E_{CORR}. King and Litke [18] saw no such shift on the introduction of a γ source (absorbed dose rate 27 $Gy \cdot h^{-1}$) to an experiment in deaerated saline solution ($[Cl^-] = 0.97\ mol \cdot dm^{-3}$) at 150°C (Fig. 12). In contrast, Glass et al. [19] observed an anodic shift of 100 mV upon irradiation of copper in a dilute groundwater solution at 30°C at an absorbed dose rate of $3 \times 10^4\ Gy \cdot h^{-1}$. The anodic shift was attributed to the formation of H_2O_2 and OH radicals in solution, because the instantaneous shift and subsequent decay in E_{CORR} could be replicated by chemically adding peroxide.

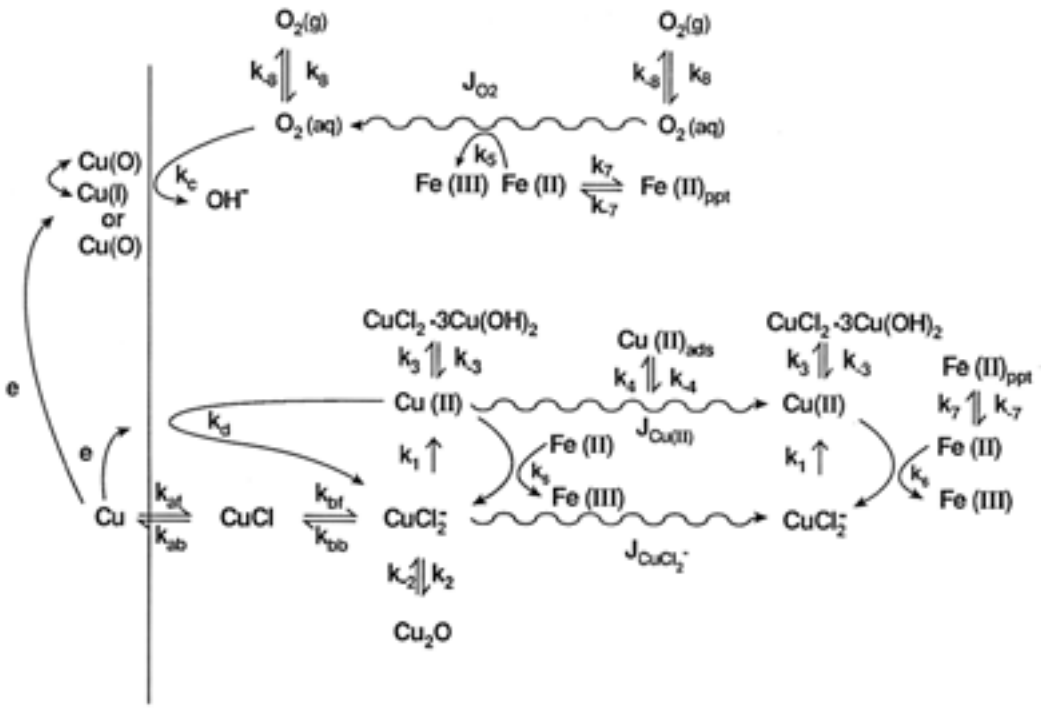

Figure 11. Mechanism of the uniform corrosion of copper in compacted buffer material.

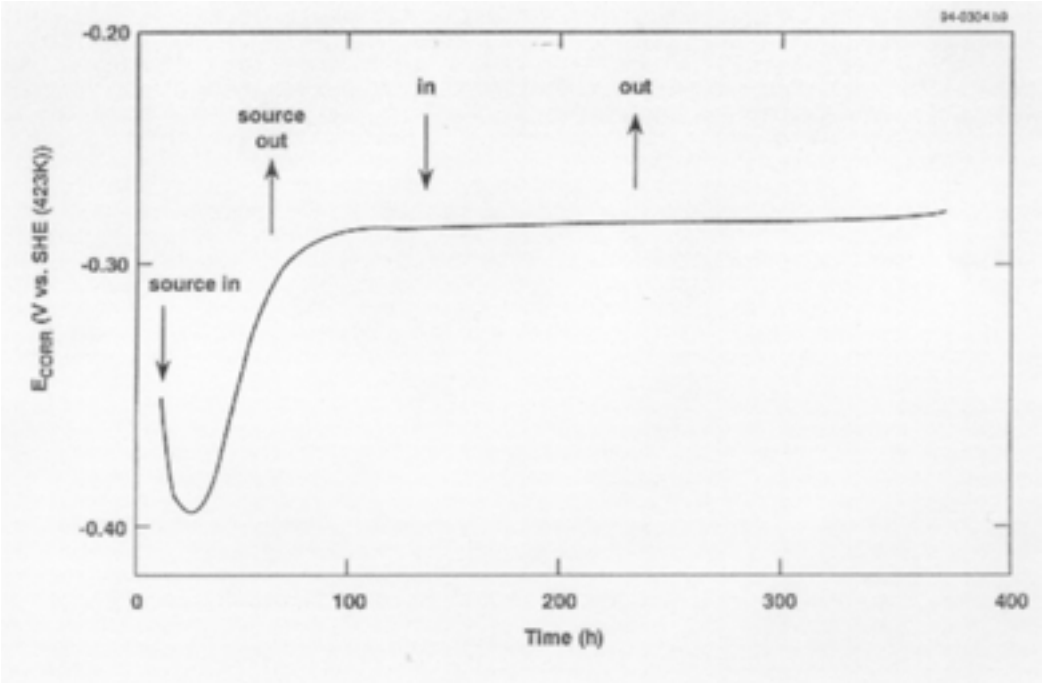

Figure 12. Effect of γ-radiation on the corrosion potential of copper in deaerated saline solution ([Cl⁻] = 0.97 mol·dm^{-3}) at 150 °C (absorbed dose rate 27 Gy·h^{-1}). The initial decrease in potential is typical of the behaviour in the presence or absence of radiation and is not itself an effect of radiation.

In fact, King and Litke [18] observed a decrease in the weight-loss corrosion rate of copper on irradiation in synthetic groundwater solution at 150°C. In both aerated and deaerated solution, the corrosion rate was lower when irradiated at absorbed dose rates of between 14 and 27 Gy·h^{-1}. The irradiated samples were covered by an adherent, apparently protective Cu_2O film, as opposed to the thicker defective mineralized film formed in the absence of irradiation [20]. It is not known whether the formation of the more protective film was the cause or a consequence of the lower corrosion rate in the irradiated environment.

A detailed experimental program has not been performed to study the effect of γ-radiation on the pitting of copper. No pitting has been observed on a range of coupons exposed to simulated disposal conditions at an absorbed dose rate of 5 Gy·h^{-1} for periods up to 5 a [21]. Other workers have observed the pitting of copper in irradiated vapour-phase experiments, but only at high-absorbed-dose rates (100 to 200 Gy·h^{-1}) [22]. It was suggested that pitting was associated with the formation of nitrogen oxides and nitric acid because of the radiolysis of air-saturated moisture films.

In general, one might speculate that irradiation might have an effect on the initiation of pitting. Lucey [23] has demonstrated the importance of CuCl and Cu_2O in the mechanism of the pitting of copper water pipes. Cuprous chloride is an n-type semiconductor and Cu_2O is a p-type oxide (although it can exhibit both p-type and n-type behaviour), and both materials exhibit photoeffects [16]. Irradiation with γ photons might also affect the structure and electronic properties of CuCl and Cu_2O layers and, hence, affect the pitting behaviour.

The possibility of SCC of copper from NH_3 or NO_2^- produced by the radiolysis of moist air has been discussed by King [8]. Neither Yunker [24] nor King and Ryan [21] observed SCC of stressed copper specimens at absorbed dose rates up to 1000 $Gy \cdot h^{-1}$ or temperatures up to 150°C. However, Makepeace [25] reports the SCC of 70-30 Cu-Zn on irradiation in moist air (100% RH) at ambient temperature. Cracking was observed at absorbed dose rates of 5.9×10^4 $Gy \cdot h^{-1}$ and 1500 $Gy \cdot h^{-1}$, but in the latter case only when the moist air was contaminated by amines formed from a neoprene rubber filter. In the high-dose-rate test, corrosion products consisted of $Cu_2(OH)_3NO_3$ and $Zn(OH)_2NO_3$, with $CuCl_2 \cdot 3Cu(OH)_2$ present near the cracks. Cracking was assumed to result from NH_3 formation [25], although radiolytically produced NO_2^- could also have been responsible [8]. It appears, however, that high dose rates (perhaps $>10^4$ $Gy \cdot h^{-1}$) are required to induce SCC.

In addition to the fact that dose rates will be low, radiation-induced SCC of copper containers in a Canadian disposal is considered unlikely for a number of other reasons. Stress corrosion requires the conjoint action of a tensile stress (or, more fundamentally, of strain at the crack tip), an aggressive SCC agent, and a susceptible material. In addition, a review of the literature on the SCC of copper alloys suggests that stress corrosion only occurs at high overall dissolution rates, requiring a sufficient supply of oxidant [8]. There is no evidence that irradiation at the absorbed dose rates expected in a Canadian disposal vault (<52 $Gy \cdot h^{-1}$) will result in the formation of either NH_3 or NO_2^-, two well-known SCC agents. Even if such species were produced, they would only be produced during the period before saturation of the disposal vault, i.e. before the imposition of the hydraulic load and before the period of greatest container strain [8]. Rapid strain of the copper shell will only occur after the vault is saturated by groundwater, but at that stage irradiation of the liquid phase will not produce aggressive SCC agents and the supply of oxidants will be limited by diffusion through the saturated buffer material.

The extent on MIC of the container has been assessed based on literature reports of the MIC of copper and the expected variation of the vault environment with time [7,17]. MIC is invariably associated with the formation of a biofilm (a combination of microbes, extracellular polymer, and other metabolic by-products) on the surface. Organic acids and other metabolites can concentrate under the biofilm, establishing a micro-environment that is different from the bulk environment. If biofilm formation does not occur, any impact from MIC should be minimal.

During the warm, oxidizing period, it is believed that the combination of elevated temperature, γ-radiation, and desiccation of the buffer will create a zone of limited microbial activity near the container surface [17]. Irradiation alone has been shown to have a dramatic impact on the number of viable microbes in buffer material [26]. Samples of uncompacted buffer were irradiated for various periods and the number of remaining viable microbes counted. The results were expressed as a D_{10} value, i.e. the absorbed dose required to reduce the indigenous microbial population by a factor of ten (Fig. 13). The highest D_{10} value measured for either native or added microbes (including several radiation-resistant strains) was ~1.7 kGy [26]. Based on this value, and the known dependence of the absorbed dose rate on time (see Fig.4) and distance into the buffer material (see Fig. 5), it is possible to predict the spatial and temporal variation of the microbial population. By defining "sterilization" as a reduction in the natural microbial population of $\sim 10^6$ $CFU \cdot g^{-1}$ by a factor of 10^7 (to 0.1 $CFU \cdot g^{-1}$), the size of the microbially depleted region around the container can be predicted [17]. Sterilization of the container surface is predicted to take between 9 and 86 days, depending on the container design and age of the fuel waste. Furthermore, a sterile zone is created,

extending up to ~40 to 60 cm away from the container, the distance increasing the higher the initial dose rate (Fig. 14) [17]. The size of this zone will also be influenced by the lack of available H_2O for microbial growth because of the desiccation of the buffer [7].

After the γ-radiation field has decayed, and once the vault has saturated with groundwater, microbial activity may resume. However, it is argued that, because the dimensions of the microbes (of the order of μm) are much greater than the mean pore size of the buffer material (of the orders of 10s of nm), repopulation of the irradiated sterile zone will not occur [7,17]. Thus, irradiation not only prevents biofilm formation and MIC initially by sterilizing the container surface, but also contributes to the long-term prevention of MIC by creating a sterile zone around the container. It should be borne in mind, however, that the predictions above are based on a minimum initial dose rate of 5.7 $Sv \cdot h^{-1}$ (for a 25.4-mm-thick copper packed-particulate container with 40-a-cooled fuel). For a 25.4-mm-thick copper dual-wall container (initial surface dose rate of 0.12 $Sv \cdot h^{-1}$ for 40-a-cooled fuel), sterilization would take ~13 a and the sterile zone around the container would be only ~14 cm thick.

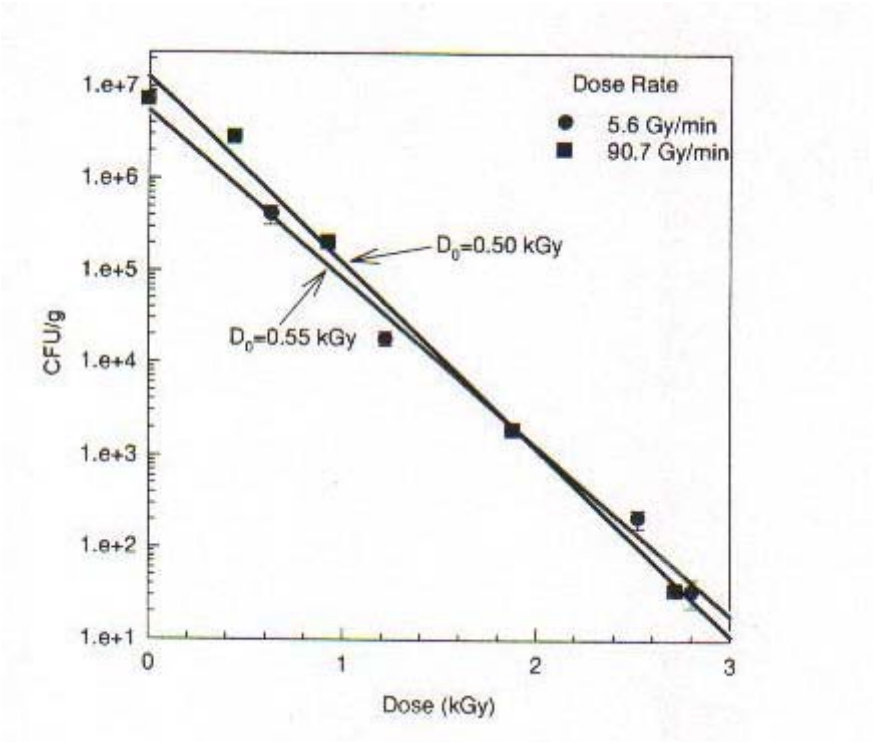

Figure 13. Typical "kill-curve" showing the effect of γ-radiation on the viable microbial population in uncompacted buffer material. The slope of such curves is quoted as a D_{10} value. Curve shown is for the radiation-resistant bacterium Acinetobacter radioresistens in a Wyoming bentonite/sand buffer mixture [26].

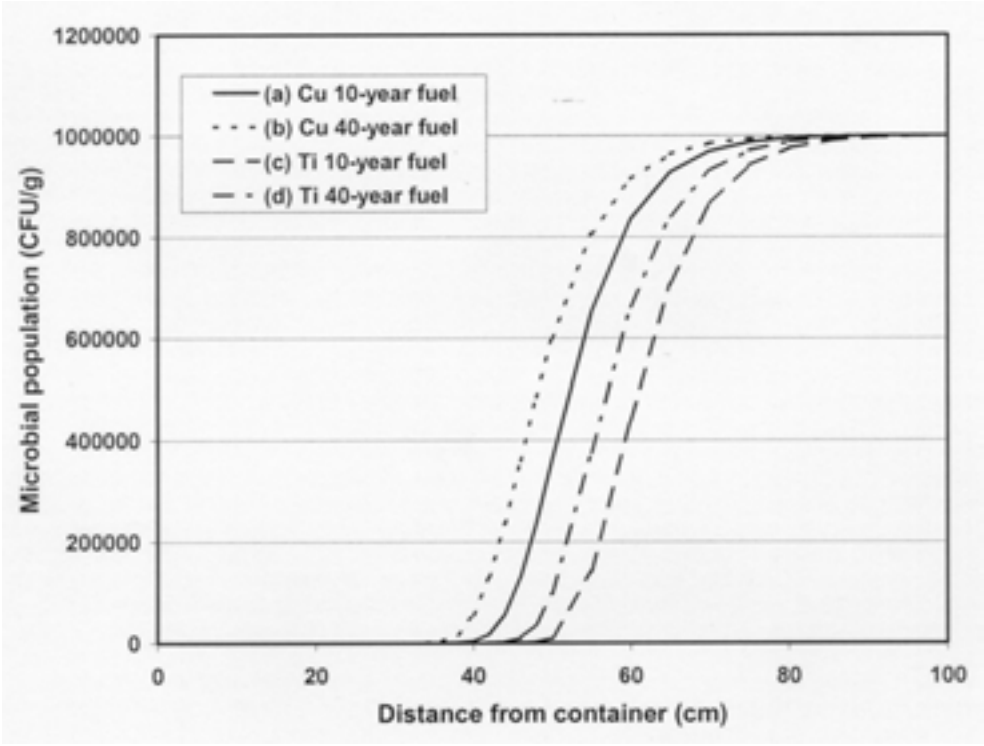

Figure 14. Predicted microbial population around nuclear waste containers of various designs illustrating the formation of a radiation-induced "sterile" zone around the container. Calculations were performed for 6.35-mm-thick titanium and 25.4-mm-thick copper containers for 10-a-cooled and 40-a-cooled fuel: (a) titanium container, 10-a-cooled fuel; (b) titanium, 40-a fuel; (c) copper, 10-a fuel; and (d) copper, 40-a fuel.

4.2. Modelling γ-radiation effects for copper containers

The models of copper container failure do not included any specific effects from γ-radiation [3]. No detrimental effects on the rate of uniform corrosion or pitting of copper have been observed under simulated disposal conditions with radiation fields representative of those expected in a Canadian disposal vault. However, from this work and that of others, it is clear how specific radiation effects could be incorporated if the dose rate is higher.

For uniform corrosion, a detailed numerical model has been developed based on the reaction mechanism shown in Fig. 11 [3]. For each of the nine species included in the model (O_2, $CuCl_2^-$, Cu^{2+}, Cu_2O, $CuCl_2 \cdot 3Cu(OH)_2$, Cu(II) adsorbed on Na-bentonite clay, Cl^-, dissolved and precipitated Fe(II)) a 1-dimensionsal mass-balance equation is written, of the form

$$\varepsilon_a \frac{\partial c}{\partial t} = \frac{\partial}{\partial x} \varepsilon_e \tau D \frac{\partial c}{\partial x} + R \qquad (6.1)$$

where

c is the pore-water concentration
D is the diffusion coefficient in bulk solution
ε_a is the accessible porosity of the buffer or backfill material
ε_e is the effective porosity of the buffer or backfill material
τ is the buffer or backfill tortuosity factor

and ΣR is the sum of the rates of reaction for the particular species.

For instance, for Cu^{2+}, the reaction term would include gains from the oxidation of $CuCl_2^-$ to Cu^{2+} by O_2 (rate constant k_1 in Fig. 11), the dissolution of $CuCl_2 \cdot 3Cu(OH)_2$ (k_{-3}) and the desorption of adsorbed Cu(II) (k_{-4}), and losses from precipitation (k_3), adsorption (k_4), and reduction by Fe(II) (k_6). These nine second-order partial differential equations are then solved numerically, subject to various boundary and initial conditions. In addition, a heat conduction equation is included

$$\rho C \frac{\partial T}{\partial t} = \frac{\partial}{\partial x} \left(K \frac{\partial T}{\partial x} \right) \tag{6.2}$$

where

T is the temperature

ρ is the buffer or backfill dry density

C is the specific heat

and K is the thermal conductivity.

Equation (6.2) is used to predict the spatial and temporal variation of T within the model, information which is then used to determine the values of the various rate constants and diffusion coefficients at each point in space and time. These equations are solved for a mathematical grid determined by the design of the disposal vault [3]. Because the model is one-dimensional, the complex 3-dimensional distribution of buffer, backfill, and rock around the containers (see Fig. 1) can only be represented by a series of layers representing the various materials. The material properties vary in their porosity, tortuosity factor, and content of Fe(II) minerals. Four such layers are typically included: the buffer materials, the backfill materials, a layer of excavation-damaged rock, and the rock mass itself, bounded on one side by the container and at the far boundary by a major water-bearing fracture. The outputs of the model are the concentrations of the nine species as a function of x and t, and various derived parameters. Two of the most important derived parameters are the corrosion rate (expressed as the corrosion current density i_{CORR}) and E_{CORR}.

This type of model could be easily extended to include the effect of oxidizing and reducing radiolysis products. In addition to the nine species already considered, a mass-balance equation of the type shown in Equation (6.1) could be written for each of the radiolysis products considered: the primary radiolysis products $e^-(aq)$, OH, H, H_2, H_2O_2, H^+, OH^- and H_2O and the secondary radiolysis products, O_2, HO_2, O_2^-, O^- and HO_2^-, produced by reactions between various primary and secondary species. The mass-balance equations for the primary radiolysis products would include a term for the production of the particular species by irradiation, which would be of the form $G \cdot R(x,t)$, where G is the yield per unit absorbed dose and R(x,t) is the dose rate as a function of distance and time. The values of G are available from the extensive literature on the radiolysis of aqueous solutions [27]. It has been suggested, however, that larger G values would be appropriate for systems involving interfaces (such as the container surface and surfaces of clay and sand particles) because of the production of additional secondary electrons at these interfaces [28]. The enhancement factor from this interfacial effect might be of the order of 1 to 10.

The ΣR term for each radiolysis product will include terms for reactions between each other and with the various copper and iron species included in the overall model. The reactions between the various radiolysis products and the values of the respective rate constants have

been well established from aqueous radiolysis studies [27]. Commonly a set of 40 to 50 such reactions is defined. In addition, a further 15 reactions can be defined involving the oxidation or reduction of $CuCl_2^-$, Cu^{2+}, and adsorbed Cu(II) [29]. The rates of these reactions are generally so fast that the concentrations of the various radiolysis products will tend to reach steady state before they have the chance to diffuse a great distance. For this reason, the mass-balance equations for these species can be simplified by omitting the diffusive mass-transport term [30].

The most significant problem in modelling the effects of radiolysis products on corrosion reactions is defining the interfacial boundary conditions. At the far boundary, e.g. at the rock/fracture interface some distance from the container, a simple zero-concentration boundary condition can be defined. The situation is more complicated, however, at the container surface. Here, the various radiolysis products can participate in three types of electrochemical reaction (Figs. 15). First, oxidizing species may be reduced on the copper surface, a process that is coupled to the anodic dissolution of copper. Second, the surface may catalyze decomposition reactions, such as the decomposition of H_2O_2 into O_2 and OH^- (or H_2O). Third, the surface may mediate recombination reactions, e.g. between $e^-(aq)$ and OH to produce H_2O and OH^-. The rate, or current density i, of each of these individual electrochemical reactions can be expressed as a function of potential E by equations of the form

$$i = i_0 \exp\frac{\alpha F}{RT}\left(E - E_{eq}\right) - \exp\frac{-(1-\alpha)F}{RT}\left(E - E_{eq}\right) \qquad (6.3)$$

where
i_0 is the exchange current density
α is the anodic transfer coefficient
F is the Faraday constant
R is the gas constant
T is absolute temperature

and E_{eq} is the equilibrium potential given by

$$E_{eq} = E^0 + \frac{RT}{nF}\ln\frac{[ox]}{[red]} \qquad (6.4)$$

where E^0 is the standard potential and [ox] and [red] are the concentrations (or products of the concentrations) of oxidants and reductants of the electrochemical couple. In Equation (6.3), the first term on the right-hand side of the equation describes the anodic (oxidation) half of the electrochemical process and the second term describes the cathodic (reduction) component.

An equation of the form of Equation (6.3) is written for each interfacial electrochemical process. For example, for the interfacial reaction of the solvated electron $e^-(aq)$, the overall process can be described by

$$e^-(aq) \leftrightarrow e^- + H_2O \qquad (6.5)$$

where the $\leftrightarrow$ symbol denotes a reversible reaction. The forward part of this reaction (going from left to right) is a reduction process involving the stripping of the electron from solution.

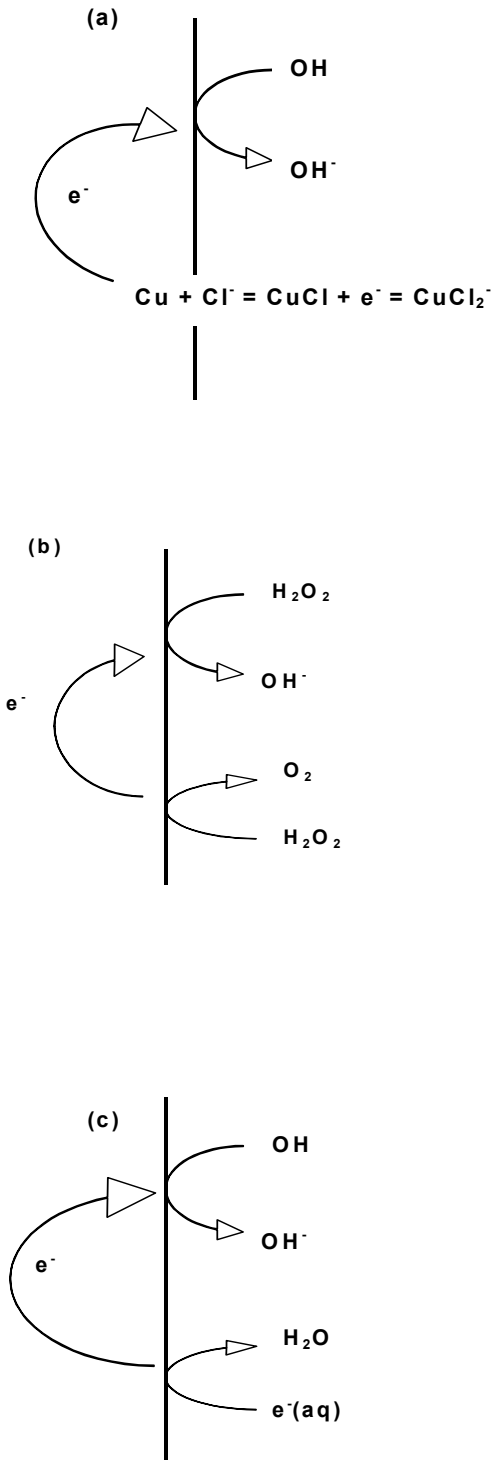

Figure.15. Various mechanisms for interfacial electrochemical reactions involving products of the radiolysis of water: (a) reduction of oxidant coupled to the anodic dissolution of copper; (b) surface-mediated decomposition reaction,; and (c) surface-mediated recombination reaction.

This is an anodic (oxidation) process and would be give rise to an anodic current. The reverse process, the solvation of an electron present in the metal, is a cathodic process. The standard potential for this reaction is -2.84 V_{SHE} [31]. In this case, and for a number of other radiolysis products, Equation (6.3) can be simplified, as the reaction is essentially irreversible because the potential of interest (E_{CORR}) is so far removed from E_{eq}. Thus, $e^-(aq)$ will act as a reductant [the forward part of reaction (6.5)], but the rate of the reverse reaction is essentially zero.

To ensure electroneutrality, the sum of the rates of all anodic (including the rate of copper dissolution) and cathodic (by convention, defined as negative) reactions must equal zero. This condition defines the potential of the surface, E_{CORR}. The condition of electroneutrality and the individual expressions of the type shown in Equation (6.3) define the boundary condition for each of the radiolysis products.

In principle, therefore, the complete set of mass-balance equations could be solved subject to these boundary conditions to predict the effect of γ-radiation on i_{CORR} and E_{CORR}. However, the analysis is hampered by the absence of data for i_0 and α for any of the reactions involving radical species. The rates of these interfacial reactions are sensitive to the values of these parameters (Fig. 16). Macdonald and Urquidi-Macdonald [31] assumed values for these parameters in their assessment of the effects of γ-radiation on the corrosion of various alloys in a thin moisture film. A better approach would be to determine values of i_0 and α experimentally, from measurements of the mixed potential of the appropriate redox reaction coupled to another electrochemical reaction whose electrochemical characteristics are well known. In the present context, the anodic dissolution of copper in Cl^- solutions could act as a suitable reaction, because its mechanism has been studied in detail [32]. Then, following the mixed-potential theory of Power and Ritchie [33], the measured E_{CORR} could be related to terms involving i_0 and α. Although the error in i_0 might be large because of the exponential relationship between E and i, this technique should be more reliable than one based on estimated values.

The current method of estimating the maximum depth of pitting on a copper container is based on a statistical extreme-value analysis of literature pit-depth data [3,16]. The data set used is from studies of buried pipes and archaeological artifacts exposed to near-surface conditions for long periods of time (up to 3000 a). Obviously, the pits observed on the buried objects were produced in the absence of γ-radiation. The available experimental evidence suggests, however, that, at the dose rates expected in a Canadian disposal vault, irradiation does not increase the extent of pitting of copper, so that the current database is adequate. Any deleterious effect of higher dose rates on the pitting of copper containers could only be modelled by this procedure if a large database of pit depths as a function of dose rate was available.

SCC, and any role of γ-radiation in promoting SCC, are not specifically included in the model to predict the lifetimes of copper containers [3]. Crack growth rates are sufficiently fast that sustained SCC would result in container failure in a relatively short period.

The strategy must, therefore, be to show that SCC does not occur. In this respect, the available literature evidence suggests that irradiation would not enhance the susceptibility of copper containers to SCC [8].

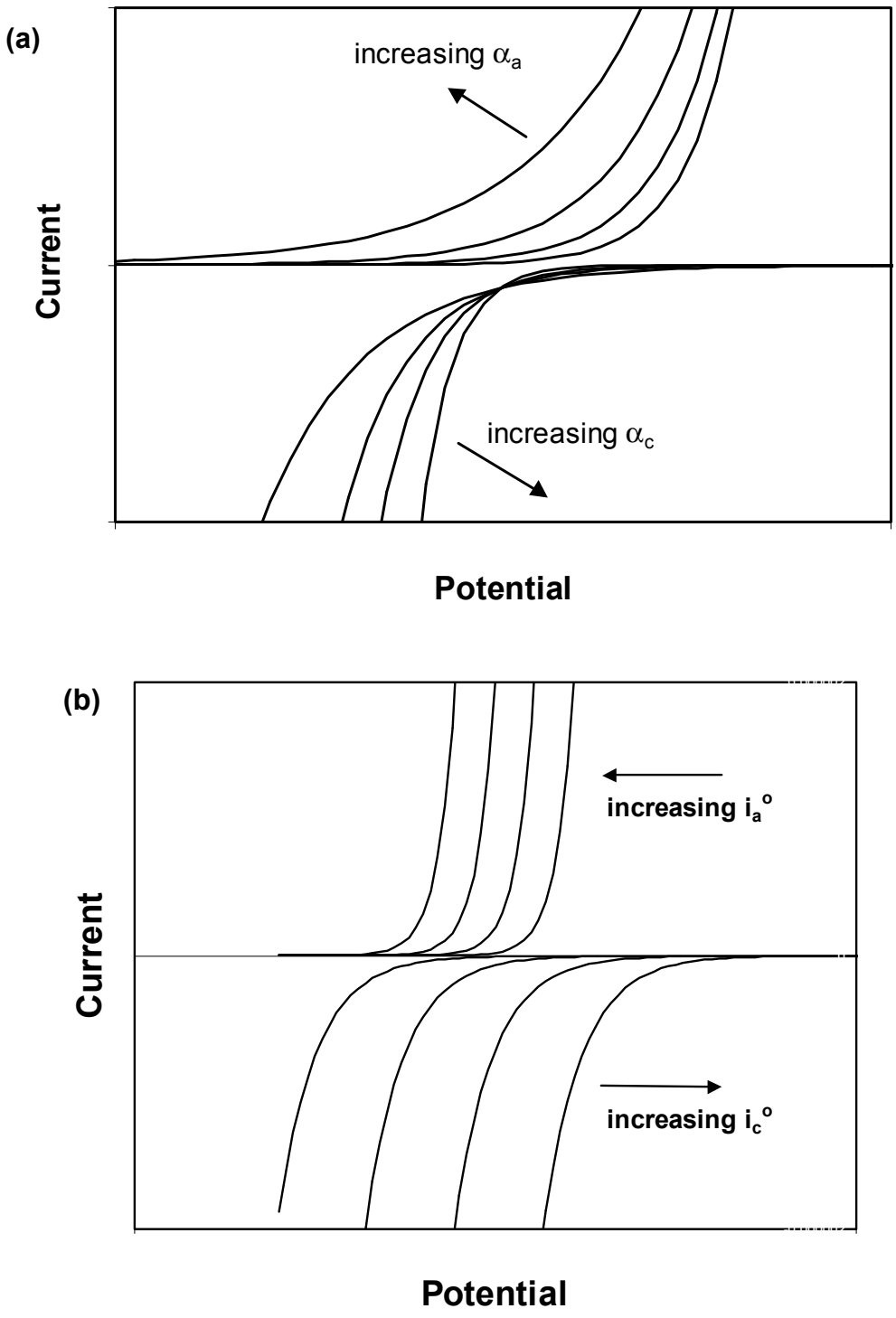

Figure 16. Impact of variability in (a) the transfer coefficient and (b) the exchange current density on the potential dependence of the rates of electrochemical processes.

Similarly, the effects of irradiation on MIC are not specifically included in the container failure model. Because, however, a central tenet of the treatment of MIC is that both the container surface and the surrounding buffer material are "sterilized," in part by γ-irradiation, the effects of radiation are implicitly included in the model (see Section 6.4.1).

5. Summary and conclusions

Irradiation of the surface and near-surface environment is a process that must be considered when predicting the lifetimes of nuclear waste disposal containers. For the dose rates expected in a Canadian disposal vault (<52 $Gy \cdot h^{-1}$), however, any impacts of γ-radiation on the corrosion process are minimal. Furthermore, some effects of irradiation are beneficial, in that they inhibit or prevent entirely certain corrosion processes. Many of these beneficial effects have been excluded from predictive models, because to include them results in a conservative underestimate of container lifetimes.

Irradiation inhibits the crevice corrosion of Grade-2 titanium but may, at high-absorbed-dose rates (>10^4 $Gy \cdot h^{-1}$), increase the rate of hydrogen absorption. The inhibitive effect of γ -radiation on crevice corrosion may be related to the production of oxidizing radiolysis products inside the crevice, which drives repassiavtion, or of reducing species, which catalyses proton reduction. This beneficial effect is implicitly included in the model for the crevice corrosion of containers made from Grade-2 titanium by using crevice-corrosion rates determined in a γ-radiation field. There is no evidence that titanium containers in a Canadian disposal vault will be subject to increased rates of hydrogen absorption, and hence earlier failure by HIC, as a result of irradiation.

For copper, the impacts of irradiation on the container lifetime are minimal. Based on E_{CORR} measurements, there is no evidence that the rate of uniform corrosion will be increased by the production of oxidizing radiolysis products at absorbed dose rates <27 $Gy \cdot h^{-1}$. Detrimental effects may be observed at much higher dose rates (10^4 $Gy \cdot h^{-1}$), and the framework of electrochemically based models has been developed to account for these effects. There is no evidence in the literature that copper containers will be more susceptible to pitting or SCC as a result of irradiation. Radiation is believed to have a beneficial effect on MIC, because it will sterilize the container surface and surrounding environment, thus preventing biofilm formation on the container surface. This effect is implicitly included in container lifetime predictions.

REFERENCES

[1] AECL (ATOMIC ENERGY OF CANADA LIMITED), Environmental Impact Statement on the Concept for the Disposal of Canada's Nuclear Fuel Waste. Atomic Energy of Canada Limited Report, AECL-10711, COG-93-1, AECL, Pinawa, Manitoba (1994).

[2] JOHNSON, L.H., et al., The Disposal of Canada's Nuclear Fuel Waste: The Vault Model for Postclosure Sssessment, Atomic Energy of Canada Limited Report, AECL-10714, COG-93-4, AECL, Pinawa, Manitoba (1994).

[3] JOHNSON, L.H., et al., The Disposal of Canada's Nuclear Fuel Waste: A Study of Postclosure Safety of In-Room Emplacement of Used CANDU Fuel in Copper Containers in Permeable Plutonic Rock: Volume 2: Vault Model, Atomic Energy of Canada Limited Report, AECL-11494-2, COG-96-552-2, AECL, Pinawa, Manitoba (1996).
[4] SHOESMITH, D.W., KING, F., and IKEDA, B.M., An Assessment of the Feasibility of Indefinite Containment of Canadian Nuclear Fuel Wastes, Atomic Energy of Canada Limited Report, AECL-10972, COG-94-534, AECL, Pinawa, Manitoba (1995).
[5] FRAPE, S.K., FRITZ, P., and MCNUTT, R.H., Water-rock interaction and chemistry of groundwaters from the Canadian Shield, Geochim. Cosmochim. Acta **48** (1984) 1617-1627.
[6] KING, F., KOLAR, M., and SHOESMITH, D.W., "Modelling the effects of porous and semi-permeable layers on corrosion processes," CORROSION/96 (Proc. Symp. Houston 1996), National Association of Corrosion Engineers International, Houston (1996) paper no. 380 (Also published as Atomic Energy of Canada Limited Report, AECL-11592, COG-96-273, AECL, Pinawa, Manitoba [1996]).
[7] KING, F., Microbially Influenced Corrosion of Copper Nuclear Fuel Waste Containers in a Canadian Disposal Vault, Atomic Energy of Canada Limited Report, AECL-11471, COG-94-519, AECL, Pinawa, Manitoba (1996).
[8] KING, F., The Potential for Stress Corrosion Cracking of Copper Containers in a Canadian Nuclear Fuel Waste Disposal Vault, Atomic Energy of Canada Limited Report, AECL-11550, COG-96-94, AECL, Pinawa, Manitoba (1996).
[9] IKEDA, B.M., et al., Crevice Corrosion of Titanium under Nuclear Fuel Waste Disposal Conditions, Atomic Energy of Canada Limited Report, AECL-9568, AECL, Pinawa, Manitoba (1989).
[10] IKEDA, B.M., and CLARKE, C.F., "Titanium corrosion under Canadian nuclear fuel waste disposal conditions," Radioactive Waste Management (Proc. 2nd Int. Conf., Toronto, 1986), Canadian Nuclear Society Toronto (1986) 605-610.
[11] IKEDA, B.M., et al, "Crevice corrosion and hydrogen embrittlement of titanium Grades-2 and-12 under Canadian nuclear waste vault conditions," Corrosion of Nuclear Fuel Waste Containers (Proc., Workshop, Pinawa, 1990, SHOESMITH, D.W., Ed.), Atomic Energy of Canada Limited Report, AECL-10121, AECL, Pinawa, Manitoba (1990) 45-66.
[12] KIM, Y.J., and ORIANI, R.A., Brine radiolysis and its effect on the corrosion of grade 12 titanium, Corrosion **43** (1987) 85-92.
[13] WESTERMAN, R.E., and TELANDER, M.R., Hydrogen Absorption and Crevice Corrosion Behaviour of Ti Grade-12 During Exposure to Irradiated Brine at 150°C, PNL/SRP-SA-14323, Pacific Northwest Laboratory, Richland, Washington (1986).
[14] WESTERMAN, R.E., PITMAN, S.G., and NELSON, J.L., General Corrosion, Irradiation-Corrosion, and Environmental-Mechanical Evaluation of Nuclear-Waste-Package Structural-Barrier Materials. PNL-4364, Pacific Northwest National Laboratory, Richland, Washington (1982).
[15] CLARKE, C.F., HARDIE, D., and IKEDA, B.M., Assessment of Materials for Containment of Nuclear Fuel Waste: Environment-Sensitive Fracture of Titanium, Atomic Energy of Canada Limited Report, AECL-10477, COG-92-162, AECL, Pinawa, Manitoba (1992).
[16] KING, F., A Model for the Corrosion of Copper containers in a Canadian Nuclear Fuel Waste Disposal Vault. Part 1. The Corrosion Model, Atomic Energy of Canada Limited Report, AECL-11472, COG-95-520, AECL, Pinawa, Manitoba (1997).

[17] KING, F., and STROES-GASCOYNE, S., "Microbially influenced corrosion of nuclear fuel waste disposal containers," Microbially Influenced Corrosion (Proc. Int. Conf., Houston, 1995), National Association of Corrosion Engineers International, Houston (1995), paper no. 35.
[18] KING, F., and LITKE, C.D., The Corrosion of Copper in Synthetic Groundwater at 150°C. Part 1. The Results of Short-Term Electrochemical Tests, Atomic Energy of Canada Limited Technical Record, TR428, AECL, Pinawa, Manitoba (1987).*
[19] GLASS, R.S., VAN KONYNENBURG, R.A., and OVERTURF, G.E., "Corrosion processes of austenitic stainless steels and copper-based materials in gamma-irradiated aqueous environments," CORROSION/86 (Proc., Symp., Houston 1985), National Association of Corrosion Engineers International, Houston (1986) (also available as, UCRL-92941, Lawrence Livermore National Laboratory, California 1985).
[20] KING, F., LITKE, C.D., and GEORGE, K.J., The Corrosion of Copper in Synthetic Groundwater at 150°C. Part II. The Characterization of Surface Films, Atomic Energy of Canada Limited Technical Record, TR-464, AECL, Pinawa, Manitoba (1989). (Unrestricted, unpublished report available from Scientific Document Distribution Office, Chalk River Laboratories, Chalk River, Ontario, Canada K0J 1J0).
[21] KING, F., and RYAN, S.R., unpublished data.
[22] REED, D.T., and KONYNENBURG, R.A., Corrosion of copper-based materials in irradiated moist air systems, Mat. Res. Soc. Symp. Proc., **212** (1991) 317-325.
[23] LUCEY, V.F., Mechanism of pitting of copper in supply waters, Br. Corros. J. **2** (1967) 175-185.
[24] YUNKER, W.H., Corrosion behavior of copper-base materials in a gamma-irradiated environment, WHC-EP-0188, Westinghouse Hanford Company, Richland, Washington (1990).
[25] MAKEPEACE, C.E., Design and analysis of corrosion experiments for testing materials exposed to gamma radiation, J. Test. Evaluation **2** (1974) 202-209.
[26] STROES-GASCOYNE, S., et al., Radiation resistance of the natural microbial population in buffer, Mats. Res. Soc. Symp. Proc. **353** (1995) 345-352.
[27] BOYD, A.W., CARVER, M.B., and DIXON, R.S., Computed and experimental product concentrations in the radiolysis of water, Radiat. Phys. Chem. **15** 177-185.
[28] ORLANDO, T.M., private communication, 1995.
[29] KING, F., IKEDA, B.M., and SHOESMITH, D.W., Radiation Effects and the Modelling of the Corrosion of Nuclear Waste Disposal Containers, Atomic Energy of Canada Limited Report, AECL-11476, COG-95-531-I, AECL, Pinawa, Manitoba (1997).
[30] WREN, C.J., private communication, 1995.
[31] MACDONALD, D.D., and URQUIDI-MACDONALD, M., Thin-layer mixed-potential model for the corrosion of high-level nuclear waste containers, Corrosion **46** (1990) 380-390.
[32] DESLOUIS, C., et al., Electrochemical behaviour of copper in neutral aerated chloride solution. I. Steady-state investigation, J. Appl. Electrochem. **18** (1988) 374-383.
[33] POWER, G.P., and RITCHIE, I.M., Mixed potential measurements in the elucidation of corrosion mechanisms-1. Introductory theory, Electrochimica Acta **26** (1981) 1073-1078.

Influence of gamma radiation on the corrosion of carbon steel, heat-generating nuclear waste packaging in salt brines

E. Smailos

Forschungszentrum Karlsruhe, Institut für Nukleare Entsorgungstechnik, Karlsruhe, Germany

Abstract. Previous corrosion studies identified carbon steels as promising materials for the manufacture of long-lived high-level waste (HLW) containers that could act as an engineered barrier in a rock-salt repository. In the present work, the influence exerted by the gamma radiation of the waste on the corrosion behaviour of the preselected TStE 355 carbon steel was investigated. The steel was examined by long-term immersion tests (maximum test duration 18 months) in three disposal relevant brines (two rich in $MgCl_2$, one rich in NaCl) at 150°C and a dose rate of 10 Gy/h. For comparison, experiments without irradiation were also performed. The results indicate that the steel resists pitting corrosion in all brines. In both cases with and without radiation, the corrosion rates of the steel in the $MgCl_2$-rich brines are significantly higher than rates in the NaCl-rich brine. However, the values determined imply corrosion allowances acceptable for thick-walled containers. A gamma dose rate of 10 Gy/h does not increase the corrosion rate of the steel in the NaCl-rich brine (about 14 - 15 µm/a). In the $MgCl_2$-rich brines, the corrosion rates in the irradiated environments (72 - 162 µm/a) are only a factor of about 1.3 to 1.5 higher than in the unirradiated systems. In view of these results, the TStE 355 carbon steel continues to be considered a promising container material and will be further investigated.

1. Introduction

Previous corrosion studies [1-4] have shown that the unalloyed fine-grained steel TStE 355 is a promising material for long-lived HLW containers that could act as a barrier for immobilization of radionuclides in a rock-salt repository. Its promising nature is based primarily on the fact that so far only general corrosion has been observed in disposal-relevant salt brines such that the long-term corrosion behaviour of the steel can be predicted in a reasonable manner. Furthermore, the corrosion rates of the steel imply acceptable corrosion allowances for thick-walled containers.

To characterize the corrosion behaviour of the fine-grained steel TStE 355 in more detail, further electrochemical and long-term corrosion studies are being performed in brine environments. An essential aspect of the corrosion studies on the steel is the investigation of the influence of radiation of the waste on its corrosion behaviour in disposal-relevant salt brines. Of the various types of radiation, only gamma radiation is present at the surface of the container. The dose rate depends on the design of the container and the nature of the waste inside.

Corrosion studies under gamma irradiation are important for two reasons. Firstly, the interaction of gamma radiation with the salt brines produces reduced/oxidizing reactive particles and stable products such as e^-_{aq}, H_2, H_2O_2, etc. [5], which may change the rate and mechanism of corrosion. Secondly, the absorption of gamma radiation in the semi-conducting protective oxide layers of metals will induce photo-radiation effects [6,7], which can change the corrosion rate by facilitating cathodic/anodic reactions at the oxide layer/electrolyte interface. Glass [7] concludes that the radiolytic products will exert the greatest effect on the corrosion process of metals.

Previous corrosion studies on carbon steels at 90°C in an $MgCl_2$-rich brine [2] have shown that a high-gamma-dose rate of 10^5 rad/h strongly enhances the corrosion rate. In contrast to this, lower dose rates of up to 10^4 rad/h did not influence the rate. It was concluded that the effect of radiation on corrosion strongly depends on the concentration of radiolytic products in the brines. Strong oxidizing agents such as H_2O_2, ClO_3^-, etc. are considered as being mainly responsible for the increase in corrosion because they are known as cathodic depolarizers.

From the corrosion studies performed so far under irradiation, two essential questions remain open: the effect of high disposal temperatures between 150°C and 200°C, and of the composition of salt brines (NaCl-rich or $MgCl_2$-rich) on the steel corrosion. Therefore, irradiation-corrosion studies were performed in the present study on the TStE 355 steel at 150°C in brines of various compositions. The experiments were conducted at a gamma dose rate of 10 Gy/h (10^3 rad/h), which is relevant for the thick-walled steel containers discussed having corrosion and mechanical allowances of about 15 cm for a service life of 300 years.

2. Steel investigated and test conditions

The preselected unalloyed fine-grained steel TStE 355 was examined in the hot-rolled and normalized condition. The metal sheet used for the preparation of the corrosion specimens had the following composition in wt%: carbon: 0.17; silicon: 0.4; manganese: 1.49; phosphorous plus sulphur: < 0.1; balance iron.

For the corrosion studies, plane specimens with dimensions of 40 x 20 x 4 mm were used. Before specimen fabrication, the metal sheet was freed from the adhering oxide layer by milling. After this mechanical treatment, the specimens were cut and cleaned with alcohol in an ultrasonic bath.

To have severe test conditions, the steel was investigated under conditions simulating an accident with an intrusion of large amounts of brine into the disposal area. To examine the influence of the brine composition on the corrosion behaviour of the steel, three disposal-relevant brines differing qualitatively and quantitatively were used as the corrosion media. Two of them, brine 1 (Q-brine) and brine 2 are highly concentrated in $MgCl_2$; the third one (brine 3) has a high concentration of NaCl. The compositions and measured pH and O_2-values of the test brines are given in Table 1. The pH values given are relative data and were measured using a glass electrode. Application of the correction formula proposed by Bates et al. [8] gives pH values at 25°C, which are higher than the measured values by 1.8 to 2.2 units for brines 1 and 2, and by 0.4 units for brine 3. The O_2-values of the brines were determined by a polarographic method using an O_2-sensor; the saturation values (1.0 - 1.4 mg O_2/l) obtained by the Winkler method were used as the reference values.

The steel was examined for general and local corrosion in the brines at a gamma dose rate of 10 Gy/h. For comparison, corrosion tests without radiation were also carried out. A test temperature of 150°C was selected, which roughly corresponds to the maximum temperature on the surface of the container according to the German concept. The experiments lasted up to 18 months.

Table 1. Compositions, pH values, and O_2 contents of salt brines used in laboratory-scale corrosion experiments

Brine	Composition (wt%)							
	NaCl	KCl	$MgCl_2$	$MgSO_4$	$CaCl_2$	$CaSO_4$	K_2SO_4	H_2O
1	1.4	4.7	26.8	1.4	---	---	---	65.7
2	0.31	0.11	33.03	---	2.25	0.005	---	64.3
3	25.9	---	---	0.16	---	0.21	0.23	73.5

pH (25°C): 4.6 for brine 1; 4.1 for brine 2; 6.5 for brine 3
O_2 (55°C): 0.8 mg/l for brine 1; 0.6 mg/l for brine 2; 1.2 mg/l for brine 3

3. Experimental set-up

The corrosion experiments under gamma irradiation were performed in the spent-fuel storage pool of KFA Jülich. The radiation source was spent-fuel elements with a gamma energy spectrum similar to that of the 10-year-old vitrified HLW. The experimental set-up is shown schematically in Fig. 1. For the experiments, autoclaves made of the corrosion-resistant alloy Ti 99.8-Pd with insert vessels of Duran glass were used. The autoclaves were placed in a circular configuration into heated cylindrical SS containers (irradiation containers). Each glass insert contained 120 ml of brine and three specimens of 60 cm^2 total surface, which were totally immersed into the brine. This configuration gave a brine-volume-to-specimen surface ratio of 2 ml/cm^2. The specimens were suspended from a frame made of glass-fibre-reinforced plastic. For irradiation, the SS containers were positioned at the bottom of the 6-m-deep water-filled spent-fuel element storage pool. The specimens and brines were heated to the test temperature of 150°C using heaters.

For the experiments in unirradiated brines (V/S = 2 ml/cm^2) at 150°C, SS pressure vessels provided with corrosion-resistant insert vessels made of PTFE were used to avoid evaporation of the brines (boiling point: about 115°C). These vessels were filled with the brines, into which the specimens were immersed. After the pressure vessels had been closed, they were stored in heating chambers at 150°C. The experiments were performed at equilibrium pressure of 0.4 Mpa. To determine the corrosion kinetics, the specimens were examined at various immersion times.

4. Post-test examination of the species

After removal from the brines, the specimens were examined for general and local corrosion. The general corrosion expressed as the average thickness reduction of the specimens was calculated from the gravimetrically measured weight losses and the material density. To determine the time dependence of the general corrosion, regression analyses of the thickness reduction values were performed by means of the SAS software (registered trademark of the SAS Institute Inc., Cary, NC, USA). Application of SAS for statistical analyses of corrosion data has already been described in previous work [4].

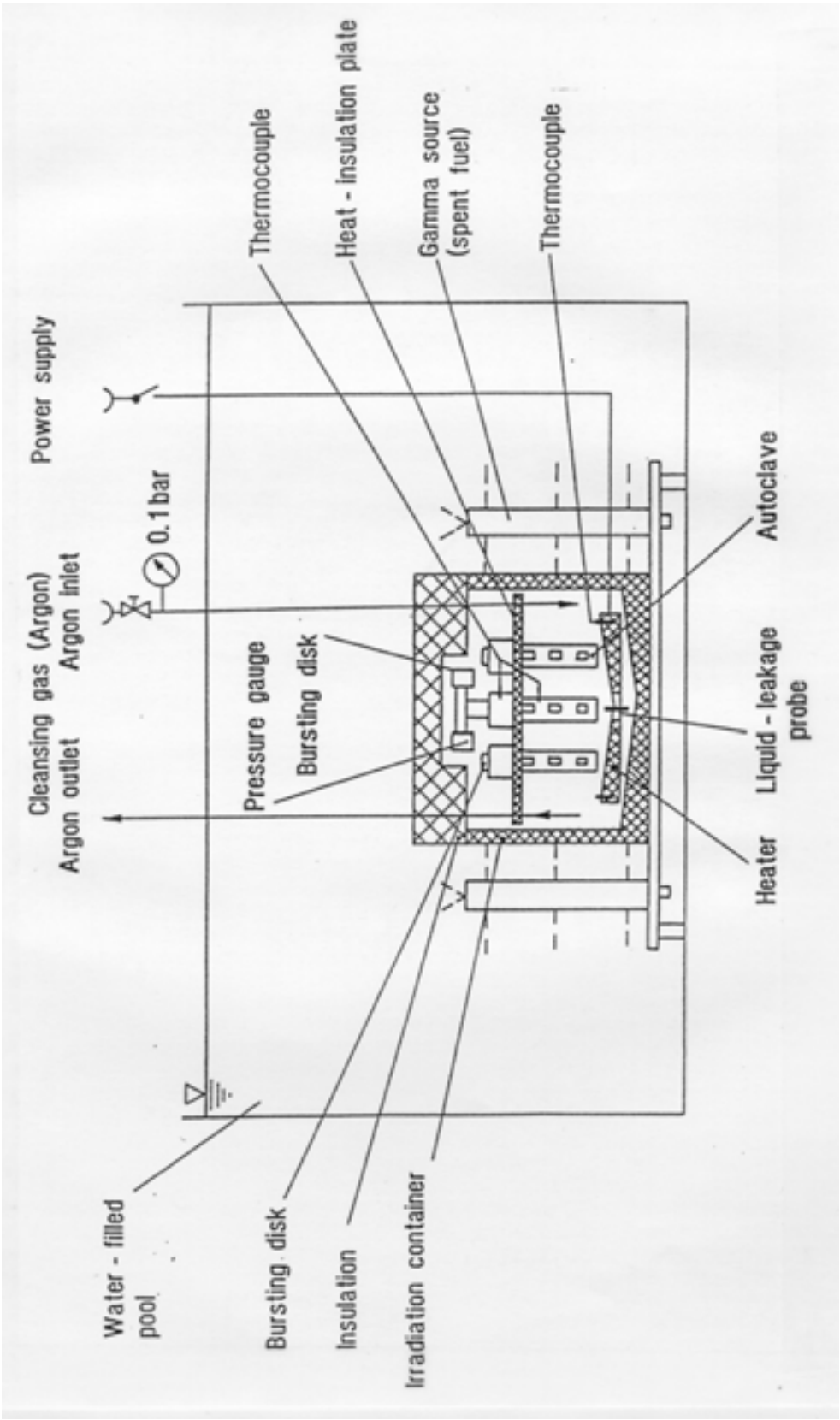

Figure 1. Irradiation-corrosion test facility.

For the regression analyses, the following equations were examined:

$$\Delta S = A + B \cdot t \tag{7.1}$$

$$\Delta S = A + B \cdot t + C \cdot t^2 \tag{7.2}$$

$$\Delta S = A + B \cdot t^N \tag{7.3}$$

where A, B, C and N are the regression coefficients, t the time, and ΔS the computed thickness reduction.

The parameter A can be interpreted as an indicator of an initial corrosion process that is influenced by the preparation of the specimens. This parameter is of minor importance for the long-term thickness reduction of the specimens. The parameter B gives a measure of the linear corrosion rate, whereas the two other coefficients (C, N) can be taken as an indication of the formation of protecting corrosion layers on the specimen surface.

Evaluation of the specimens with regard to local corrosion was carried out by measurement of the pitting depths, surface profilometry and metallography. Additional information on the corrosion mechanism was obtained from the analysis of the corrosion products by means of X-ray diffraction.

5. Results

The time-dependence of the thickness reduction of the TStE 355 steel in irradiated (10 Gy/h) and unirradiated brines at 150°C and a V/S-ratio of 2 ml/cm^2 is plotted in Figs. 2 through 4. The results show a linearly increase of the thickness reduction with exposure time. The results of the linear regression analyses for the thickness reduction of the steel in the test brines are compiled in Table 2. In both cases with and without gamma radiation, the corrosion rates (B) of the steel in the $MgCl_2$-rich brines 1 and 2 are significantly higher than those in the NaCl-rich brine 3. The higher corrosivity of the $MgCl_2$-rich brines compared to the NaCl-rich brine is attributed to their higher HCl concentration. This could be explained by the higher Cl^--concentration and the hydrolysis of Mg^{2+}. The acceleration of steel corrosion in brines containing high amounts of $MgCl_2$ is in line with the results reported by Westerman et al. [9].

The imposition of a 10 Gy/h radiation field on the 150°C brine environment increases the linear corrosion rates of the steel specimens in the brines 1 and 2 from about 47 µm/a to 72 µm/a, and from 120 µm/a to 163 µm/a, respectively. In brine 3, the corrosion rate in the 10 Gy/h irradiated environment (13.7 µm/a) is very close to the value attained in the unirradiated system (15.3 µm/a).

Surface profiles and metallographic examinations of corroded specimens have shown that the steel is resistant to pitting corrosion in irradiated and unirradiated brines. In all brines, a non-uniform general corrosion was observed. However, the measured maximum penetration depth of this uneven corrosion corresponds to the values of the average thickness reduction.

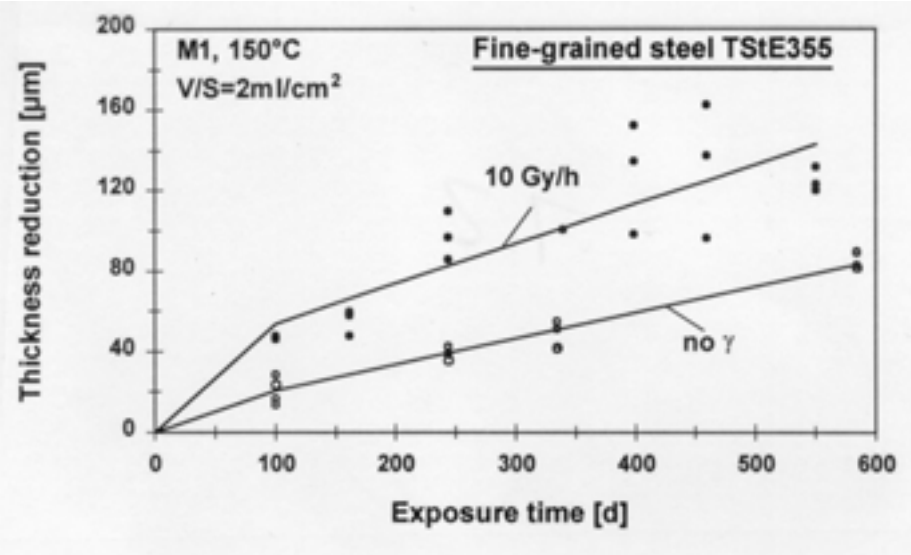

Figure 2. Thickness reduction of the TStE355 steel in the $MgCl_2$-rich brine 1 (Q-brine) with and without gamma radiation.

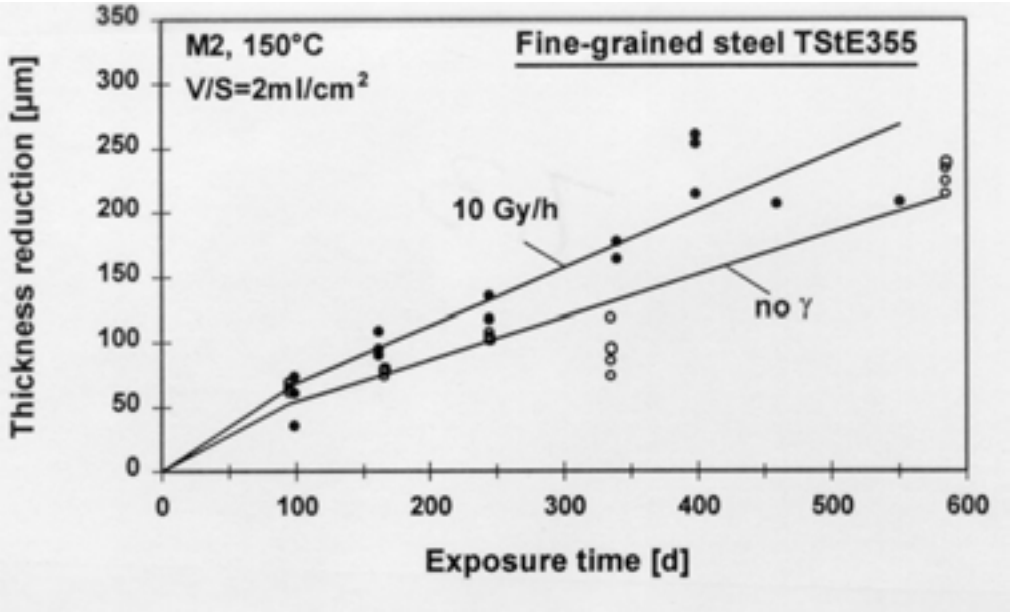

Figure 3. Thickness reduction of the TStE355 steel in the $MgCl_2$-rich brine 2 with and without gamma radiation.

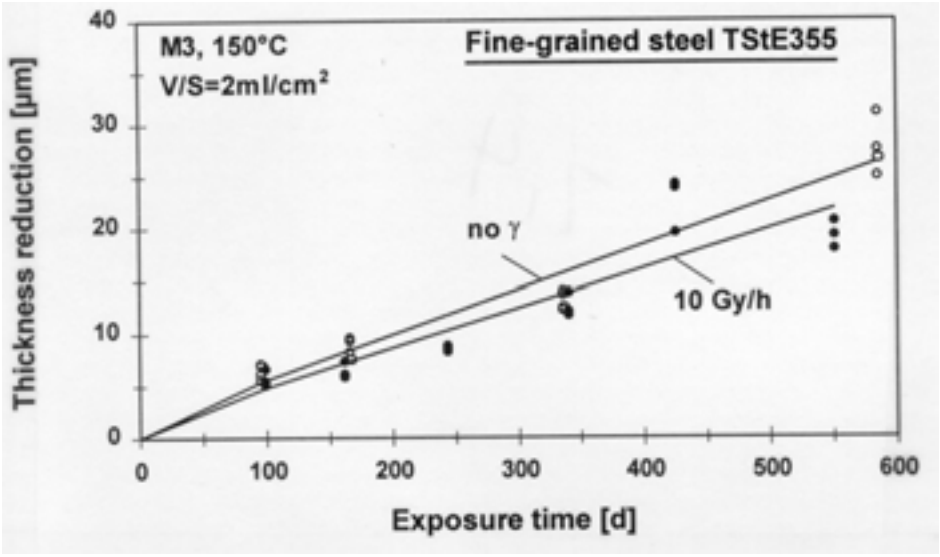

Figure 4. Thickness reduction of the TStE355 steel in the NaCl-rich brine 3 with and without gamma radiation.

Table 2. Results of linear regression analyses for the thickness reduction ($\Delta S = A+Bt$) of the TStE 355 steel in irradiated and unirradiated brines at 170°C ($V/S = 2ml/cm^2$)

Corrosion medium	D (Gy/h)	Number of specimens	A (µm)	Standard error of A (µm)	B (µm/a)	Standard error of B(µm/a)
brine 1	0	16	8.0	2.5	47.1	2.5
	10	19	34.1	10.6	72.6	11.0
brine 2	0	20	20.9	9.7	119.6	10.6
	10	15	23.6	17.5	162.4	20.4
brine 3	0	16	1.3	1.0	15.3	1.0
	10	18	1.6	1.1	13.5	1.8

Brines 1 and 2 : $MgCl_2$-rich; brine 3 : NaCl-rich.

Fig. 5 shows optical micrographs of steel specimens after 166 days of exposure to the test brines at 150°C and 10 Gy/h.

Tenacious black corrosion products were present on all steel specimens following exposure to NaCl-rich brine 3, which is consistent with the low corrosion rates observed both with and without irradiation. On the contrary, loose corrosion products were observed on the surface of the specimens exposed to the $MgCl_2$-rich brines. X-ray diffraction analyses have shown that the corrosion products formed in the unirradiated NaCl-rich brine consist of Fe_3O_4 (magnetite).

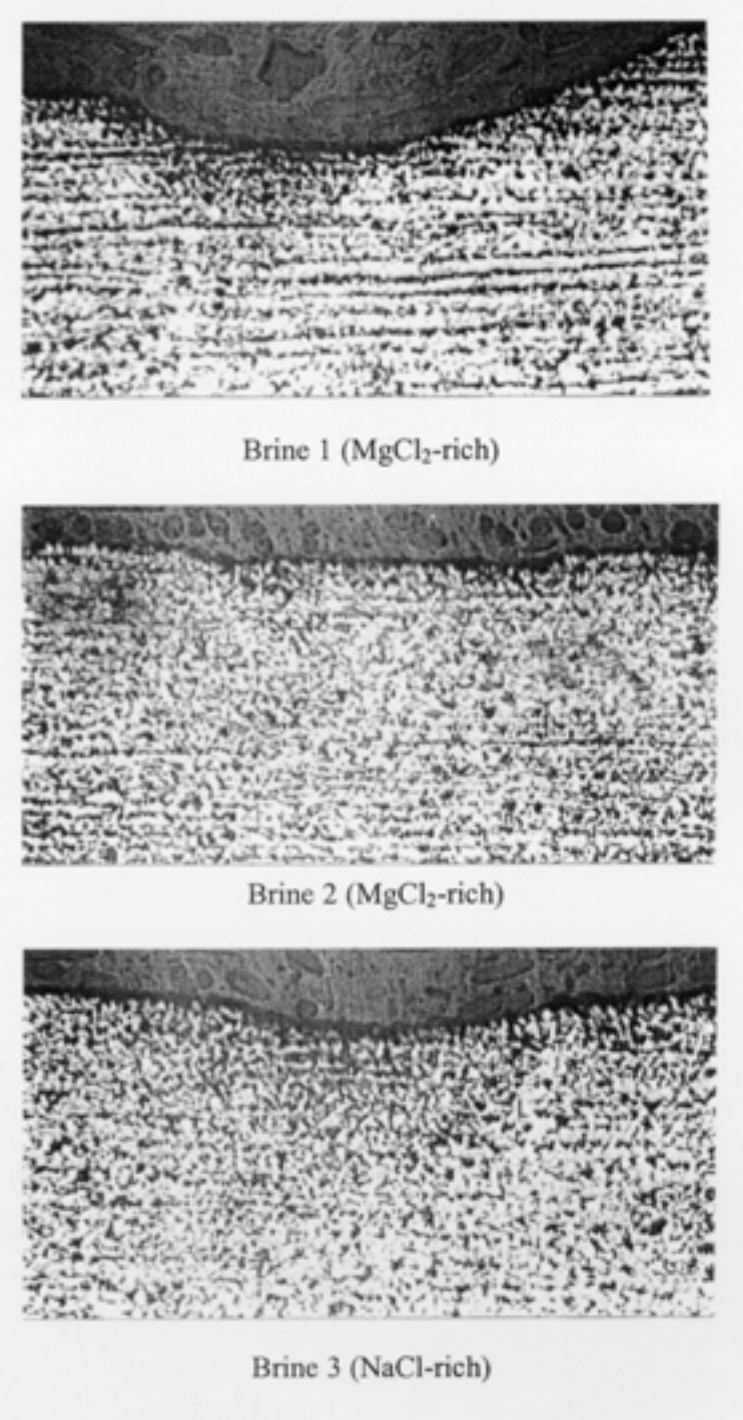

Figure 5. Optical micrographs of the TStE355 steel after 166 days exposure to brines at 150°C and 10 Gy/h.

In case of the unirradiated $MgCl_2$-rich brines, the corrosion products primarily consist of $(Fe,Mg)(OH)_2$/ $Fe_2(OH)_3Cl$ and Fe_3O_4. After exposure to irradiation of 10 Gy/h, Fe_2O_3 and β-FeOOH (Akaganeite) were identified in addition to the abovementioned phases as corrosion products in all three test brines.

6. Conclusions

In salt brines relevant for a rock-salt repository, the TStE 355 is resistant to pitting corrosion and the linear corrosion rates at 150°C imply corrosion allowances acceptable for thick-walled containers. Under the test conditions applied (V/S = 2 ml/ cm^2), corrosion allowances of about 5 mm in NaCl-rich brine and 15 to 35 mm in $MgCl_2$-rich brines are needed for steel containers with a service life of 300 years.

A gamma dose rate of 10 Gy/h does not increase the corrosion rate of the TStE 355 steel in NaCl-rich brine at 150°C. In $MgCl_2$-rich brines, the corrosion rate in the irradiated environments is a factor of about 1.3 to 1.5 higher than in the unirradiated system.

Generally, it can be stated that the corrosion results obtained in this study confirm the promising nature of the unalloyed TStE 355 steel for the manufacture of long-lived containers for heat-generating wastes. For the final evaluation of carbon steels for long-lived containers, however, further investigations are needed. These involve above all the clarification of questions relating to the synergetic effect of salt impurities and radiolytic products on corrosion at high temperature as well as the examination of the influence of pH and welding on the corrosion process in brines. Such investigations are in progress.

ACKNOWLEDEGEMENTS

The author thanks Mr. B. Fiehn and Mrs. R. Weiler for the experimental assistance, Mrs. M. Schlieker for the X-ray diffraction analyses, and the Commission of the European Union, Brussels, Belgium, and the IAEA, Vienna, Austria, for supporting this work. This work was performed in the frame of the EU programme "Management and Storage of Radioactive Waste" (Research Contract No. FI4W-CT90-0030) and of the IAEA CRP "Irradiation Enhanced Degradation of Materials in Spent Fuel Storage Facilities" (Research Agreement No. 7511/CF).

REFERENCES

[1] SMAILOS, E., et al., "Advanced corrosion studies on selected packaging materials for disposal of HLW canisters in rock salt," Waste Management '88 (Proc. Symp., Tucson, Arizona, 1988), Vol. 2, U.S. Department of Energy, Washington, D.C., (1988) 985-994.

[2] SMAILOS, E., SCHWARZKOPF, W., and STORCH, R., "Corrosion studies on packaging materials for high-level waste disposal in a rock-salt repository," 12th Scandinavian Corrosion Congress and Eurocorr 92 (Proc., Conf., Espoo, Finland, 1992), 327-338.

[3] FARVAQUE, A.M., and LEISTIKOW, S., "Electrochemical studies of the corrosion behaviour of a low carbon steel in simulated salt repository environments," 12th Scandinavian Corrosion Congress and Eurocorr 92 (Proc., Conf., Espoo, Finland, 1992), 339-347.

[4] SMAILOS, E., et al., Corrosion of carbon steel containers for heat-generating nuclear waste in brine environments relevant for a rock-salt repository, Mat. Res. Soc. Symp. Proc., **257** (1992) 399-406.
[5] JENKS, G.H., Radiolysis and Hydrolysis in Salt-Mine Brines, ORNL-TM-3717, Oak Ridge National Laboratory, Oak Ridge, Tennessee (1977).
[6] BJALOBZESKIJ, A.V., "Korrosion durch radioaktive Strahlung," in K. Schwabe (Hrsg.), Akademie Verlag, Berlin, S.82 (1971).
[7] GLASS, R.S., Effects of Radiation on the Chemical Environment Surrounding Waste Canisters in Proposed Repository Sites and Possible Effects on the Corrosion Process, SAND 81-1677, Sandia National Laboratory, Albuquerque (1981).
[8] BATES, R.G., STAPLES, B.R., and ROBINSON, R.A., Ionic hydration and single ion activities in unassociated chlorides at high ionic strength, Analytical Chemistry **42** (1970) 867.
[9] WESTERMAN, R.E., et al., Corrosion and Environmental Characterization of Iron-Base Nuclear Waste Package Structural Barrier Materials, PNL-5426, Pacific Northwest Laboratory, Richland, Washington (1986).

ABBREVIATIONS

µg	microgram
µS/cm	microSiemens per centimetre
µm	micrometer
a	year
AECL	Atomic Energy of Canada Ltd
AES	Auger electron microscope
AFR	away-from-reactor (spent fuel storage not connected to a reactor site)
AGR	advanced gas reactor
Al	aluminium
appm	atom parts per million
aq	aqueous
AR	at-reactor (spent fuel storage at a reactor site)
ASG	anti-stacking groove
ASTM	American Society for Testing and Materials
ATR	advanced test reactor
BARC	Bhabha Atomic Research Centre
BWR	boiling water reactor
CANDU	Canadian deuterium uranium reactor
CBB	crevice bent beam
CFU	colony-forming unit
CIRUS	research reactor at the Bhabha Atomic Research Centre, Mumbai, India
CRIEPI	Japanese Research Institute
DHRUVA	research reactor at the Bhabha Atomic Research Centre, Mumbai, India
DIW	deionized water
DM	demineralized
dpa	displacements per atom
ECN	electrochemical current noise
ECP	electrochemical potential
EPN	electrochemical potential noise
EPRI	Electric Power Research Institute
FA	fuel assembly
FEG-STEM	field-emission-gun scanning-transmission electron miscrope
FFTF	fast flux test facility
GCR	gas-cooled reactor
GWd/t	gigawatt-days/tonne (unit of nuclear fuel burnup)
Gy	gray
h	hour
HAZ	heat-affected zone (altered metal zone adjacent to weld metal)
HIC	hydrogen-induced cracking
HLW	high-level waste
IASCC	irradiation-assisted stress corrosion cracking
IG	intergranular
IGSCC	intergranular stress corrosion cracking
kJ/mol	kiloJoules per mole
KW/L	kilowatts per litre
LOP	limit of proportionality
LMR	liquid metal reactor
LWR	light water reactor
MeV	million electron volts

MIC	microbially influenced corrosion
MIM	metallographic microscope
mm	millimetre
mol dm^{-3}	moles per cubic decimetre
MOX	mixed oxide (nuclear fuel comprising a mix of oxides, e.g., oxides of uranium and plutonium)
Mpa	mega Pascal
mpy	mils per year (1 mil = 25.4 μm)
NACE	National Association of Corrosion Engineers, International
ORIGEN	Oak Ridge generation code (describes generation and depletion of radioactive species in nuclear fuel)
ORNL	Oak Ridge National Laboratory
PCI	pellet-clad interaction
PHWR	pressurized heavy water reactor
PIE	post-irradiation examination
PNNL	Pacific Northwest National Laboratory
ppm	parts per million
PWR	pressurized water reactor
R/h	Roentgen/hour
Rad	unit of energy absorbed from ionising radiation equal to 100 ergs/g
RBMK	power reactor of Soviet design (pressure tube/graphite stack design)
RCM	Research Coordination Meeting
RH	relative humidity
RIS	radiation-induced segregation
rpm	revolutions per minute
SAS	software copyrighted by SAS Institute
SEM	scanning electron microscope
SCC	stress corrosion cracking
SCCIG	model developed by EPRI to calculate SCC
SCE	saturated calomel electrode
SFSP	spent fuel storage pool
SG	spacer grid
SIM	simulated
SNF	spent nuclear fuel
SS	stainless steel
SSRT	slow strain rate test
Sv/h	Sieverts/hour
TEM	transmission electron microscope
TIG	tungsten inert gas (welding method)
TTS	time, temperature, sensitization (type of diagram for SS)
U	metallic uranium
V/S	volume-to-surface ratio
WWER	power reactor of Soviet design (PWR type)
wt%	weight percent
W/cm	watts/centimeter
Zry	Zircaloy

LIST OF PARTICIPANTS

Agarwar, K.	Bhabha Atomic Research Centre, India
Chichov, V.	Research Institute of Inorganic Materials (VNIINM), Russian Federation
Hashizume, K.	Kyushu University, Japan
Johnson, A.B., Jr.	Pacific Northwest National Laboratory, United States of America
King, F.	NOVA Research and Technology Centre, Canada
Mills, S.	Nuclear Electric plc, Barnwood, Gloucester, United Kingdom
Smailos, E.	Forshungszentrum Karlsruhe, Institut fur Nukleare Entsorgungstechnik, Germany
Sugisaki, M.	Kyushu University, Japan